

**Development and characterization of silicide coating for  
Nb-1Zr-0.1C alloy**

*By*

**Megha Tyagi**

(Enrolment number: **ENGG01201304014**)

**Bhabha Atomic Research Centre, Mumbai**

*A thesis submitted to the  
Board of Studies in Engineering Sciences*

*In partial fulfilment of requirements*

*for the Degree of*

**DOCTOR OF PHILOSOPHY**

*of*

**HOMI BHABHA NATIONAL INSTITUTE**



**May, 2019**

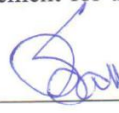
# Homi Bhabha National Institute

## Recommendations of the Viva Voce Committee

As members of the Viva Voce Committee, we certify that we have read the dissertation prepared by Ms. Megha Tyagi entitled "Development and characterization of silicide coating for Nb-1Zr-0.1C alloy" and recommend that it may be accepted as fulfilling the thesis requirement for the award of Degree of Doctor of Philosophy.

**Dr. (Smt.) S.B. Roy**

Chairman - Name & Signature with date

 9.5.19.

**Dr. R. Tewari**

Guide / Convener - Name & Signature with date

 9/5/19

**Dr. S. K. Ghosh**

Co-guide - Name & Signature with date

 9/5/19

**Prof. Rahul Mitra**

Examiner - Name & Signature with date

 9.5.19

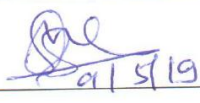
**Dr. G. Sugilal**

Member 1- Name & Signature with date

 9.5.19

**Dr. (Smt.) S. Mukhopadhyay**

Member 2- Name & Signature with date

 9/5/19

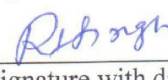
**Dr. Deep Prakash**

Member 3- Name & Signature with date

 09/05/2019

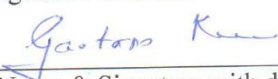
**Dr. R.N Singh**

Member 4- Name & Signature with date

 09.05.2019

**Dr. G.K. Dey**

Technology Adviser - Name & Signature with date

 9/5/2019

Final approval and acceptance of this thesis is contingent upon the candidate's submission of the final copies of the thesis to HBNI.

I/We hereby certify that I/we have read this thesis prepared under my/our direction and recommend that it may be accepted as fulfilling the thesis requirement.

Date: 09/5/19 

Place: HBNI,  
Mumbai

Signature  
Co-guide (if any)

  
Signature  
Guide

## STATEMENT BY AUTHOR

This dissertation has been submitted in partial fulfillment of requirements for an advanced degree at Homi Bhabha National Institute (HBNI) and is deposited in the Library to be made available to borrowers under rules of the HBNI.

Brief quotations from this dissertation are allowable without special permission, provided that accurate acknowledgement of source is made. Requests for permission for extended quotation from or reproduction of this manuscript in whole or in part may be granted by the Competent Authority of HBNI when in his or her judgment the proposed use of the material is in the interests of scholarship. In all other instances, however, permission must be obtained from the author.



Megha Tyagi

## DECLARATION

I, hereby declare that the investigation presented in the thesis has been carried out by me. The work is original and has not been submitted earlier as a whole or in part for a degree / diploma at this or any other Institution / University.



Megha Tyagi

## List of Publications

1. Megha Tyagi, B.Vishwanadh, S.K Ghosh, R. Tewari “A Study on Reaction Kinetics and Development of Silicide Coatings on the Nb-1Zr-0.1C Alloy by Molten Salt Technique” Royal Society of Chemistry Advances, 6 (2016) 99331-99338.
2. Megha Tyagi, B.Vishwanadh, S.K Ghosh, R. Tewari “Synthesis and characterization of silicide coating on niobium alloy produced using molten salt method” Materials Science Forum Vols. 830-831 (2015) 683-686 .
3. Megha Tyagi, S.K Ghosh, R. Tewari “High temperature behaviour of Niobium Silicide Coating on Nb-1Zr-0.1C Alloy” Surface Engineering (2019)  
doi:10.1080/02670844.2019.1622204

### **Paper & poster presented in Conferences**

1. Presented poster titled " Synthesis and characterization of silicide coating on niobium alloy produced using molten salt method" at ICAMPS 2015, Thiruvananthapuram.
2. Presented poster titled " Optimization of parameters for silicide coating on the Nb-1Zr-0.1C alloys" at EMSI 2015, Mumbai.
3. Presented paper titled "Oxidation Behaviour of Silicide Coatings Produced by Molten Salt Technique on the Nb-1Zr-0.1C Alloy" at TMS 2017, San Diego, USA.
4. Presented paper titled " Development and characterization of Molybdenum and silicide based coatings on Nb based structural materials for advanced high temperature reactor" at Smart Materials and Structures 2018, Vienna, Austria.

*Dedicated to  
my dear parents*

---

# Acknowledgments

---

It is with a feeling of great pleasure that I express my most sincere heartfelt gratitude to Dr. R. Tewari, my Ph.D. supervisor for his constructive suggestions and support during the progress of my work. I owe a depth of gratitude to Dr. S.K Ghosh, my co-supervisor for giving me good suggestions and encouraging me during the course of my tenure . I am greatly indebted to my supervisors for their guidance throughout the course of preparing this dissertation.

I would like to express my sincere thanks to all of my colleagues in Physical Metallurgy Section, Bhabha Atomic Research Centre, especially Mr. R. D. Hankare and Dr. Naveen Kumar N. for their help and support received in carrying out experiments. It would have been impossible to bring this work into this form without their effort. I am also thankful to Dr. Vishwanadh B., Mr. Nachiket Keskar, Dr. K. V. Mani Krishna , Dr. Suman Neogy and Mr. Vishal Singh for their valuable suggestions and help in analyzing the results.

I would also like to thank all the staff members of my department and for their invaluable help and guidance. A special thanks to my friends Mr. Lokesh Goel and Mr. Nilabja Sarkar for their constant support and encouragement. Lastly, I am thankful to my family members who have directly or indirectly provided a helping hand to reach the pinnacle of success.

**Megha Tyagi**

---

# Table of Contents

---

	Page no.
Synopsis	xi
List of Figures	xxii
List of Tables	xxiv
List of Abbreviations	xxvi
<b>Chapter 1 Introduction</b>	<b>1</b>
1.1 Background	1
1.2 Physical metallurgy of Nb based systems	5
1.2.1 Nb-Zr binary phase diagram	5
1.2.2 Nb-C binary phase diagram	6
1.2.3 Nb-O binary phase diagram	6
1.2.4 Nb-Si binary phase diagram	8
1.3 Objectives of study	9
1.4 Outline of thesis	10
<b>Chapter 2 Literature Survey</b>	<b>13</b>
2.1 Nb and Nb alloys	13
2.1.1 Nb-C alloys	15
2.1.2 Nb-1Zr alloys	19
2.1.3 Nb-1Zr-0.1C alloy	20
2.2 Oxidation behaviour of Nb	22
2.3 Oxidation barrier coatings	25
2.3.1 Pack cementation method	27

2.3.2	Molten salt method	29
2.4	Oxidation barrier coatings of Nb and Nb alloys	34
<b>Chapter 3</b>	<b>Experimental Methods</b>	<b>40</b>
3.1	Sample preparation and furnace fabrication	40
3.2.1	Sample preparation	40
3.2.2	Design of furnace	40
3.2	Silicide coating on Nb alloy by molten salt method	42
3.3	Oxidation and Annealing Experiments	44
3.4	Characterization techniques	45
3.4.1	Microstructural Investigations and Phase Identifications	45
3.2.4	Composition analysis	46
<b>Chapter 4</b>	<b>Optimization of Coating Parameters</b>	<b>49</b>
4.1	Optimization of Silicide Coating Process	49
4.1.1	Optimization of composition of salt	49
4.1.2	Effect of stirring	50
4.1.3	Optimization of time and temperature	51
4.2	Discussion	59
4.3	Summary	60
<b>Chapter 5</b>	<b>Mechanisms of molten salt coating process</b>	<b>63</b>
5.1	Microstructural characterization	64
5.2	Discussion	75
5.3	Summary	79
<b>Chapter 6</b>	<b>High temperature Behaviour of Silicide coating</b>	<b>82</b>
6.1	High temperature studies on the silicide coated samples	83
6.1.1	Microstructural characterization	84

6.2	Isothermal oxidation study	92
6.3	Discussion	94
6.4	Summary	100
<b>Chapter 7</b>	<b>Conclusion</b>	<b>102</b>
7.1	Optimization of coating parameters	102
7.2	Reaction Kinetics	103
7.3	High temperature behaviour of silicide coating	104
<b>Scope of Further Research</b>		
<b>References</b>		

## Synopsis

---

Niobium based alloys possess good high temperature strength, adequate ductility at low temperature, good nuclear properties and high liquid metal corrosion resistance which make them an attractive choice for high temperature structural material applications in nuclear and aerospace engineering fields [1-6]. Among various niobium alloys, Nb-1Zr-0.1C alloy has been identified for structural applications in compact high temperature reactors, because in addition to the aforementioned properties, the alloy shows good weldability, formability and suitable creep properties above 1000°C. One of the limitations of the Nb alloy is its poor oxidation resistance at and above 400°C. The poor oxidation resistance has been attributed to the formation of a non-protective oxide layer. One way of improving the oxidation resistance of the alloy is by adding suitable alloying elements. However, choices of alloying elements are rather limited as most of the elements, which enhance their oxidation resistance, reduce the melting temperatures of the alloy and thereby adversely affect the high temperature properties of the alloy [7]. Thus, the protective coating, another method of improving oxidation resistance of the alloy, becomes an essential requirement to protect the Nb alloy from oxidation at high temperatures. The approach of providing oxidation resistance by surface coating is advantageous as it does not alter the mechanical and thermal properties of the substrate. In this regard, silicide based coatings stands out among all other coatings, as these coatings have nearly same value of the coefficient of thermal expansion as of Nb alloys, which suffices the material property to undergo thermal cycling. Also, silicide coatings form an impervious oxidation resistant layer of oxides of Si which generally exhibits good self-healing characteristics [8]. These qualities make silicide coating an attractive choice for the surface protection of the Nb alloys.

There are many methods for providing silicide coating on the Nb alloys. For example, chemical vapour deposition, physical vapour deposition techniques, sputtering based technique etc., to name a few. Among these various techniques, due to its simplicity in construction and ease of operation, molten salt technique, a diffusion coating formation process, is widely used to deposit oxidation-resistant coatings on various refractory metals alloys including Nb-based alloys [9]. The advantages offered by molten salt technique, such as, low temperature operation and shorter processing time than other coating methods [10-12], make it a promising technique having wider applications. Therefore, in the present study molten salt technique has been used to provide silicide coating on the Nb-1Zr-0.1C alloy. In most of the cases, molten bath, consisting NaCl- KCl as supporting salt, having composition close to the eutectic composition (50:50) has been used [13]; though use of other molten salts for applications other than coating are reported in the literature [14,15].

In the present study, the main aim is to develop silicide based coating on the Nb-1 Zr-0.1 C alloy to improve its oxidation behaviour at high temperatures. For this purpose, a systematic study has been carried out to optimize the coating parameters in terms of time and temperature to obtain uniform and homogenous coating. Using the optimized parameters, experiments were carried out to deduce the reactions governing the system. Finally, high temperature behaviour of the developed silicide coating for different time and temperatures was studied. Based on this study, a plausible mechanism governing the system at high temperatures has been proposed.

This thesis has been divided into seven chapters. A brief introduction about Nb based alloys, phase diagrams and their applications are given in the chapter 1. Chapter 2 deals with the literature review on the development of different coating methodologies which have been used to provide coating on Nb based alloys. The details of the experimental methods employed in the

present study are given in Chapter 3. Chapters 4, 5 and 6 present a detailed description of the obtained experimental results and their discussions. In chapter 7 all the results of the present study are summarized. A Summary of each chapter pertaining to experimental results has been given in the following sections:

#### **Chapter 4: Optimization of parameters to develop silicide coating**

This chapter deals with the optimization of several variables including, composition of salt, time and temperature to develop a uniform silicide coating on the Nb alloy. A eutectic salt mixture comprising NaCl, KCl, NaF and two Si sources-  $\text{Na}_2\text{SiF}_6$  and Si powder was selected to carry out studies on the development of silicide coating on Nb alloys. In order to obtain the optimized temperature and time window, coating experiments were carried out at different temperatures. As the eutectic temperature of the salt mixture is ( $\sim 750^\circ\text{C}$ ), all the temperature selected for the experiments were kept above this temperature. Upon exceeding temperature of the bath above  $1000^\circ\text{C}$ , extremely poor quality coatings were observed and therefore the most suitable temperatures where coating could be successfully developed were identified as  $800^\circ\text{C}$  and  $900^\circ\text{C}$ . By changing the duration of coating at these temperatures further optimization was carried out. In order to facilitate the process of coating, stirring of the bath at different rates was also carried out; which did not show promising results and therefore it was not pursued further. Similarly, concentration of Si containing constituents were also varied and optimum composition of the salt was worked out. Several experiments of adding of pure silicon intermittently during the coating experiments were also carried to achieve the optimum thickness of the coatings. In order to estimate the thickness and variation in the thickness of the coating, at different temperature and time periods, cross sections of the Si-coated samples were characterized using optical, SEM and XRD techniques.

The surface morphologies of the samples dipped at 800 °C for 2 and 4 h showed the presence of a smooth coating whereas samples which dipped for 6 h showed granular appearance with the formation of pits on the surface. The sizes of pits increased with increasing temperature and time. To study the thickness of the coating, cross section of the samples were observed under SEM. For the samples coated at 800°C, an increase in the coating thickness from 8 μm to 12 μm was noticed with increase in the dip time from 2 h to 4 h (Fig.1). However, further increase in the immersion time from 4 h to 6 h, a decrease in the coating thickness from 12 to 5 μm was observed. Reduction in the coating thickness was also observed with an increase in temperature from 800°C and 900°C. The composition profile across the coating thickness in all the coated samples showed that the silicide phase mainly comprised the NbSi<sub>2</sub> phase.

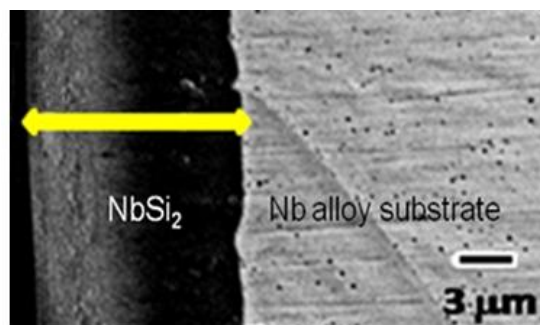


Figure-1 SEM micrograph of cross sectional view of Nb-Si coating produced by molten salt method at 800°C and 4 h.

The XRD patterns of all the samples also showed the appearance of NbSi<sub>2</sub> reflections in all the patterns confirming the EDX results. These coating were of single phase which compositionally and by XRD analysis was identified as the hexagonal NbSi<sub>2</sub> phase.

These parametric experiments have shown that the optimum time and temperature to produce maximum thickness (~12 μm) of continuous uniformly thick silicide coating onto the Nb alloy was 4 h at 800 °C. Stirring did not help in improving the thickness but compromised the uniformity of the coatings. Addition of metallic-Si intermittently also did not yield any positive

results. Based on increasing pits upon increasing time or temperature, it was inferred that etching of silicide phase was taking place, which could be attributed to the buildup of F<sup>-</sup> ions with increasing time and temperature. This could also be one possible reason resulting in the reduction of the coating thickness.

## **Chapter 5: Reaction kinetics**

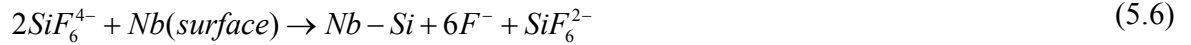
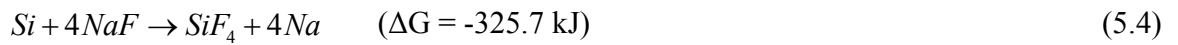
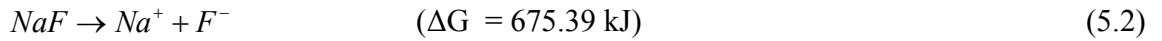
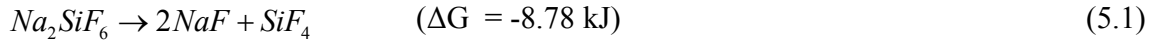
This chapter deals with the details of the studies carried out in determining the role of various species of Si sources and in understanding the underlying mechanism of silicide coating. By varying concentrations of Na<sub>2</sub>SiF<sub>6</sub> and Si, three salts (S1, S2, S3) were produced to develop coatings on samples at 800°C. Post experiments, apart from investigating the coated samples, these salts were also examined by X-ray Photoelectron spectroscopy (XPS) technique to determine various states of silicon (Si<sup>0</sup>, Si<sup>+2</sup> and Si<sup>+4</sup>) present in the salts as well as using ion chromatography concentrations of F<sup>-</sup>, Si ion and the etched Nb were determined .

Surface morphologies of the samples, which were dipped in S1 salt, containing only Na<sub>2</sub>SiF<sub>6</sub>, showed the formation of large number of pits on the surface whereas the samples dipped in salt S2, containing only metallic Si, and salt S3, containing both Si and Na<sub>2</sub>SiF<sub>6</sub>, showed the presence of relatively smooth coating surfaces. In the case of samples dipped in salts S2, isolated pits were observed whereas for the samples dipped in salt S3, the size of the pits as well as their number density was considerably low. Cross-sections of the samples revealed no coating on the samples dipped in salt S1 and maximum thickness of the coatings on the samples, which were dipped into the salt S3. EDS and XRD data analyses revealed presence of the NbSi<sub>2</sub> as the major phase on the surfaces of the samples dipped in salt S2 and S3; but presence of

metallic- Nb as the major phase on the surface of the samples dipped in S1 confirmed no silicide coating on the sample.

Ion chromatographic analysis showed that the concentration of fluoride ions and etched Nb was highest in salt S1 whereas least concentration of etched Nb was observed in salt S3. The presence of etched Nb in all the three salts thereby confirmed the etching effect of F<sup>-</sup> ions. XPS analysis showed that Si in the salt S1 was present in the Si<sup>4+</sup> state only whereas the presence of Si<sup>4+</sup>, Si<sup>2+</sup>, Si<sup>0</sup> ions was observed in the salts S2 and S3.

Based on the microstructural and chemical data analysis of samples and salts, following possible reactions were examined in details



Based on microstructural, chemical, thermodynamic analyses and on the basis the presence of Si in different electronic states in different salts, entire set of equations were analysed and equations for each salts were identified. It was established that the occurrence of a disproportionation reaction in the molten salt producing metastable species, SiF<sub>6</sub><sup>4-</sup> is a prerequisite for producing the layer of silicide coating on the alloy. By comprehending these observations, a mechanism of silicide coating, which is schematically shown in Figure 2, has been proposed.

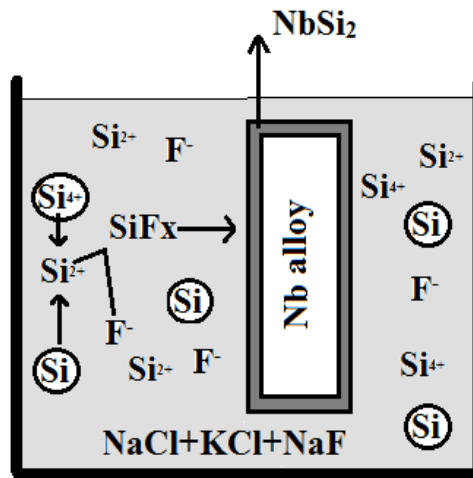


Figure-2 Schematic representation of formation and deposition of  $\text{Si}^{2+}$  ions in molten salt for silicide coating on Nb alloy substrate. In the figure it has been shown that  $\text{SiF}_x$  species decomposes on the surface of the Nb alloy where  $\text{F}^-$  goes back into the solution and Si ion get deposited on the surface [16].

## Chapter 6: High temperature behaviour of silicide coating

This chapter is focussed on the high temperature behaviour of the silicide coated samples. For this purpose, isothermal oxidation experiments as well as heat treatment at various times ranging from 1-10 h and temperatures ranging from 1000-1400 °C were carried out. Silicide coated samples when subjected to isothermal oxidation at 1000 °C or above, they disintegrated into the powder exhibiting poor oxidation resistance of the silicide phase. XRD analyses of the powders showed that the major oxide phase was  $\text{Nb}_2\text{O}_5$  and the  $\text{SiO}_2$  phase was nearly absent in the samples. Cross sectional views of the samples heat treated at various temperatures, on the other hand, showed the formation of two distinct layers, i.e, porous layer (layer 1) and a non-porous layer (layer 2) (Fig.3). EDS analysis showed that the stoichiometry of both the layers matched with  $\text{Nb}_5\text{Si}_3$ . By detailed EDS analysis it has also been established that for the formation of the  $\text{Nb}_5\text{Si}_3$  phase, both, inward diffusion of Si from the  $\text{NbSi}_2$  layer and outward diffusion of Nb from the bulk matrix have occurred during the heat treatment. Based on the concentrations

variation of elements formation of the  $Nb_5Si_3$  phase towards the matrix and presence of the unreacted  $NbSi_2$  phase at the outermost layer was rationalised. It was also established that due to paucity of time Nb could not diffuse across the entire length during this heat treatment (Fig.3).

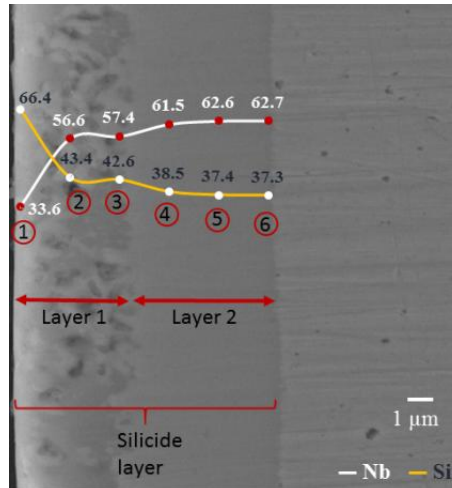
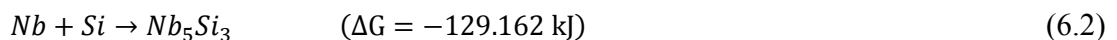
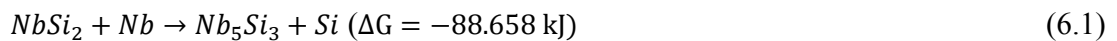


Figure- 3 SEM Micrograph of cross section samples after heat treatment at 1200°C-2h.

This observation was further confirmed by increasing temperature and time of heat treatment, where higher Nb concentration in porous layer was observed. Also, increase in the thickness of non porous layer and stagnancy in porous layer was observed, which could be attributed to nearly complete consumption of  $NbSi_2$ . In order to rationalize the microstructural observations and formation of phases after various heat treatments, mechanism of formation of various silicide phases and pores in the  $NbSi_2$  layer, in form of the following equation was proposed:



Considering microstructural evidences and thermochemical feasibility of the proposed equations, it was established that initially the reaction proceeds according to the equation 6.1 and after the complete consumption of  $NbSi_2$  phase, equation 6.2 becomes the dominant mechanism

for the formation of  $\text{Nb}_5\text{Si}_3$  and thus increase in the thickness is observed only in the non-porous layer.

In addition, attempts of re-coating the samples after the post heat treatment to improve the oxidation resistance behaviour did not yield any fruitful results. Therefore, this study has shown that the single layer of  $\text{NbSi}_2$  on the Nb alloy could not prevent oxidation of the material. Based on microstructural and thermodynamic analyses, a plausible mechanism explaining the formation of various phases at high temperatures has been proposed.

### **Conclusions**

The important conclusions drawn from the present study are as follows:

- (i) Based on the optimization of parameters studies, composition of salt, time and temperature parameters to develop maximum thickness of uniform and homogenous coating has been established. It was shown that the optimum time of 4 h and temperature of  $800^\circ\text{C}$  is required to produce uniform silicide coating of maximum thickness of  $\sim 12\ \mu\text{m}$  onto Nb-1Zr-0.1C alloy using molten salt technique.
- (ii) Reaction kinetics studies revealed the role of each Si species produced by subsequent reactions in the salt. It has been found that the presence of both the Si sources-  $\text{Na}_2\text{SiF}_6$  and Si powder was important to produce uniform and homogenous coating. Detailed analysis of reaction mechanism has shown presence of active species  $\text{SiF}_4$  is essential for the formation of the silicide coatings.
- (iii) High temperature behaviour studies of the silicide coated samples have shown that at high temperature, single layer of  $\text{NbSi}_2$  gets transformed into two-layer system with the major phase as  $\text{Nb}_5\text{Si}_3$ . Isothermal oxidation studies revealed that the single layer of  $\text{NbSi}_2$

developed using molten salt technique could not provide sufficient oxidation resistance to Nb-1Zr-0.1C alloy.

## References

- [1] B.P. Bewlay, M.R. Jackson, P.R. Subramanian, J.-C. Zhao, *Metall. Mater. Trans. A.* 34 (2003) 2043-2052.
- [2] J.R. Stephens, D.W. Petrasek, R.H. Titran, *Refractory Metal Alloys and Composites for Space Power System*, Report number NASA TM-100946 (1988).
- [3] J.H. Westbrook, R.L. Fleischer, eds., *Intermetallic Compounds - Principles and Practice*, John Wiley & Sons, Ltd, Chichester, UK, 2002.
- [4] P. Subramanian, M. Mendiratta, D. Dimiduk, M. Stucke, *Mater. Sci. Eng. A.* 239 (1997) 1-13.
- [5] B.P. Bewlay, J.J. Lewandowski, M.R. Jackson, *JOM.* 49 (1997) 44-46.
- [6] B.P. Bewlay, M.R. Jackson, P.R. Subramanian, *JOM.* 51 (1999) 32-36.
- [7] R.A. Perkins, K.T. Chiang, G.H. Meier, R.A. Miller, *Effect of alloying, rapid solidification, and surface kinetics on the high temperature environmental resistance of niobium*, Report number AFSOR TR. 89-0909 (1989).
- [8] K. S. Chan, *Oxid. Met.* 61 (2004) 165-194.
- [9] A. J. Gay, J. Quakernaat, *J. Less Common Met.* 40 (1975) 21 -28.
- [10] J. K. Yoon, G. H. Kim, J. H. Han, I. J. Shon, J. M. Doh , K. T. Hong, *Intermetallics* 13 (2005) 1146-1156.
- [11] M. Li, L. Song, J. Le, X. Zhang, B. Pei , X. Hu, *Mater. Trans.* 45 (2004) 2785-2787.
- [12] S. Majumdar, P. Sengupta, G. B. Kale , I. G. Sharma, *Surf. Coat. Technol.* 200 (2006) 3713-3718.
- [13] R.O. Suzuki, T. Nishibata, K. Nakanishi, M. Ishikawa, K. Ono, *Mater Technol.* 71 (2000) 130-137.

- [14] R. Serrano-López, J. Fradera, S. Cuesta-López, *Chem. Eng. Process* 73(2013) 87-102.
- [15] Brajendra Mishra, David L. Olson, *J. Phys. Chem. Solids* 66 (2005) 396-401.
- [16] R.O. Suzuki, M. Ishikawa, K. Ono, *J. Alloys Compd.* 336 (2002) 280–85.

---

## List of figures

---

1.1	Nb-Zr binary alloy equilibrium phase diagram [13]	7
1.2	Nb-C binary alloy equilibrium phase diagram [13]	7
1.3	Nb-O binary alloy equilibrium phase diagram [13]	8
1.4	Nb-Si binary alloy equilibrium phase diagram [13]	9
2.1	Comparison of (a) DBTT and (b) density for various refractory metals [15]	14
2.2	Stress vs. Temperature Comparison for different alloy systems [5]	22
2.3	Formation of various Nb-oxide phases with increase in Oxygen% [33]	23
2.4	Schematic representation of pack cementation technique [55]	28
2.5	Schematic representation of formation and deposition of Si ions in molten salt for silicide coating on metallic substrate ( eg.- Nb)	30
2.6	Schematic representation of silicide layer formation mechanism in group A and B metals [62]	33
3.1	Schematic representation of the experimental setup	43
4.1	SEM micrographs of cross sectional view of Nb-Si coating produced by molten salt method with continuous stirred bath	51
4.2	Optical images showing surface morphology of Si coated Nb alloy samples for dip time of (a) bare Nb alloy, (b) 2 h, (c) 4h; (d) 6 h (800 °C), (e) 2h and (f) 6 h (900 °C), location of the pits are marked in the figure	54
4.3	SEM micrographs of cross sectional view of Nb-Si coating produced by molten salt method at different time periods (a) 2 h, (b) 4 h, (c) 6 h (800 °C), (d) 2 h and (e) 6 h (900 °C)	56
4.4	Composition profiles of Si coated samples by EDS at (a) 2 h, (b) 4 h, (c) 6 h (800	58

	°C) and (d) 2 h (900 °C).	
4.5	XRD patterns showing formation of different Nb-Si phases at 800 °C and 900°C	58
5.1	Optical images showing surface morphology of Si coated Nb alloy produced when samples were dipped into (a) bare Nb alloy, (b) S1 and (c) S2 (d) S3; location of the pits are marked in the figure.	66
5.2	SEM micrographs of cross sectional view of Nb-Si coating produced when samples were dipped into salt (a) S1, (b) S2 and (c) S3	67
5.3	Composition profiles of Si coated samples by EDS dipped in salt (a) S2 and (b) S3	68
5.4	XRD patterns showing formation of NbSi <sub>2</sub> phase formed when samples were dipped into salt (a) S1, (b) S2 and (c) S3	69
5.5	Si-2p XPS spectra of the molten salt bath (a) S1, (b) S2 (c) S3	71
5.6	De-convoluted Figures for the Si-2p XPS spectra of the different Samples	73
5.7	F-1s XPS spectra of the molten salt bath (a) S1, (b) S2 and (c) S3	74
6.1	SEM Micrographs of cross section samples after heat treatment at (a) 1200°C- 2h (b)1200°C- 4h, (c)1350°C- 6h, (d)1350°C- 10h, (e)1400°C- 10h, *Layer 1- porous ; Layer 2 – non-porous layer. The points marked show the region from where composition of the silicide layer was identified which is listed in Table 6.2	88
6.2	SEM Micrograph of cross section sample after re-coating post heat treatment. Three distinct layers of silicides could be observed in the image. The points marked show the region from where composition of the silicide layer was identified which is listed in Table 6.3	89
6.3	Plot of fractional frequency Vs pore size for the samples heat treated at (a)1200 °C- 4h, (b)1350 °C- 6 h (c) 1350 °C- 10 h	92
6.4	Isothermal oxidation behaviour of (a) Set-1 (as-coated), (b) Set-2 (heat treated) and (c) Set-3 (re-coated post treatment) samples.	93
6.5	XRD patterns of powder of the samples oxidized at 1000 °C for 1 hr showing formation of Nb <sub>2</sub> O <sub>5</sub> .	94
6.6	Schematic representation of proposed reaction mechanisms.	96

---

## List of Tables

---

1.1	Properties of Bcc Refractory Metals	2
1.2	Composition and applications of refractory metal alloys	3
2.1	Effect of various alloying elements in Nb [22]	17
2.2	Mechanical properties of Nb-1Zr alloy at different temperatures [16]	19
2.3	Comparison of maximum operating temperature for nominal corrosion different alloys	22
2.4	Comparison of various coating methods	26
2.5	Stable silicide phases in binary system of M- Si	31
2.6	Comparisons of the salt compositions used to develop coating using molten salt technique	35
3.1	Typical chemical composition of the Nb-1Zr-0.1C alloy	40
3.2	Composition of molten salts used in the study	43
3.3	Time and temperature considered for heat treatment	45
3.4	Crystallographic information of the various kinds of crystal structures present in the Nb-O and Nb-Si phases	46
5.1	Composition of molten salts used in the study	63
5.2	Volume percentage of phases present in samples dipped in various salts estimated by Rietveld analysis	70
5.3	Nb and F <sup>-</sup> ion concentration in various molten salts estimated by ion chromatography	70
5.4	Summary of the thickness of the coating phases present and weight gain in various salts	75
5.5	Post experiment salt analysis of salt S1,S2 and S3	77

6.1	Time and temperature considered for heat treatment	83
6.2	Chemical Composition Determined by EDS at the Positions Marked on the SEM micrographs Fig. 3(a) and 3(c)	88
6.3	Chemical Composition Determined by EDS at the Positions Marked on the SEM micrographs (Fig. 6.3)	89
6.4	Pore size data analysis	90
6.5	Effect of temperature and time on silicide coated samples	97

---

## List of Abbreviations

---

BRM	Bcc Refractory Metals
CHTR	Compact High Temperature Reactors
CTE	Coefficient of Thermal Expansion
CVD	Chemical Vapour Deposition
DBTT	Ductile To Brittle Transition Temperature
EDS	Energy Dispersive X-Ray
FE-SEM	Field Emission-Scanning Electron Microscope
FWHM	Full Width half Maximum
JCPDS	Joint Committee on Powder Diffraction Standards
LPPS	Low Pressure Plasma Spray
NFC	Nuclear Fuel Complex
PVD	Physical Vapor Deposition
SEM	Scanning Electron Microscope
SPS	Spark Plasma Sintering
XPS	X-Ray Photoelectron Spectroscopy
XRD	X-Ray Diffraction

# **Introduction**

---

## **1.1 Background**

In 1960, attention of material experts was drawn towards the refractory metal base structural materials for aerospace applications [1]. These applications, apart from ability to perform at high temperature conditions, demand low density, high melting point and adequate strength at the operating temperatures to bring down the launch weight. High ductility at low temperatures and high solubility for interstitial were additional requirements added from the workability viewpoint. Metals, such as niobium (Nb), molybdenum (Mo), tungsten (W), rhenium (Re), tantalum (Ta), etc., are designated as refractory metals owing to their metallurgical properties, such as high melting temperature ( $T > 2000\text{ }^{\circ}\text{C}$ ). Nb, Ta, Mo, W possess same crystallographic structure as body centered cubic whereas Re has hexagonal closed packed structure. In general, by extending the definition, W, Ta, Mo Nb and V have been named as bcc refractory metals (BRM) and Re, Pt, Os, Ir and Rh form another class of refractory metals. Table 1.1 lists some of the properties of BRM.

BRM found several usages in the nuclear energy applications, in electronic industry, aerospace applications and chemical industry to name a few. Nb and Mo as alloying elements are used in steel industry. Due to their excellent performance in the environment with respect to temperature, corrosion and stress, BRMs and their alloys are considered as promising structural material in aerospace and nuclear fields [2–7]. Few of the commonly used refractory metal alloys compositions and their applications are presented in Table 1.2. In general, use of iron-nickel and nickel cobalt alloys is limited up to the temperature range of 700-1000  $^{\circ}\text{C}$  [8]. Beyond this temperature range these alloys lose their high temperature strength and become non-usable. The structural ceramics, which can provide sufficient

strength, are not very attractive choice due to their high ductile to brittle transition temperature, which is well above the room temperature in most of the cases. In addition, propensity for thermal shock cracking is high in the ceramic based materials. Therefore, for high temperature applications ( $T \sim 1500$  °C), refractory metal alloys are the most suitable candidate for structural purposes.

**Table 1.1** *Properties of Bcc Refractory Metals.*

<b>Property</b>	<b>Niobium</b>	<b>Tantalum</b>	<b>Molybdenum</b>	<b>Tungsten</b>	<b>Vanadium</b>
<b>Density g/cc</b>	8.6	16.6	10.2	19.3	6.0
<b>Melting Point, K</b>	2711	3269	2883	3683	2183
<b>Tensile strength,(GPa) at 1273K</b>	0.04–0.1	0.1	0.1–0.2	0.3–0.5	0.007
<b>Young’s Modulus, (GPa) at 1273K</b>	110	170	280	365	98

BRM based alloys exhibit good creep strength and compatibility with liquid alkali as long as impurities, such as oxygen, nitrogen and carbon, are within the limit of few ppm. BRM based alloys have good formability and can be formed into any shape. As they do not undergo any allotropic phase transformation, design of heat treatments and thermo-mechanical processing is relatively easy. The major drawback of the refractory metal alloys, however, is their poor oxidation resistance at high temperatures [9]. Refractory metal alloys, on the basis of the oxidation behaviour at high temperatures, could be categorised into two groups. The first group consists of Nb and Ta. These metals have very high oxygen solubility that results in internal oxidation at low oxygen pressure also. The second group comprises of Mo and W. These metals have relatively low oxygen solubility and form volatile oxides under oxidizing environment. Out of all the refractory metals, Nb and Mo, stand out as most suitable candidate materials for structural applications owing to design consideration of density. The significant degradation caused by volatile oxide,  $\text{MoO}_3$ , limits Mo application in the nuclear field. On the other hand, oxides of Nb are not volatile and generally form complex oxides in the presence of other alloying elements (e.g., Ti). In addition, because of

their superior corrosion resistance against liquid Pb and its alloys and easy fabricability, Nb and its alloys have been considered as structural material for nuclear applications.

**Table 1.2** *Composition and applications of refractory metal alloys*

<b>Alloy</b>	<b>Nominal Composition (wt.%)</b>	<b>Applications</b>
<b>C-103</b> <b>Nb-1Zr</b> <b>PWC-11</b> <b>WC-3009</b> <b>FS-85</b>	Nb-10Hf-1Ti Nb-1Zr Nb-1Zr-0.1C Nb-30Hf-9W Nb-28Ta-10W-1Zr	Thrust chambers & radiation skirts for rocket and aircraft engines, piping for liquid alkali metal containment, sodium vapour lamp electrodes. Liquid metal container and piping.
<b>Ta-2.5W</b> <b>Ta-10W</b> <b>T-111</b>	Ta-2.5W Ta-10W Ta-8W-2Hf	Heat exchangers, linings for towers, valves and tubings. Hot gas valves, rocket engine skirts, corrosion resistant valves in the chemical industry
<b>Mo-TZM</b>  <b>TZC</b> <b>Mo-30W</b> <b>MHC</b>	Mo-(0.5-0.8)Ti-(0.1-0.2)Zr-(0.013-0.02)C Mo-1Ti-0.3Zr-0.03C Mo-30W Mo-1.5Hf-0.05C	Tooling materials in the isothermal forging of superalloys, structural materials for HTR, container material for molten zinc.
<b>W-3Re</b> <b>W-5Re</b> <b>W-25Re</b>	W-3Re W-5Re W-25Re	High temperature thermo-couples, Heaters etc.

Among the various nuclear reactors, compact high temperature reactors (CHTR) are envisaged to operate at temperatures in the vicinity of 1000 °C for several years in unmanned conditions. For such high temperatures of operation with liquid Pb-Bi as coolant, the most suited alloys for structural applications are Nb or Mo based alloys. Mo based dilute alloy like TZM or TZC, have been studied in details [8]. As, in most of the cases, these alloys are fabricated through powder metallurgy route, they suffer from structural integrity related issues. The contamination of oxygen led to the loss of room temperature ductility. In addition to Mo base alloys, dilute Nb alloys, Nb-1Zr, PWC-11, PWC-13 have also been examined for several applications. Among BRMs, niobium has the lowest density (8.4 g/cc), exhibits highest low temperature ductility (20 at.% -173 °C) and highest solubility of interstitial

elements, and least sensitivity in ductility with interstitial content. In view of such attractive properties, it is not surprising that niobium was the first refractory metal selected on prospective basis for the structural material for high temperature applications.

Initial efforts for the development of the material were directed towards obtaining high temperature strength without compromising its ductility and protection against oxidation at elevated temperatures exceeding 1000 °C. As a result, first few alloys of niobium developed could be divided into three broad groups [10]; low ( alloying element% < 5%) , medium ( alloying element% ~5%- 15%) and high alloy groups ( alloying element% > 15%) [11]. Most of these alloys find applications in the temperature range from 1000-1200 °C for a long-term operation whereas for short time working temperature range was 1200-1700 °C. These alloys possess a combination of beneficial properties such as high temperature strength, liquid metal corrosion resistance, irradiation damage resistance, low neutron absorption and good metallurgical processing properties. As a result, these alloys are the most promising for the use in nuclear reactors and accelerator driven systems (ADS). By virtue of these properties various niobium based alloys (Nb-1Zr, PWC- 11 and C-103) have been considered as potential materials for high temperature nuclear as well as space applications[10]. These alloys are most suitable structural materials in the temperature range between 900 and 1200 °C. Among various Nb alloys, the Nb-1Zr based alloys have been proposed for various high temperature applications, as these alloys exhibit high resistance to liquid alkali metal corrosion and remain single phase from room temperature to the melting point in addition to aforementioned properties. Carbon addition in the Nb-1Zr alloy improves its high temperature strength and increases creep-resistance to provide additional design and safety margins through the formation of the primary carbide phase. An earlier studies on Nb-Zr-C alloy [12] shows that the Nb-1Zr-0.06C alloy has excellent microstructural stability at temperatures of interest with or without applied load. The total creep strain in the sample of

this alloy was less than 0.1% after 4 years (35,000 hours) at 1077 °C under a stress of 10 MPa. With further addition of carbon the strength in the material was gained at the cost of reduction in ductility and poor fracture strength and the composition of the alloy system was optimized to Nb-1Zr-0.1C. The Nb-1Zr-0.1C alloys meet all the properties from the high temperature strength view point. It also shows excellent corrosion resistance against liquid metal corrosion, but the oxidation of the alloys are extremely poor. The presence of carbon in the alloy makes the oxidation properties of the alloy even inferior to the Nb-1Zr alloy. Therefore, the use of Nb-1Zr-0.1C alloy is restricted either to inert atmosphere or in the conditions where suitable environmental barrier coatings are provided.

In the present study, environmental barrier coating for the potential application of Nb-1Zr-0.1C as the structural material for compact high temperature nuclear reactor has been studied. It is, therefore, pertinent to discuss details about the physical metallurgy of the Nb-Zr-C alloys.

## **1.2 Physical metallurgy of Nb based systems**

In the present research work, suitable coatings on Nb-1Zr-0.1C alloy have been investigated in detail. It is, therefore, pertinent to examine the relevant phase diagram and different phases present in various systems (Nb-Zr, Nb-C, Nb-O and Nb-Si). Figs.1.1 and 1.2 show the equilibrium binary alloy phase diagrams of Nb-Zr and Nb-C systems, respectively [13]

### 1.2.1 Nb-Zr binary phase diagram

The binary Nb-Zr equilibrium phase diagram (Fig. 1.1) shows existence of three equilibrium solid solution phases:  $\alpha$ -Zr,  $\beta$ -Zr and  $\beta$ -Nb.  $\beta$ -Zr,  $\beta$ -Nb have bcc crystal structures and the  $\alpha$ -Zr has hcp structure. Pure Zr and pure Nb melt at 1855 °C and 2469 °C, respectively. The phase diagram shows that pure Nb consists of single phase  $\beta$ -Nb and it exists up to the melting point.

In contrast, pure Zr shows allotropic transformation, liquid phase transforms to  $\beta$ -Zr at 1855 °C and it exists in the temperature range of 1855 to 863 °C. At 863 °C,  $\beta$ -Zr transforms to  $\alpha$ -Zr. At 620 °C, the binary phase diagram of Zr-Nb shows monotectoid reaction where high temperature  $\beta$ -Zr transforms to  $\alpha$ -Zr and  $\beta$ -Nb. The solid solubility of Nb in  $\alpha$ -Zr is 0.6 wt.% at monotectoid reaction temperature. Considering the alloy composition in the present study, i.e., Nb-1Zr, according to the Nb-Zr binary equilibrium phase diagram shows that the alloy will have a single  $\beta$ -Nb phase from room temperature to its melting temperature.

### 1.2.2 Nb-C binary phase diagram

Fig. 1.2 shows the equilibrium Nb-C binary phase diagram. It shows the existence of  $\text{Nb}_2\text{C}$ , NbC and  $\text{Nb}_6\text{C}_5$  carbide phases. According to equilibrium Nb-C binary phase diagram, the Nb-0.1C alloy will have  $\beta$ -Nb and disordered hexagonal  $\text{Nb}_2\text{C}$  phases below melting temperature to 2500 °C. Below 2500 °C to 1200 °C temperature, the alloy will have  $\beta$ -Nb and ordered hexagonal  $\text{Nb}_2\text{C}$  phases [14]. Below 1200 °C to room temperature, the alloy will have  $\beta$ -Nb and orthorhombic  $\text{Nb}_2\text{C}$  phases. Considering both Nb-Zr and Nb-C binary alloy phase diagrams, at room temperature the alloy Nb-1Zr-0.1C should have  $\text{Nb}_2\text{C}$  carbide precipitates in the  $\beta$ -Nb matrix.

### 1.2.3 Nb-O binary phase diagram

Fig. 1.3 shows the equilibrium Nb-O binary phase diagram. It shows the existence of mono, di and penta-oxides of Nb. The oxides of Nb; NbO,  $\text{NbO}_2$  and  $\text{Nb}_2\text{O}_5$  have ordered defective rock salt structure, rutile and polymorph structure respectively. The solubility of oxygen in niobium varies from 0.25 wt.% at 500 °C to 0.72 wt.% at the eutectic temperatures. Two eutectics are observed in the phase diagram at composition 10.5 and 21 wt.% O. The temperature of eutectic reactions,  $L \rightarrow \text{Nb} + \text{NbO}$  and  $L \rightarrow \text{NbO} + \text{NbO}_2$  is found out be 1915 °C and 1810 °C, respectively. The congruent melting temperature of  $\text{NbO}_2$  is established as

1915 °C and 1945 °C for NbO. A peritectic reaction between NbO<sub>2</sub> and Nb<sub>2</sub>O<sub>5</sub> occurs at 1510 °C.

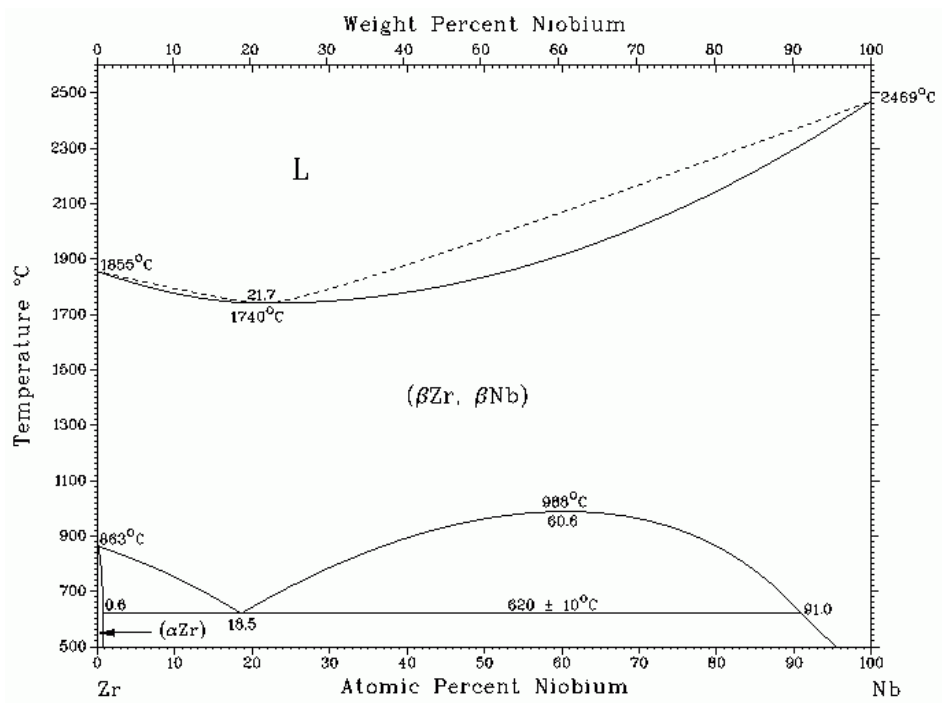


Figure 1.1: Nb-Zr binary alloy equilibrium phase diagram [13].

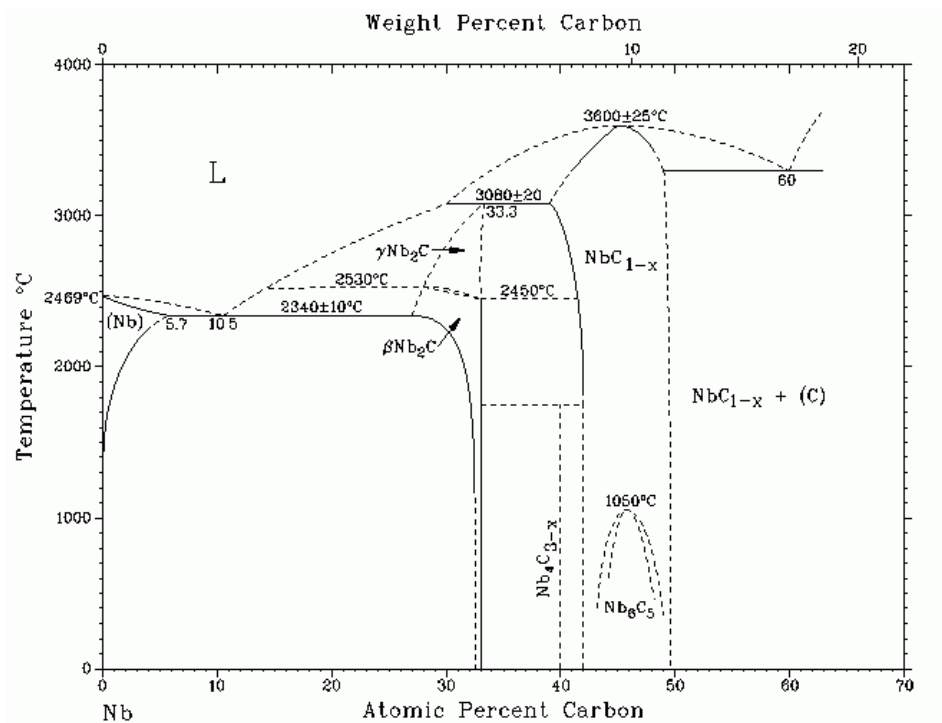
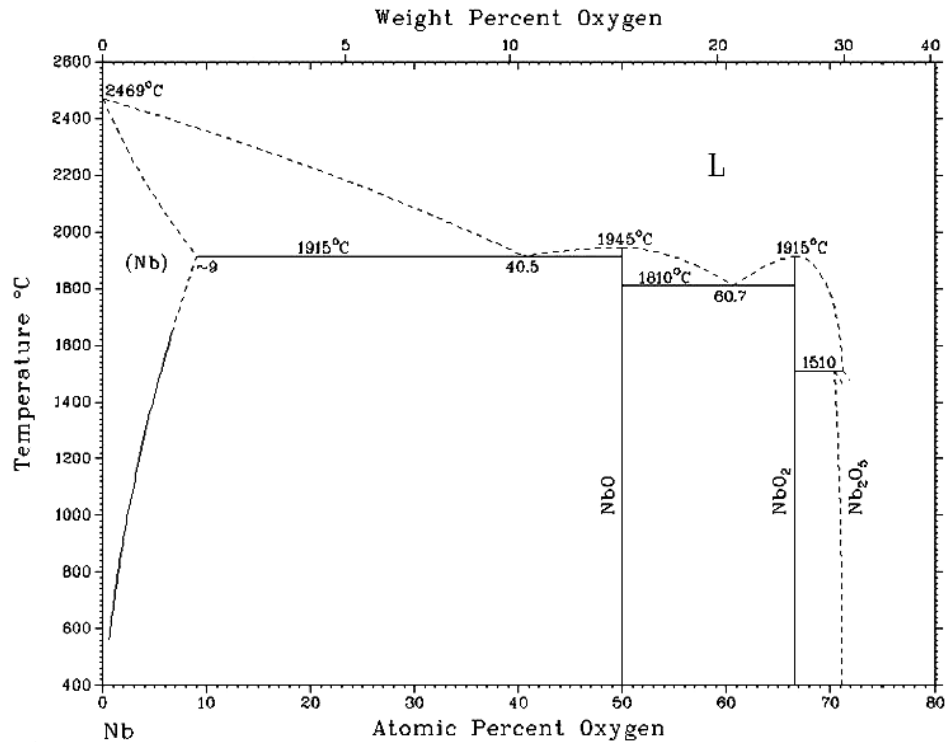


Figure 1.2: Nb-C binary alloy equilibrium phase diagram [13].



**Figure 1.3:** Nb-O binary alloy equilibrium phase diagram [13].

#### 1.2.4 Nb-Si binary phase diagram

The binary Nb-Si phase diagram exhibits seven stable phases 1) liquid, L, (2) bcc W-type terminal solid solution, Nb, (3) tetragonal Ti<sub>3</sub>P-type, Nb<sub>3</sub>Si, (4) tetragonal W<sub>5</sub>Si<sub>3</sub>-type  $\beta$ -Nb<sub>5</sub>Si<sub>3</sub>, (5) tetragonal Cr<sub>5</sub>Si<sub>3</sub>-type  $\alpha$ -Nb<sub>5</sub>Si<sub>3</sub>, (6) hexagonal CrSi<sub>2</sub>-type, NbSi<sub>2</sub> and (7) the diamond cubic terminal solid solution, Si.

Pure Nb and pure Si melts at 2469 °C and 1414 °C respectively. A wide two-phase field between the terminal Nb-Si solid solution and the intermetallic Nb<sub>5</sub>Si<sub>3</sub> which is bounded by the eutectoid isotherm at 1770 °C. The Nb<sub>5</sub>Si<sub>3</sub> phase shows no change in Si solubility with temperature and the terminal Nb phase shows only a small change in Si solubility at temperatures above 1200 °C. The phase diagram shows the existence of a high-temperature  $\beta$  phase which is a line compound having a stoichiometric composition of Nb<sub>3</sub>Si and the  $\beta$  to Nb + Nb<sub>5</sub>Si<sub>3</sub> eutectoid transformation at ~1770 °C. The congruent melting temperature of Nb<sub>5</sub>Si<sub>3</sub> and NbSi<sub>2</sub> is established as 2520 °C and 1940 °C, respectively. The temperature of

eutectic reactions,  $L \rightarrow \beta\text{-Nb}_5\text{Si}_3 + \text{NbSi}_2$  and  $L \rightarrow \text{NbSi}_2 + \text{Si}$  is found out to be 1900 °C and 1400 °C, respectively.

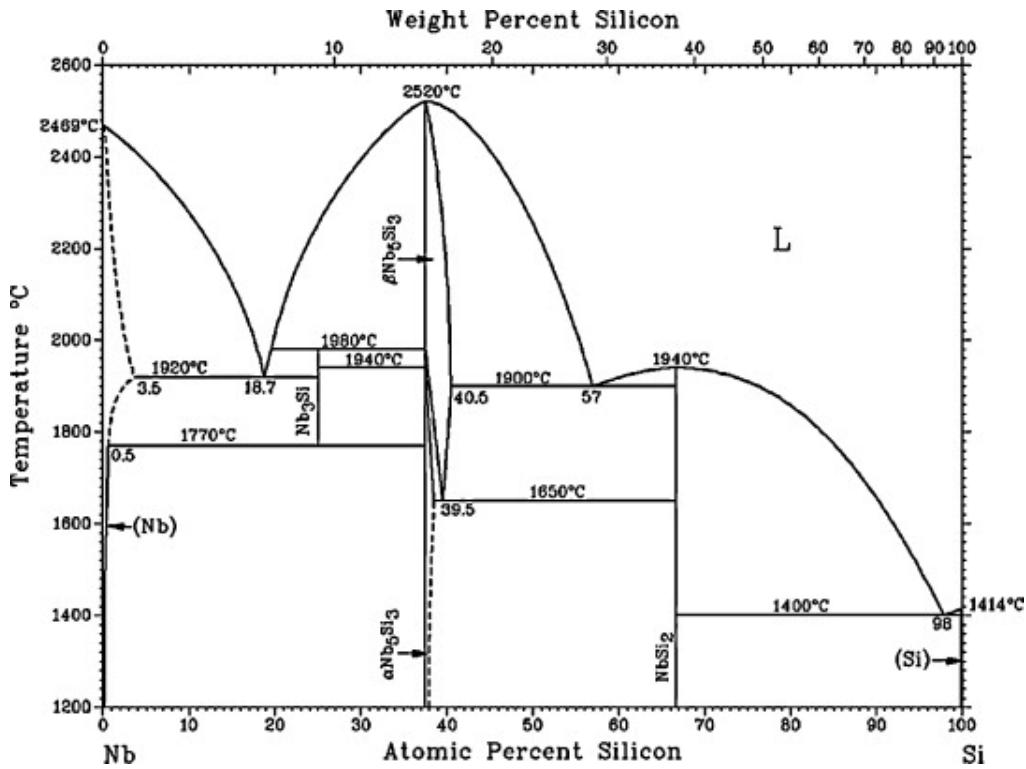


Figure 1.4: Nb-Si binary alloy equilibrium phase diagram [13].

### 1.3 Objectives of study

In spite of having high applicability of the Nb-Zr-C alloys, one of the main concerns of using Nb based alloys for high temperature applications is their poor oxidation resistance. In addition, studies on the high temperature behaviour of this alloy under oxidizing environment are very limited. These alloys get easily oxidized even at temperature as low as 400 °C in air which severely restrict their usage in ambient atmosphere. In general, approach of alloy addition or surface coating is employed to improve oxidation resistance of Nb alloy. Due to non-favourable nuclear properties of many alloying elements their usage for nuclear applications are restricted. For such applications surface coating is the preferred mode of providing oxidation resistance to Nb alloys and, therefore, detailed study on the approach of

providing a surface coating in order to exploit high temperature and oxidation resistance properties of the components made of niobium needs to be carried out.

In the present study, attempts have been made to address the issue of low oxidation resistance of the Nb alloy at higher temperatures by providing oxidation resistant coating. Owing to the edge over other coatings available for surface protection of Nb based alloys, experiments were carried out to develop silicide based oxidation resistant coating on Nb alloy. The main objectives of the present study are

1. Development of uniform and homogenous silicide coating using molten salt technique
2. Detailed microstructural characterization of the silicide coating
3. To understand the coating formation mechanism
4. Study the high temperature behaviour of as-coated samples

Initially, parameter optimization experiments were carried out at different temperatures and time periods. Further, using the optimized parameters, silicide coating was developed and detailed microstructural characterization of the coating was carried out. In addition, detailed studies were carried out to understand the underlying mechanism of formation of coating on Nb alloy. Also, annealing experiments were carried out to study the high temperature behaviour of the as-coated samples. Subsequently, the heat treated as-coated samples were characterized and their behaviour at elevated temperatures was understood.

#### **1.4 Outline of Thesis**

The outline of the thesis is as follows: Chapter 2 deals with the literature review on the topics related to the Nb based alloys, their oxidation behaviour and surface coating methodologies available to improve its high temperature behaviour. Details of the experimental methods are provided in chapter 3. Chapter 4 deals with the effect of various coating parameters. It also includes identification and characterization of various silicide phases formed. Chapter 5 deals with the understanding of coating mechanism involved

during silicide coating on Nb alloys. Chapter 6 gives details about the high temperature behaviour of the silicide coated Nb based alloys. It gives detailed microstructural characterization of as-coated and heat treated samples. Finally, the main conclusions drawn are summarized in Chapter 7.



---

# Literature Survey

---

This chapter is broadly divided into four sections. In section 1, detailed literature review on niobium based alloy with specific mention of Nb-1Zr-0.1C alloy is presented. In section 2, oxidation behaviour of Nb alloys is reviewed and summarised. In section 3, various methods of providing oxidation barrier coatings are reviewed and compared. Section 4 provides various methods of silicide coatings with emphasis on the molten salt coating, which is the subject of research of present thesis.

## **2.1 Nb and Nb alloys**

During the period of 1955 to 1963, niobium and its alloys were used in nuclear reactors as structural, cladding and corrosion barrier materials. This metal has been tested and used for fast breeder reactors and the nuclear rocket. In the latter applications, the use of niobium was due to its ability to form an effective barrier, when converted to carbide, to hot hydrogen corrosion. In the former system, its use is based on high temperature strength and resistance to liquid metal corrosion.

Commercially pure niobium is a soft, ductile metal with a relatively low modulus and modest high temperature strength. Nb has lowest Ductile to Brittle Transition Temperature (DBTT) among BRMs. For example, DBTT of pure-Nb is  $\sim -198.15$  °C (75 K), which is not easily achievable; whereas that of W is  $126.85$  °C (400 K), which is above the room temperature. Therefore, in comparison to other BRMs, Nb is less prone to brittle transition. The comparison of DBTT and density for various refractory metals is given in Fig. 2.1 (a).

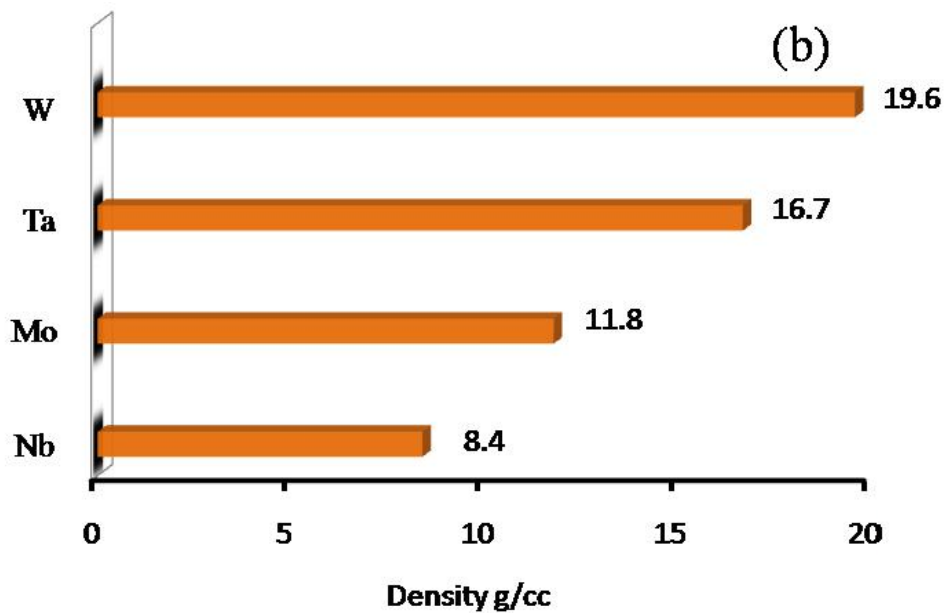
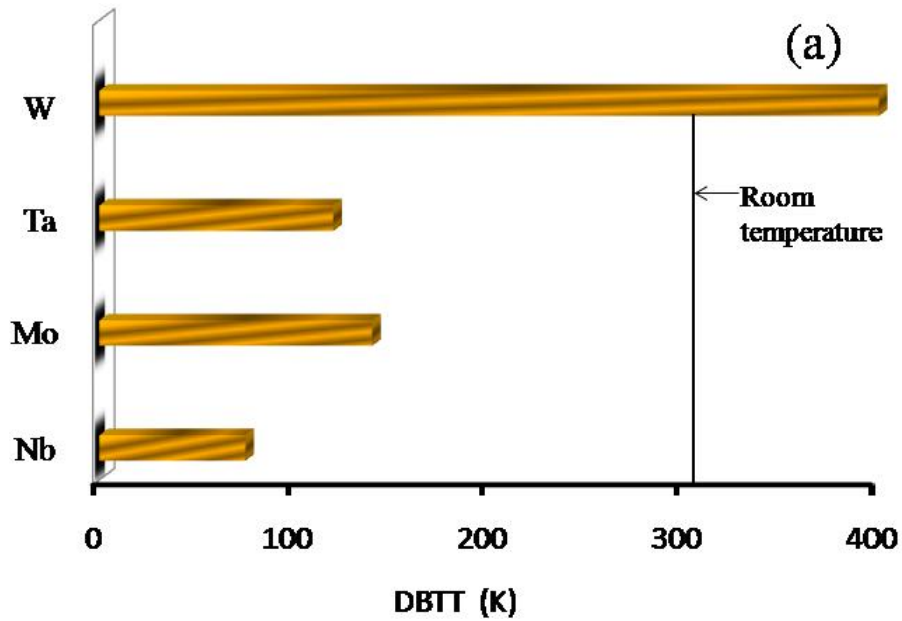


**Figure 2.1:** (a) Comparison of DBTT and (b) density for various refractory metals [15].

Excellent progress has been achieved through alloying and thermo-mechanical working to achieve high, short and long time mechanical strengths of the Nb based alloys, but only modest progress has been made in overcoming its inherent lack of oxidation resistance

through alloy changes. For alloying additions, general approach is to improve high temperature strength without compromising room temperature ductility. This is achieved by adding elements, which provide solid solution strengthening as well as precipitation hardening. However, for oxidation resistance, the choice of elements is very limited, as most of these elements have limited solubility and at low temperatures they form complex compounds which bring down the fracture toughness of the material substantially. Table 2.1 summarises the effects of some of the alloying addition to Nb alloys. With respect to the alloy studied in the present work, a brief description of Nb-C, Nb-1Zr and Nb-1Zr-0.1C alloys have been provided in the next sections.

### 2.1.1 Nb-C alloys

Delgrosso *et al.*[16] have found that in Nb-C alloys, relatively soft matrix (82-93 DPH) containing extremely hard carbides imposed problems during the forming of the alloy. Therefore, they focussed their attention on reducing the hardness of carbides and at the same time strengthening the matrix phase. Among series of elements, addition of zirconium in this regard turn out to be the best solution as on the one hand it increased the hardness of the matrix from 20 to 70 DPH and on the other hand, significantly reduced the hardness of the carbide phase, typically by a factor of two to three. Thus, addition of Zr to Nb-C alloy, reduced difference in hardness between matrix and carbide phases as well as changed morphology of the carbide phases. This way it was shown that Zr could improve the fabricability of the Nb-(Zr)-C alloys. Beyond 1 wt.% effectiveness of Zr in imparting hardness reduces significantly and at 3-4 wt.% zirconium concentration the carbide phase in Nb-Zr-C alloys did not show any significant increase in the hardness until the carbon concentration had risen to above 11,000 ppm. Hence, an alloy containing Zr less than 4 at% and C less than 4 at.% appear to meet all the property requirements for the structural material. It is worth mentioning here that increasing concentration of carbon has a strong tendency to

form large whiskers directly from the liquid phase, which make the material extremely brittle [17]. In order to avoid the formation of such large carbides, fine Nb-carbides were added into the melt to achieve fine dispersion of the carbide phase.

Recently, the effect of carbon addition on the mechanical properties of Nb-/Mo-W ternary alloys has been investigated [18]. It was found that with small amount of carbon addition led to the formation of the carbide phase into the Nb-Mo-W ternary alloys, which improved both the 0.2% yield stress and the ductility. This was attributed mainly to the presence of carbides improving the grain boundary strength and changing the fracture mode from inter- to transgranular, thereby improving the ductility of the Nb-Mo-W alloys. More recently, Nomura *et al.* [19] also investigated mechanical properties and creep behavior of Nb-Ti-C ternary alloys containing 40 mol% TiC. Their results showed that Nb-40 mol% TiC alloy exhibited a very high strength at high temperatures. Similar results have been reported for the Mo-40 mol% ZrC alloy [20]. The mechanical behavior of Nb-based alloy containing ZrC phase has also been investigated by Y.Tan *et al.* [21]. Their results indicate that the 0.2% flow stress of the Nb/ZrC alloys increases with increasing ZrC content from room to elevated temperature. However, the compressive ductility and fracture toughness decreased with increasing ZrC content. These studies have shown that to have most suitable toughness at room temperature and strength at high temperatures the concentration of the carbon should not increase beyond 0.3%.

**Table 2.1** *Effect of various alloying elements in Nb*[22]

<b>Element</b>	<b>Effect of alloying element in Nb</b>
<b>Tungsten</b>	Additions increase the strength of both short-time tensile and time-dependent stress rupture properties, tungsten additions also increases density and degrades fabricability; such degradation may become serious in alloys containing more than ~10% W.
<b>Molybdenum</b>	Additions are superior to W in short-time, low-temperature strengthening capability but are more limited in temperature- time strengthening capabilities; Mo also degrades fabricability.
<b>Vanadium</b>	Additions are more effective for short-time strengthening in comparison to W and Mo. Compared to tungsten and molybdenum additions, vanadium additions have less effect on fabricability and thus most useful in alloys designed for low-temperature service .
<b>Tantalum</b>	Additions have little direct effect on mechanical behavior; they are essentially non-strengthening. However, these additions increase the creep strengths as a result of a higher alloy melting point. Strength-to-weight ratio would increase only slightly.
<b>Zirconium</b>	Additions are very effective strengtheners in small amounts (0.5 to 2%), reflecting their reactive nature and their ability to combine with interstitial elements, particularly oxygen and carbon. Large amounts (> 2%) are also strengthening, It is a necessary alloying element when the alloy is used in contact with alkali liquid metals.
<b>Oxygen</b>	Oxygen is one of the first alloying element in Nb alloys which strengthened by the formation of oxide phase. In oxygen containing alloys, an intermediate step of aging was necessary to realize the full potential of oxide dispersoids. Aging between 900-1100 °C provided uniformly distributed fine size oxide phase which are in the matrix. For example, Nb-Ti-O alloys showed ~ 6 nm size of TiO <sub>2</sub> particles aligned along the elastically soft <100> directions. Alloys containing such oxide precipitates with volume as high as 2% exhibited ultimate tensile strength of nearly 1 GPa. However, higher concentration leads to the rapid growth of oxide particles resulting in substantial reduction in the strength as well as room temperature ductility.
<b>Nitrogen</b>	Nitride containing alloys were produced by melting in nitrogen containing plasma or by arc melting with nitride containing charges. Long aging of nitride alloys showed the decomposition of the large nitride phase and redistribution of the smaller precipitates which were coherent with matrix. Such precipitates remain highly dispersed up to 1500°C. These nitride precipitates slow down the recrystallization process substantially. In most of the cases due to eutectic or eutectoid phase reactions because of which formation of long fibers of nitride occurs lowering the rupture strength.

<b>Carbides</b>	Among all precipitates carbides were considered the only suitable interstitial compounds because they exhibit minimal susceptibility to liquid-metal corrosion. It has been shown that NbC, ZrC, HfC, , TaC, Ta <sub>2</sub> C and TiC should be relatively stable in a niobium matrix. Out of these carbides HfC and ThC <sub>2</sub> were eliminated on the basis of their nuclear properties. Ti and Ta carbides were excluded because the addition of either titanium or tantalum to Nb-C or more complex alloys produced negligible improvement in the high temperature strength. Of this group, therefore, niobium and zirconium carbide are the most suitable precipitates. The zirconium carbide particles also enhance strength, creep strength and brittle failure resistance of the alloy by creating distortions in the crystal lattice, and therefore, making it difficult for dislocations to propagate through the lattice.
<b>Chromium</b>	Additions improves the oxidation resistance but in case of addition more than 9%, Laue phase comprises room temperature ductility. At elevated temperatures, dissolution and re-precipitation of the Laue phase destabilizes the microstructure.
<b>Aluminium</b>	Additions improves the oxidation resistance but reduces the melting point of the alloy. However, decrease in the room temperature ductility is observed if the concentration of Al is more than 4%
<b>Nickel</b>	Additions result in the formation of Nb <sub>3</sub> Ni phase. Additions does not affect high temperature strength significantly.
<b>Silicon</b>	Addition of Si by more than 9-10% results in ductile to brittle region transformation. Improvement in oxidation resistance is observed but NbSi <sub>2</sub> and Nb <sub>5</sub> Si <sub>3</sub> phases become brittle.

### 2.1.2 Nb-1Zr alloys

Table 2.2 shows mechanical properties of the Nb-1Zr alloy at different temperatures. From this table it could be observed that the solid solution strengthening provided by Zr remain effective only up to 1095 °C. Reduction in the yield strength and ultimate tensile strength beyond this temperature is due to extreme softening shown by Nb matrix, which is shown in form of large reduction in area or in high ductility. The data at 1315 °C shows that the addition of 1% Zr to Nb, the alloy strengthened to the same degree by the addition of 3000 p.p.m carbon.

**Table 2.2** *Mechanical properties of Nb-1Zr alloy at different temperatures* [16]

<b>Test temperature (°C)</b>	<b>Yield strength (MPa)</b>	<b>Ultimate strength (MPa)</b>	<b>Elongation, %</b>	<b>Reduction in area</b>
<b>Room temperature</b>	222.7	330.94	31	88
<b>205</b>	106.18	200.63	29	95
<b>425</b>	108.24	221.32	23	92
<b>650</b>	124.79	248.90	18	88
<b>870</b>	106.18	186.15	15	82
<b>980</b>	103.42	255.79	23	86
<b>1095</b>	128.24	230.97	14	76
<b>1205</b>	77.91	91.70	39	99
<b>1315</b>	41.36	48.26	27	—

As shown in Table 2.2, Nb-1Zr alloy serves to improve the mechanical properties of niobium at elevated temperatures. The Nb-1Zr alloy retains its strength up to temperatures of about 750 °C, whereas pure niobium quickly loses its mechanical strength beyond about 500 °C. The addition of 1% zirconium to niobium not only provides high temperature strength by solid solution strengthening but also serves as a grain refiner for niobium. Therefore, in

addition to solid solution strengthening, Zr contributes to the strength by grain refinement also. In addition, the rate of grain growth of the pure metal is greater than that of the alloy. As a result, in high temperature service applications, Nb-1Zr is expected to be less prone to embrittlement than pure niobium. Zirconium forms a second phase by reacting with free interstitial oxygen atoms within the niobium matrix, which if distributed uniformly, provides additional high temperature strength. The addition of 1% zirconium does not have a statistically significant effect on the room temperature strength of niobium. However, Nb-1Zr offers improved high temperature properties compared to commercially pure niobium. These observation supports findings that zirconium acts more as a dispersion strengthener in niobium.

### 2.1.3 Nb-1Zr-0.1C Alloy

As mentioned earlier, addition of carbon alone in Nb matrix does not significantly improve strength but reduces its ductility significantly. When both zirconium and carbon are added together to niobium, the yield, rupture and creep strengths are improved by three to five fold as compared to Nb-1Zr alloy (Fig. 2.2). The resulting alloys become both fabricable and ductile. Maximum strengthening is achieved when carbides are dissolved during the extrusion process and re-precipitated as fine particles uniformly distributed throughout the matrix, as well as in subgrain boundaries and dislocation sub cell walls. [16]

Mehmet Uz *et al.* [23] have carried out the effect of thermos-mechanical processing on the microstructure of the Nb-1%Zr-0.1%C alloy. They have worked mainly on as-solidified, extruded (at 1627 - 1277 °C) and annealed samples. The as-solidified microstructures have coarse grain (up to 500 microns) size with coarse (>1 $\mu$ m) intra and intergranular Nb<sub>2</sub>C precipitates. After extrusion the resulted microstructure showed presence of the Nb<sub>2</sub>C phase and a small amount of (Zr,Nb)C phase and all the precipitates were aligned along the extrusion direction. The hardness of the samples depends upon the

temperature of extrusion, which was attributed to higher solid solubility of C with increasing temperature of extrusion. This would lead to dissolution and subsequent re-precipitation of carbides during the high temperature processing.

Changes in the phase composition and morphology of the carbide precipitates, when the alloy is maintained under stress for long periods at high temperatures, may lead to changes in its mechanical properties. Therefore, several researchers have investigated the possible structural and morphological changes in the precipitates in the alloy during prolonged stressing at high temperatures. Maksimovich *et al.* [24–27] have carried out these experiments and showed that after prolonged holding at 900 and 1100°C, the volume fraction and average size of NbC carbides have increased. It is attributed to the acceleration of the dissolution of fine particles and the growth of carbides due to diffusion of atoms of alloying elements into the matrix. With increasing holding time (up to 1000 hrs or more) at 900°C the consumption of fine particles by large particles practically ceases. It was noticed that the rate of increase in the particles size under loading condition is lower than without loading condition. The reason for this could be due to the generation of dislocations under loading condition. Dislocations acts as favourable sites for the accumulation of dispersed precipitates.

It appears that presence of carbides in Nb alloys does not affect the liquid metal properties adversely. The strain around particles appears to be sufficiently low to participate in any form of liquid corrosion. Because of these properties Nb-1Zr-0.1C alloy is one of the best choice for those structural materials which have to expose to liquid metal coolant at high temperature. Table 2.3 provides a comparison of the Nb alloys with respect to other alloys for liquid metal corrosion.

**Table 2.3** Comparison of maximum operating temperature for nominal corrosion different alloys

Material	Maximum Temperature of Operation for Nominal Corrosion (° C)			
	Na	Li	K	Pb, Pb-Bi
Stainless Steel	600	450	600	400
Cr-Mo Steels	600	500	--	425
Ti and alloys	--	550	--	--
Nb-1Zr	900	1300	750	--
Nb-1Zr-0.1C	~900	~1300	750	--

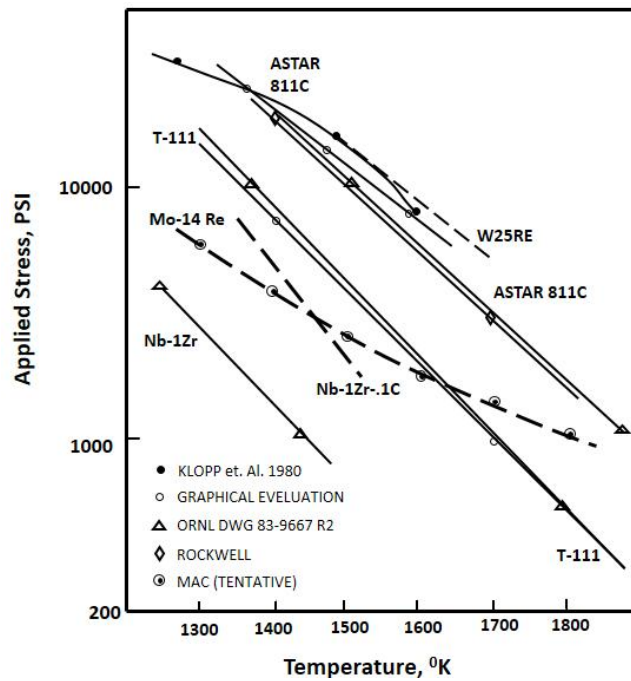


**Figure 2.2:** Stress vs. temperature comparison for different alloy systems [5].

## 2.2 Oxidation Behaviour of Nb

The oxidation behaviour of Nb, due to formation of various stable and metastable oxides, is complex in nature. The oxidation of niobium with time has been extensively studied in literature [28–32].

It has been observed that Nb when exposed to oxidizing environment, oxidation commences with initial dissolution of oxygen in Nb and formation of lower Nb- oxides:

NbO, NbO<sub>2</sub> (Fig. 2.3), these oxides exist only as thin layers and do not play any major role in the oxidation process at high temperatures.

In the next stage, preferentially oriented layer of  $\alpha$ -Nb<sub>2</sub>O<sub>5</sub> is formed which on subsequent recrystallization becomes randomly oriented.

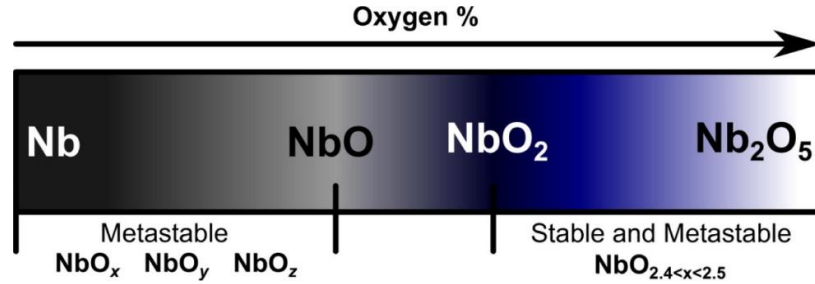


**Figure 2.3:** Formation of various Nb-oxide phases with increase in Oxygen% [33].

Transformation from  $\alpha$ -Nb<sub>2</sub>O<sub>5</sub> to  $\beta$ -Nb<sub>2</sub>O<sub>5</sub> is observed with increase in oxidation time. Also, during the growth of Nb<sub>2</sub>O<sub>5</sub> layer, transformation from the black adherent layer to white in-adherent porous layer is observed. High oxidation rate of Nb could be attributed to the large volume of oxide to metal ratio (~2.5). With further growth in the oxide scale, compressive stresses are generated owing to the dimensional constraint imposed by metal. These stresses result in the formation of cracks, which allows further penetration of oxygen into the material.

Since 1955, research on the oxidation behaviour of Nb and on the development of Nb-based alloy system has been pursued with the aim to achieve balance between oxidation resistance and mechanical properties. Extensive research on the oxidation behaviour of Nb carried out during 1955- 1975 has been reviewed by Stringer [34]. The work carried out prior to 1975 was mainly confined to the alloy development in empirical way. During this time, efforts were made to produce compact, adherent oxides with better oxidation resistant properties. The efforts were not successful in improving the oxidation resistance of niobium-base ductile alloys, and it was recognized by a number of investigators that such alloying

additions are needed so as to produce a surface oxide other than a modified  $\text{Nb}_2\text{O}_5$  was required.

During 1975-1976 period, studies carried out by Svedberg [35] on the oxidation behaviour of Nb based intermetallics showed that slowest oxidation rate is observed in those alloys (e.g. Nb-Al, Nb-Fe) where mixed oxide layer with rutile type structure is formed. Based on the type of protective scale formed, the metals could be classified into three groups. First group, which includes systems like Nb-Al, where selective oxidation of Al in  $\text{NbAl}_3$  forms a semi-protective layer oxide  $\text{Al}_2\text{O}_3 + \text{NbAlO}_4$ . The second group includes systems, where the formation of compound oxides is slower than the binary oxides forming on either pure element. This phenomenon is observed in Nb-Fe system, where formation of rutile structured compound  $\text{NbFeO}_4$  is observed. The third group includes the formation of protective and rutile structured ternary oxides such as  $\text{NbCr}_2\text{O}_4$ .

In Nb-Al alloy system, recent studies have shown that  $\text{NbAl}_3$  initially forms an alumina scale but cannot sustain its growth as a protective layer [36]. Binary Nb-Al alloys with lower aluminum contents (<75 at.%) also do not form protective alumina scales in air at 1200 °C. Svedberg [35] also reported that lower aluminides of Nb ( $\text{Nb}_2\text{Al}$ ) undergo rapid oxidation with linear kinetics. However, ternary additions of Ti in the Nb-Al alloys modify their oxidation behaviour. Wukusick [37] studied the oxidation behaviour in a series of Nb-Al-Ti alloys in the range of (16-24 at.%) Nb- (46-50 at.%)Al - (26-40 at.%)Ti. He showed that by adding large amount of titanium, between 593-982°C the pest behaviour in the Nb-Al alloy could be suppressed owing to the formation of titanium oxide. In the temperature range of 1004-1298 °C, high oxidation rate of Al led to the formation of duplex oxides,  $\text{TiO}_2 + \text{Al}_2\text{O}_3$  in the  $\text{TiO}_2$  matrix was observed. With further increase in temperature, formation of a protective, continuous  $\text{Al}_2\text{O}_3$  scale was reported.

Many researchers have also carried out basic studies on the oxidation behaviour of niobium silicides. Lavendel [38] reported formation of silicate glasses comprising niobium oxides on the exposure of NbSi<sub>2</sub> to air temperatures up to 1538°C. NbSi<sub>2</sub>, when subjected to rapid heating to 1650 °C, forms oxides of pure Si but they revert back to mixed oxides at lower temperature. Therefore, alloying of NbSi<sub>2</sub> becomes essential to improve the oxidation resistance of the intermetallics. The effect of addition of alloying elements, such as titanium and chromium in NbSi<sub>2</sub> has been reported in literature [39]. However, large additions of these alloys have detrimental effect on the ductility of niobium.

Nevertheless, the protective oxides based on alumina and silica formed by the selective oxidation of aluminium and silicon from intermetallic compounds of niobium under some conditions could not be formed on ductile niobium base alloys under any conditions. Till date, researchers have not been able to develop a high-temperature niobium-base alloy with the ability to form a protective oxide scale. Even though, some of the alloys tested have potentially useful properties, the alloying elements usually act to the detriment of at least one property. Therefore another approach of providing surface coating to improve the oxidation resistance behaviour of Nb has become attractive choice as it does not alter mechanical properties of the substrate. The various coating methodologies employed to improve the oxidation resistance behaviour of various refractory metals for example, Nb are discussed in the following section.

### **2.3 Oxidation barrier coating**

In order to widen the horizon of Nb applications, protective coating is necessary for high-temperature applications of Nb based alloys in oxidizing environments as they undergo oxidation at temperature as low as 400 °C. In general, for high temperature oxidation resistance, a coating should exhibit following properties:

- Oxygen and metal ion diffusion should be restricted by coating.

- The coating should have a low vapour pressure at the operating temperature,
- The melting point of the coating should be above the operating temperature,
- It should have low reactivity with the high temperature environment

To improve the oxidation resistance properties, a large number of coating techniques are available, such as, physical vapour deposition (PVD), chemical vapour deposition (CVD), pack cementation, thermal spray coating, hot dipping, vacuum plasma coating, laser surface alloying and molten salt [40–52].

**Table 2.4** Comparison of various coating methods.

Coating technique	Advantages	Disadvantages
<b>CVD</b>	<ol style="list-style-type: none"> <li>1. Good growth rates of coating.</li> <li>2. Can deposit materials that are hard to evaporate.</li> <li>3. Co deposition of materials simultaneously is possible.</li> </ol>	<ol style="list-style-type: none"> <li>1. Difficult to get suitable precursors and very expensive</li> <li>2. By products can be hazardous.</li> <li>3. High operable temperature is required</li> </ol>
<b>PVD</b>	<ol style="list-style-type: none"> <li>1. Process is environmental friendly.</li> <li>2. Good control over chemical composition of coating.</li> </ol>	<ol style="list-style-type: none"> <li>1. Low deposition rate.</li> <li>2. Line of site process, difficult to coat uniformly on intricate/complex geometry</li> <li>3. Complex procedure with high operable cost</li> </ol>
<b>Pack cementation</b>	<ol style="list-style-type: none"> <li>1. Non line of sight process.</li> <li>2. Batch process can coat multiple substrates simultaneously</li> </ol>	<ol style="list-style-type: none"> <li>1. High operable temperature.</li> <li>2. Expensive to scale-up</li> <li>3. Incorporation of contaminants in the coating</li> </ol>

<b>Molten Salt</b>	<ol style="list-style-type: none"> <li>1. Non line of sight process.</li> <li>2. Low operable temperature</li> <li>3. Good mechanical bonding between coating and substrate.</li> <li>4. Easy and economical setup.</li> <li>5. Good growth rates of coating</li> </ol>
--------------------	-------------------------------------------------------------------------------------------------------------------------------------------------------------------------------------------------------------------------------------------------------------------------

Each of these techniques presents various advantages and disadvantages depending upon the component to be coated and the end-use application. Although, many of these methods are in practice, however, they are not free from limitations.

A comparison of various coating method used for Nb based alloys is presented in table 2.4. The two most common techniques used to provide surface coating on Nb alloys are discussed in detail below.

### 2.3.1 Pack cementation method

Pack cementation is an in-situ chemical vapour deposition (CVD) batch process that has been used to produce corrosion- and wear-resistant coatings on inexpensive or otherwise inadequate substrates for over 75 years.

Pack cementation is a widely applicable in the case of complex shaped structures where it produces uniform and adherent coatings throughout the surface. The coating layers and the substrates are found to be compatible with respect to adhesion, thermal expansion, etc. This method is widely used to confer oxidation resistance on ferrous alloys as well as nonferrous especially for super alloys and refractory metal alloys [53,54]. Usually relatively expensive aluminum or binary alloys grade reagent is used during the pack process. Pack cementation processes include aluminizing, chromizing, and siliconizing.

In pack cementation process, components are packed in metal powders in sealed heat-resistant retorts and heated in a furnace to precisely controlled temperature–time profiles. The schematic illustration of a coating obtained by pack cementation is shown in Fig. 2.4.

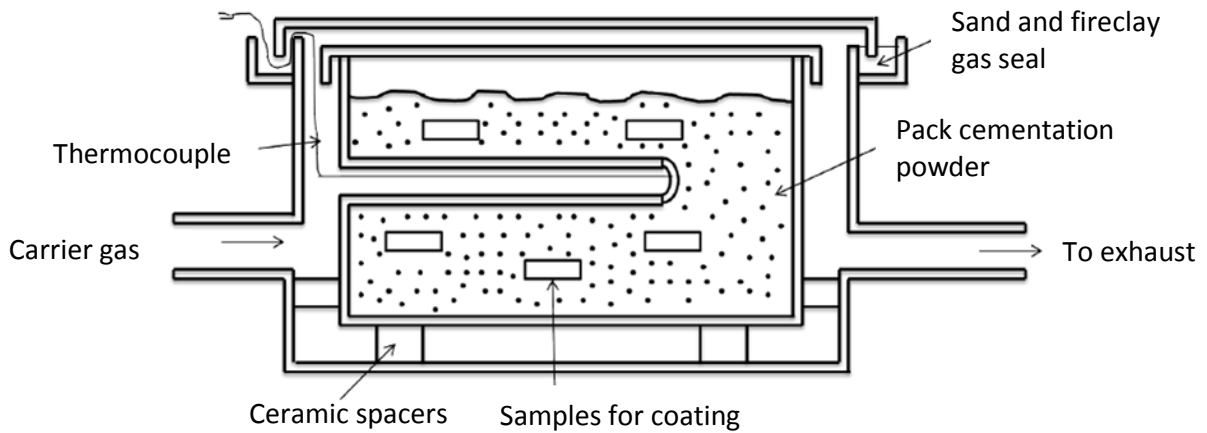


**Figure 2.4:** Schematic representation of pack cementation technique [55].

The powder pack is composed of a master alloy or pure element powder to be enriched at the substrate surface, a halide salt activator and inert filler. The halide activator decomposes at high temperature to produce volatile halide vapours of the elements because of which HAPC (Halide activated pack cementation) technique is classified as in-situ chemical vapour deposition technique. The chemical potential gradient drives the gas phase diffusion of the metallic halides to result in surface deposition. The different steps for a silicide coating using halides and schematic illustration of the coated sample are shown below:

Step One: Decomposition and formation of volatile silicon halide



Step two: Deposition on the substrate



Where X is a halide, generally corresponds to Cl or F and M corresponds to metal.

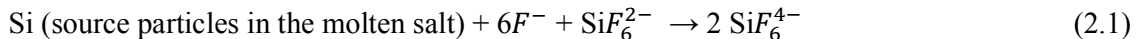
However, because pack cementation method works on the principle of chemical vapour deposition from the dilute halide gas phase, it requires encapsulation, high operable temperatures (1000- 1200 °C) and long reaction time (8-36 h). It is therefore difficult to HAPC scale up a HAPC process. This issue is particularly of concern in the case of long objects where the size of equipment, furnace and packs become extremely large.

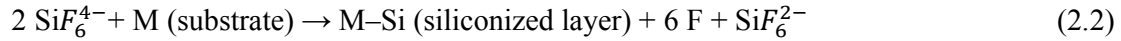
### 2.3.2 Molten salt method

Another coating method, molten salt can be employed to deposit coating on pure iron and other refractory metals [56,57]. The molten salt media is capable to carry Si to the metallic substrate. The coating techniques using molten salt are classified into two categories: electrolytic and electroless plating. Ueda *et al.* [58] studied the electrolytic plating on iron substrate in the molten LiCl-KCl-LiF-K<sub>2</sub>SiF<sub>6</sub> bath impressing 0.6-1.0 V (vs. Li/Li<sup>+</sup>) at 500°C. The deposits were found to be powdery or dendritic in nature. However, 200 µm thick smooth silicide coating was developed using non-electrolytic method, by immersing iron substrate into molten KCl- NaCl-NaF-Na<sub>2</sub>SiF<sub>6</sub>-Si bath below 1000 °C.

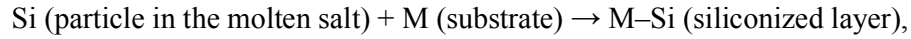
Therefore, molten salt is an electroless plating operable in open air at 973–900 °C, lower than the pack cementation processing temperature. It has been shown that the silicon deposits on the metal surface in the salt react with the substrate metal and form the metal silicide.

The principle of this deposition in the molten salt has been reported in Refs. [56, 57, 59–61]. Fig 2.5 shows a typical molten salt bath considered for silicide coating. When Na<sub>2</sub>SiF<sub>6</sub> and Si powder are added in the supporting salt of NaCl–KCl, a disproportionational reaction between Si and Si<sup>4+</sup> ions deposits a siliconized layer on the metallic substrates, M, as,





The deposited Si from  $\text{Si}^{2+}$  penetrates into the metal surface, and forms an alloy (M-Si) with the metal substrate. The total reaction,



shows that the reaction is driven by the difference between the thermodynamic activity of pure silicon and that of the siliconized layer.

In the thermodynamic sense of the disproportionation reaction, as illustrated above, the deposition reactions from the silicon sources are fundamentally same for both, pack cementation in the gaseous state and for the electroless plating in the molten salt.

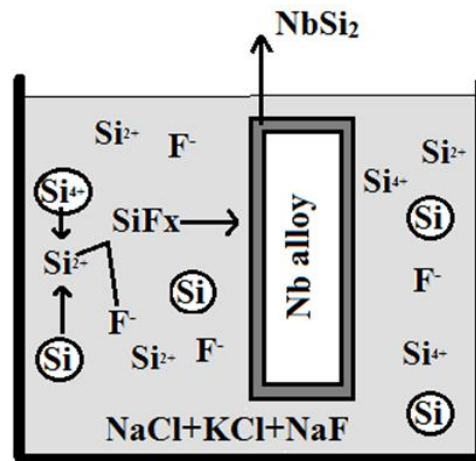


**Figure 2.5:** Schematic representation of formation and deposition of Si ions in molten salt for silicide coating on metallic substrate (e.g., - Nb).

The former uses gaseous species as silicon carrier and the latter the ionic Si. The amount of silicon atoms in the media, however, is much larger in the molten salt than in the gaseous phase. It can enhance silicide formation even at lower temperatures, if the rate-determining step is not diffusion in the solid.

The diffusion coating developed using molten salt technique involves reduction, deposition, ion interchange, diffusion, and the formation of new compounds. In this case, the coatings, are solid solutions, or intermetallic compounds, or both, and are composed of alloys of the coating materials and the substrate. They form an integral part of the base metal and so bonding strength is excellent. The properties of these kinds of coatings can be controlled by a careful choice of the elements in the system and by proper control of the thermodynamics and kinetics of the reaction.

Based on the studies carried out on the development of coating on various refractory metals such as Mo [57], Nb [61], Ni [59], Cr and Co, the deposited silicides are classified into two groups: the substrate on which di-silicide ( $MSi_2$ ) precipitated (Group A) and that on which lower silicide ( $MSi_n$ ,  $n < 2$ ) was formed (Group B).

**Table 2.5** Stable silicide phases in binary system of M- Si

Group	Substrate	Stable silicides in the Binary system
<b>A</b>	Mo	$MoSi_2$ , $Mo_5Si_3$ , $Mo_3Si$
	Nb	$NbSi_2$ , $Nb_3Si$ , $Nb_5Si_3$
	Cr	$CrSi_2$ , $CrSi$ , $Cr_5Si_3$ , $Cr_3Si$
<b>B</b>	Fe	$FeSi_2$ , $FeSi$ , $Fe_3Si$
	Ni	$NiSi_2$ , $NiSi$ , $Ni_3Si_2$ , $Ni_2Si$ , $Ni_5Si_2$
	Co	$CoSi_2$ , $CoSi$ , $Co_2Si$

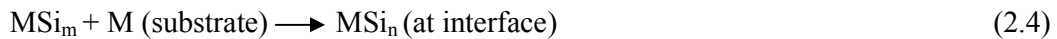
Group A consists of Mo, Nb and Cr and group B consists of Fe, Co and Ni. Table 2.5 summarizes the various stable silicide phases formed in the group A and B metals.

Fig. 2.6 schematically shows the mechanism of silicide layer formation in metals pertaining to group A and group B. The formation model (A) and model (B) (Fig. 2.5) represent the formation mechanism of silicide rich phases and formation of lower silicides respectively.

The Si produced from the proportional reaction between Si and  $Si^{4+}$  ions (Eq. (2.1)) gets deposited on the surface. After attaining sufficient concentration of Si, formation of the first layer of  $MSi_2$  phase occurs on the metal surface during initial stages (Fig. 2.6 (A)). Subsequently, the deposited Si diffuses into this  $MSi_2$  phase and reacts with the substrate. After the formation of a thick layer of  $MSi_2$  phase, the Si supply to the interface get delayed and because of short supply of Si formation of lower silicide,  $MSi_n$  ( $n < 2$ ) starts forming (Fig. 2.6):

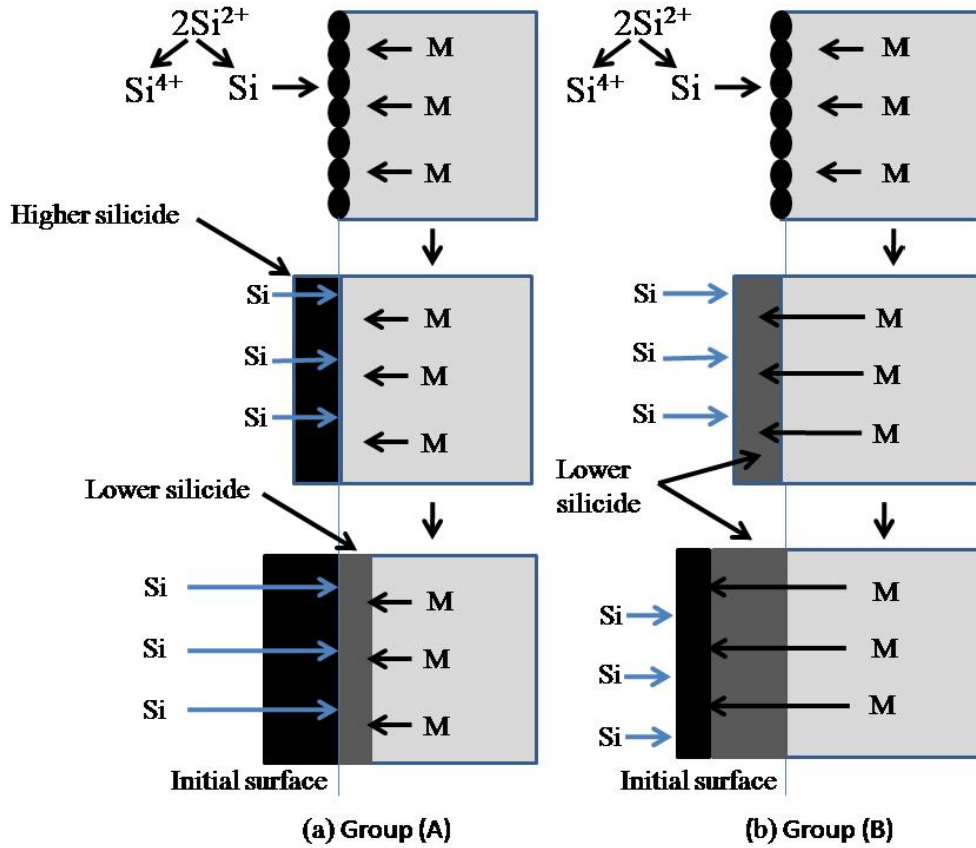


Fig. 2.6 (b) shows the formation model (B) of the lower silicides. In the metals pertaining to Group B the first step of Si deposition is same as in the case of group A. The deposited Si forms  $MSi_2$  phase first, but decomposes into the lower silicides,  $MSi_m$ . However, in Group B the base metal diffuses through the thin  $MSi_m$  layer toward the surface and reacts with Si to form silicide. After the formation of thick layer of the lower silicide, the metal supply to the surface is delayed and the higher silicides,  $MSi_n$  ( $m < n$ ), are formed following the equation 2.4:



In case of Nb–Si system, there are three stoichiometries compounds, i.e.  $NbSi_2$  (tetragonal),  $Nb_5Si_3$  (tetragonal), and structured  $Nb_3Si$  (cubic). Among these, Niobium disilicide ( $NbSi_2$ ) is the most oxidation resistant because other two silicides lack Si content to cover the full surface by forming  $SiO_2$ .  $NbSi_2$  makes Nb alloy a promising candidate material for high temperature structural applications. It is a high melting–point ( $\sim 1960$  °C) material

with excellent oxidation resistance and has a moderate density ( $5.53 \text{ g/cm}^3$ ). NbSi<sub>2</sub> based heating-elements have been used extensively in high-temperature furnaces. The low electrical resistance of silicides in combination with high thermal stability, electron-migration resistance, and excellent diffusion-barrier characteristics are important for various applications.



**Figure 2.6:** Schematic representation of silicide layer formation mechanism in group A and B metals. [62].

The major problem associated with NbSi<sub>2</sub> based silicide coatings is the mismatch of the coefficient of thermal expansion (CTE) with substrate and oxide layer. Another basic problem with NbSi<sub>2</sub> based coatings arises due to differences between the thermal expansion coefficients of NbSi<sub>2</sub> and Nb. During deposition at temperatures in the range 1000 – 1050 °C, the coating and substrate are nearly unstressed. However, the difference between the thermal

expansion coefficient of Nb ( $7.3 \times 10^{-6} \text{ K}^{-1}$ ) and NbSi<sub>2</sub> ( $9.8 \times 10^{-6} \text{ K}^{-1}$ )[63,64] creates tensile stresses in the coating on cooling because the NbSi<sub>2</sub> contracts more than the niobium substrate.

Although the cracks may heal on reheating to or above the application temperature, they will not completely reseal themselves. Thus, a coating is needed that either has a lower application temperature or forms oxides that will seal the cracks on reheating. Many cracks within the oxide scale may also be induced by the large volume expansion inherent to oxidation of NbSi<sub>2</sub> coating. Another factor which induces cracks is the thermal stress from a CTE mismatch between the oxide scale and the NbSi<sub>2</sub> coating during cooling. It has also been observed that defects, such as pores and cracks, in the oxide scale are formed in the isothermal oxidation temperature. Therefore, additional heat treatments could be given to NbSi<sub>2</sub> coating to overcome some of these problems associated with defects or stress due to mismatch of CTE.

The formation of silicide rich phase or lower silicide phase in the substrate depends upon the type of substrate. It is important to note that in the molten salt technique, composition of the bath also plays an important role to develop coating on different refractory metals. Various studies have been carried out to optimize the composition of the molten salt to coat metals like Fe, Ni, Mo and Nb. Table 2.6 gives a brief information about the various composition of salts reported in the literature.

Therefore, considering factors, such as ease of operation, economical aspects and lesser reaction time, molten salt technique stands out as the most promising coating technique in the present time for protecting niobium based alloys. The coating developed using this method is metallurgically bonded to the substrate and becomes an integral part of the base material. It is also possible to provide a good coating in intricate shapes as liquid salt can penetrate into otherwise inaccessible regions.

#### 2.4 Oxidation barrier coatings for Nb and Nb alloys

For Nb based alloys, mainly two types of protective (aluminide and silicide) coatings have been reported in literature due to their superior properties [65–67]. Reason for their suitability is that both the elements (Al, Si) form various intermetallic compounds. These intermetallic compounds provide high temperature strength as well as protective coating by the formation of  $\text{Al}_2\text{O}_3$  or  $\text{SiO}_2$  layers on the surface of the components which protect it from oxygen penetration. Even if the compounds of these elements are used, they provide necessary protection against oxidation. For example, deposition of niobium silicide on a niobium substrate forms a protective silicate (SiO) layer. Between Al and Si, the process of coating is simpler in the case of Al, but from alloying view point Al has limited solubility and induces brittleness in the Nb alloys. In contrast to this, Si offers wider solubility range and therefore is more suitable from metallurgical view point but development of Si- based coating is a complex process.

**Table 2.6** Comparisons of the salt compositions used to develop coating using molten salt technique.

Literature	Salt Composition (mol %)				
	NaCl	KCl	NaF	$\text{Na}_2\text{SiF}_6$	Si
<b>Gay and Quakernaat</b> [59]	40.88	32.05	22.13	4.94	23.63
<b>Hosokawa</b> [68]	50	50	-	-	100
<b>Belyaeva et al.</b> [69]	40.88	32.05	22.13	4.94	23.63
<b>Oki and Takinawa</b> [70]	40.98	32.12	22.00	4.90	100
<b>Suzuki et al.</b> [61]	36.58	36.58	21.95	4.89	21.85

Huijbregts and Brabers [71] studied the oxidation behavior of niobium and niobium coated with aluminium in the temperature range of 400 – 600 °C in different atmospheres: superheated steam at 1 atmosphere, a mixture of steam and air, and in air. They found out that when a crack is present, NbO is formed which grows between niobium and niobate. Also, cracks may arise by oxidation of free aluminium between NbAl<sub>3</sub> grains or by thermal stresses during cooling in a dense NbAl<sub>3</sub> diffusion layer. This showed that aluminum based coating should be as free from defects as possible. Murukami *et al.* [72] attempted to prepare a coating consisting of a ternary compound of Nb, Si and Al on niobium substrate by low pressure plasma spray (LPPS) technique, but the coating layer easily spalled from the Nb substrate. Matsuura *et al.*[46] proposed a new method for surface modification based on the arc surface alloying and its feasibility has been investigated performing niobium aluminide coating on a niobium base metal. They concluded that when tungsten arc was used to melt an aluminum plate placed on a niobium block, the niobium surface was also melted and a melt pool of an Al–Nb binary alloy was formed on the niobium block. The melt pool solidified into niobium aluminides on the surface of the niobium block forming a thick NbAl<sub>3</sub> layer on the top surface of the coating layer. When an Al–Si alloy plate was used instead of the aluminum plate, a thick layer containing niobium alumina–silicide layer was formed on the niobium block.

Kumon *et al.*[73] applied hot dipping of a Nb substrate into molten Al and subsequent they provided anodic oxidation to the Al films. This dip coating seems to be the simplest coating method. However, when this technique is extended to silicon, it has some practical issues. The lowest melting temperature in the Nb–Si system is as high as 1668 K [74], so that it is practically difficult to deposit directly niobium silicide from the Si melt. Coatings of Cr–Si or Ti–Si binary silicide on the Nb substrate, therefore, were applied using their lower eutectic melting [75]. Other methods such as vacuum deposition or chemical vapor

deposition have been applied to deposit silicon onto the Nb substrate. These attempts need elevated temperatures of over 1273 K and prolonged times for silicon deposition and diffusion.

Li *et al.* [76] and Yoon *et al.* [77] prepared NbSi<sub>2</sub> layers with a thickness of around 25-66 μm on Nb substrates by pack cementation where Nb substrates were embedded in a pack mixture of fine Si powder, halide activators (NaF, MgF<sub>2</sub>), and inert fillers (SiC, Al<sub>2</sub>O<sub>3</sub>), this mixture being heated at 1323-1373K (1050-1100 °C) for 23 h in a vacuum or an Ar atmosphere. NbSi<sub>2</sub> has also been coated on Nb plates and bulks by electroless plating using molten salt and by spark plasma sintering (SPS).

Milanese *et al.* [78] reported that NbSi<sub>2</sub> phase grows much faster than the other Nb rich phases (such as Nb<sub>5</sub>Si<sub>3</sub>) in the presence of high Si activity from the pack. In order to improve the high temperature oxidation resistance of refractory metals, multilayers Al–Si composite coatings of about 50 and 40 μm thickness were formed on niobium and tantalum metals, respectively, by pack cementation technique by Majumdar *et al.* [79]. Substrate metals embedded in the pack consisting of Al, Si powders and activator NH<sub>4</sub>F intimately mixed in the prescribed proportions were heat treated at 1300 K (1027 °C) for 16 h. They concluded that the coating process was dominated by the diffusion of silicon. The thickness of the di-silicide layers was larger as compared to alumina-silicide layers in case of both the refractory metals (Nb and Mo).

Formation of a thin adherent Al<sub>2</sub>O<sub>3</sub> layer on the surface of a matrix comprising of a ternary compound of Nb, Si and Al has also been reported by Murukami *et al.*[72] which indicated that the coating was also resistant to oxidation. Suzuki *et al.* [61] have prepared NbSi<sub>2</sub> coating with a thickness of approximately 10 μm by heating a Nb substrate in NaCl-KCl molten salt with NaF, Na<sub>2</sub>SiF<sub>6</sub>, Si and SiO<sub>2</sub> at 900 °C for 2h. Ukegawa *et al.* [80] have found a NbSi<sub>2</sub> coating of over 50μm in thickness and a dense Nb matrix with a Nb<sub>5</sub>Si<sub>3</sub> layer

(dozens of  $\mu\text{m}$ ) in between by heating NbSi mixture powder and Nb powder at 1673K and 40 MPa for 0-4h.

Yamada *et al.* [74] have prepared powders and polycrystalline bulks of metal silicides such as  $\text{FeSi}_2$ ,  $\text{MnSi}$ ,  $\text{MoSi}_2$  and  $\text{NbSi}_2$  at 773-900 °C. The preparation temperature of the metal silicides with Na was over 300 K lower than that without Na. According to the phase diagram of the Na-Si system, a Na-Si melt containing Si up to about 50 mol.% exists at 700-1100 K (427-827 °C). It was considered that the formation of the metal silicides at relatively low temperature was enabled by the reaction of source metals with Si dissolved in the Na-Si melt. In the present study, a novel method was employed for the preparation of  $\text{NbSi}_2$  coating at the surface of Nb plates by heating Nb plates in a Na-Si melt. The effects of heating temperature and time on the formation of  $\text{NbSi}_2$  layers and the oxidation resistance of  $\text{NbSi}_2$ -coated Nb plates were investigated.

Studies have shown that silicide based coatings are the best oxidation resistant coating system for Nb metals and alloys, as they exhibit most of the requirements for high temperature applications. The beneficial effects of silicides coatings on high temperature oxidation resistance are twofold. First, with sufficient concentration, Si can form a continuous vitreous silica layer between the metal and scale interface. This silica layer has a low concentration of defects, allowing it to become a good diffusion barrier and provide excellent oxidation resistance. The Nb-silicide coating exhibits most of the desired properties and can be most successfully accomplished by the molten salt coating technique.



## Experimental Methods

For the present study, the electron beam melted samples of the Nb-1Zr-0.1C alloy were obtained from Nuclear Fuel Complex (NFC), Hyderabad, India. Table 3.1 shows typical chemical composition of the alloy. As cast samples were subsequently deformed and annealed. Details of these could be obtained from reference [81].

**Table 3.1** Typical chemical composition of the Nb-1Zr-0.1C alloy.

Zr (wt. %)	C (wt. %)	Impurities	Nb (wt. %)
0.9-1.2	0.1-0.13	H – 4 ppm N – 41 ppm O – 132 ppm	Balance

### 3.1 Sample preparation and furnace fabrication

#### 3.1.1 Sample preparation:

Annealed samples of the Nb-1Zr-0.1C alloy were cut into pieces of 15 mm x 15 mm x 1 mm. Initially, these samples were mechanically polished using sand papers up to 1500 grade. These mechanically polished Nb samples were later fine-polished using colloidal silica suspension to get flat mirror surface finish. The surfaces of polished Nb samples were ultrasonically cleaned by submerging the samples in a solution of hydrogen peroxide and water at room temperature for 10 – 15 minutes with repeated renewal of the solution. This treatment gave a scratch and debris free mirror polished surface without any artefact.

#### 3.1.2 Design of furnace:

In order to carry out the coating experiments, a special furnace was needed to fulfil the following conditions:

- (1) The furnace should have provision to let out all the gaseous products generated during the experiment. As these gaseous products are hazardous in nature, special provisions are required to treat them prior releasing to the atmosphere.
- (2) As samples were to be inserted at coating temperature, special provisions were required to immerse the samples in the bath.
- (3) The salt in molten state contains substantial amount of halide ions, it was necessary that salt should be contained in an inert material and the moisture content within the furnace should be as low as possible.
- (4) Nb, Si and other ions are prone to oxidation at coating temperature, it was necessary to provide a cover of inert gas throughout the experiment to stop oxidation of the sample.
- (5) In addition provisions for adding Si and stirring during experiments were needed.

In order to incorporate all these aforementioned facilities in the design of the furnace, the following main features were considered:

- Sample size,
- Operable temperature range,
- Provision for gas purging and thermocouple ,
- Crucible size and material of the crucible.

A furnace with operable temperature of 1200°C was designed to carry out coating experiments. K-type thermocouple was selected considering the temperature range of the furnace and concentration of fluorides in the bath. Depending upon the size of samples, the quantity of the salt was calculated and based on the estimate of volume of sample and salts appropriate size of the crucible was selected. As the molten bath comprised of fluorides and chloride salts, high density alumina crucible was selected to avoid unwanted reactions

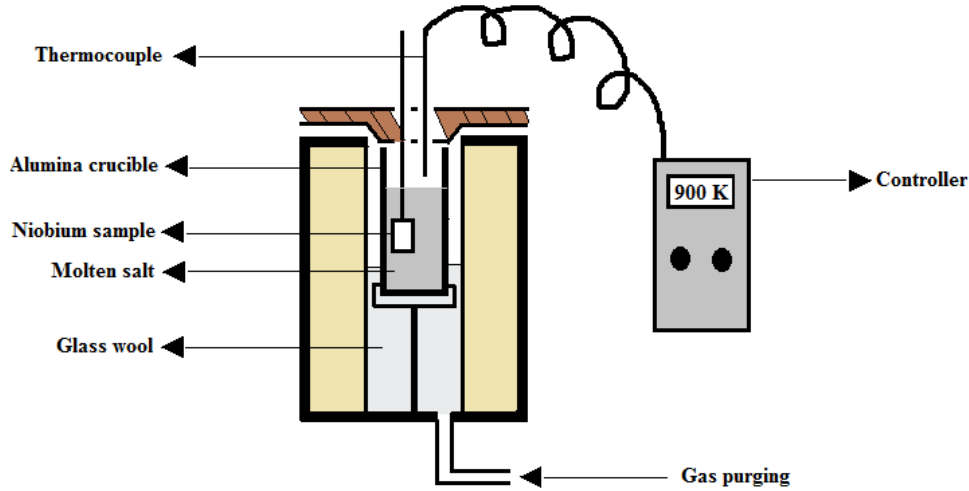
between the salt and the crucible. Provisions were made to purge the argon gas, to maintain the inert atmosphere while lowering the sample in the bath at high temperatures.

Figure 3.1 schematically represents the diagram showing the experimental setup of molten salt silicide coating. The setup consists of an alumina crucible filled with salt mixture placed inside the uniform heating zone of the furnace. The cylindrical region is covered by glass wool from the bottom region. A small space is allowed through glass wool for argon gas purging to remove the moisture and to carry out the experiments under inert atmospheric conditions. Series of thermocouples are inserted inside the furnace near to mid region of the crucible to measure the average temperature of the salt mixture. The thermocouples are connected to a temperature control system to control the furnace/system temperature to predefined value with an accuracy of  $\pm 5^{\circ}\text{C}$ . Prior to carrying out experiments, uniform heating zone in the furnace was identified and marked. The crucible was then placed at the middle of the heat zone and allowed to get thermalized to the temperature for half an hour. Once the desired temperature was achieved in the crucible, with the help of prior determined length of Nb wire, samples were carefully lowered. In order to ensure that samples were immersed inside the liquid salt, a tube acting as a guide was used. During insertion, drop in temperature was determined and the time was accounted from the point where temperature of the system reached to the desired value after inserting the sample. Typical time required to reach the equilibrium temperature was 3-5 minutes. Therefore, accuracy in the time measurement is  $\pm 5$  minutes.

### **3.2 Silicide coating on Nb alloy by Molten salt method**

For the purpose of silicide coating, a molten salt composing 36.58 mol% NaCl-36.58 mol% KCl- 21.95 mol% NaF – 4.89 mol%  $\text{Na}_2\text{SiF}_6$  were used. The intention behind using NaCl and KCl in this proportion was to have composition as close to the eutectic composition as possible [61]. The eutectic composition avoids the formation of two phase region (liquid +

solid) and therefore partitioning of components into any one of phase. After series of experiments, three compositions of the salts having different proportion of NaF, Si and  $\text{Na}_2\text{SiF}_6$  were determined. These are listed in Table 3.2.



**Figure 3.1:** Schematic representation of the experimental setup.

**Table 3.2** *Composition of molten salts used in the study*

Salt	Composition (mol %)				
	NaCl	KCl	NaF	$\text{Na}_2\text{SiF}_6$	Si
<b>S1</b>	36.58	36.58	21.95	4.89	-
<b>S2</b>	36.58	36.58	21.95	-	21.85
<b>S3</b>	36.58	36.58	21.95	4.89	21.85

About 150-200 g of salt mixture and silicon powder (21.85 mol% for salt mixture) was filled into an  $\text{Al}_2\text{O}_3$  crucible. The coating experiments were conducted at temperatures 800 and 900 °C for different time periods (2, 4 and 6 h). In order to provide inert atmosphere during experiment, high purity Ar gas was passed through the furnace tube. In order to remove moisture content from the salt mixture, it was heated at a temperature of 400 °C (673 K) for 2 hours and subsequently temperature was gradually raised to 800 °C (1073 K). The

mixture of salt started to melt at 700 °C, but to ensure homogeneous mixture, temperature was increased to 800 °C. Subsequently, required addition were made and temperature of the system was brought to the desired temperature of coating experiments. To provide silicide coating to the samples of the alloy, samples were suspended and immersed in molten salt with the help of a tungsten wire. After holding at the coating temperature for a predefined time period, the crucible was allowed to cool inside the furnace.

During the process of silicide coating, large amount of volatile species are generated. In order to trap these volatile species, the outgoing gases were allowed to pass through a column of water before leaving them out to the atmosphere. The coated samples were taken out, cleaned ultrasonically in acetone to remove any loosely embedded salt and were weighed to determine the weight gain. The dimensions of the coated samples were also measured to record for the changes in dimensions.

### **3.3 Oxidation and Annealing Experiments**

To study the oxidation behaviour of the as-coated Nb alloy before and after annealing, oxidation experiments were carried out at 1000 °C for a period of 1 h in an open air furnace at a heating rate of 2°C/min. For this purpose, to avoid inducing thermal shock to the coating, samples were inserted at room temperature and later, the temperature of 1000 °C was achieved gradually from room temperature with the heating rate of 2 °C/min.

The annealing treatment was carried out to facilitate the formation of Nb<sub>5</sub>Si<sub>3</sub> phase and for this purpose samples were subjected to a post silicide heat treatment. For this post silicide heat treatment, several heat treatments by varying temperature and time were carried out, as listed in Table 3.3. The heat treatment was carried out in a vacuum furnace maintaining vacuum at 10<sup>-6</sup> bar with the heating of 2°C/min was used.

**Table 3.3** *Time and temperature considered for heat treatment*

<b>Temperature (°C)</b>	<b>Time( h)</b>
1200	2,4
1350	6,10
1400	10

### **3.4 Characterization techniques**

In order to study morphology of various phases and to identify the various phases formed after heat-treatment and oxidation, detailed characterization was carried out using following techniques.

#### 3.4.1 Microstructural Investigations and Phase Identifications

The microstructures of the silicide coated samples were characterized using following methods:

- (a) Optical microscope,
- (b) Scanning electron microscope (SEM), and
- (c) X-ray diffraction.

##### (a) Optical microscopy

To prepare samples for optical microscopy, the specimens were mounted in conducting resin and were mechanically polished using successive grades of emery papers. Final mirror finishing of the samples was obtained using diamond paste with the particle size <1  $\mu\text{m}$ . Microstructural investigations were carried out on Zeiss microscope. Samples were examined in bright field as well as in differential interference contrast mode.

##### (b) Scanning electron microscopy (SEM)

Samples prepared for optical microscopy were directly used for SEM examination using the back-scattered and secondary electron modes of imaging. A field emission scanning electron microscope (FE-SEM-Zeiss Auriga) equipped with Oxford Instrument's Energy Dispersive Spectroscopy (EDS) detector was used for microstructural investigation as well as for

chemical composition analysis of various phases. The general SEM operating conditions used were,

Voltage = 20 keV, Detector- SE

(c) X-ray diffraction (XRD)

X-ray diffraction was used to identify phases present in the coated samples. X-ray diffraction patterns were obtained utilizing Cu-K $\alpha$  radiation with a wavelength of 1.5406 Å in a Bruker D8 Discover X-ray Diffractometer. XRD scans were obtained at a speed of 0.1°/sec. The XRD patterns of the various Nb-O and Nb-Si phases were analysed with the help of JCPDS data base software. Table 3.4 summarizes the crystallographic information of the various kinds of crystal structures present in the Nb-O and Nb-Si phases.

**Table 3.4** *Crystallographic information of the various kinds of crystal structures present in the Nb-O and Nb-Si phases*

Phase	Crystal structure	Lattice parameters
<b>Nb-O</b>		
NbO	Cubic	a= 0.421
NbO <sub>2</sub>	Tetragonal	a= 0.969 ; c = 0.598
Nb <sub>2</sub> O <sub>5</sub>	Tetragonal	a= 2.044 ; c = 0.382
<b>Nb-Si</b>		
NbSi <sub>2</sub>	Hexagonal	a= 0.481 ; c = 0.659
Nb <sub>5</sub> Si <sub>3</sub>	Tetragonal	a = 0.657; c=1.188

### 3.4.2 Composition analysis

#### (a) X-ray Photoelectron spectroscopy (XPS)

In order to identify various states of elements present in the salts of different compositions, S1, S2, S3, (given in Table 3.2), X-ray Photoelectron Spectroscopy (XPS) of the salts was carried out. For XPS the SPECS instrument, a PHOBIOS 100/150 Delay Line Detector (DLD) with 385 W, 13.85 kV and 175.6 nA (sample current) and Al K $\alpha$  (1486.6 eV) dual anode as the source was used. The XPS signal was taken with pass energy of 50 eV. As an internal reference for the absolute binding energy, the C-1s peak (284.5 eV) was used.

#### (b) Ion chromatography

Metrohm ion chromatography instrument with detectability limit of 0.01 ppm was used to determine the concentration of F<sup>-</sup>, Si ion and the etched Nb in the salts (S1, S2 and S3). In this technique, ions were separated on an ion exchange column followed by a suppressor column to remove eluent ions of high conductance. A conductivity detector was used to measure conductance of ions.



---

# Optimization of Coating Parameters

---

This chapter deals with the optimization of several variables, mainly including composition of salt, time and temperature to develop a uniform silicide coating on the Nb alloy. A eutectic salt mixture comprising NaCl, KCl, NaF and two Si sources- $\text{Na}_2\text{SiF}_6$  and Si powder was selected to study the development of silicide coating on Nb alloys. In order to facilitate the coating process, the bath was stirred at different rates intermittently and its effect on coating was also studied. The concentration of Si containing constituents were also varied and optimum composition of the salt was worked out. Experiments of adding of pure silicon intermittently during the coating were also carried to achieve the optimum thickness of the coatings. Optimized temperature and time window was obtained by systematically varying temperature and time of coating experiments and estimating the thickness and variation in the thickness of the coating with temperature and times. For this purpose, cross sections of the Si-coated samples were characterized using optical, SEM and XRD techniques. These results are summarized in the following sections

## 4.1 Optimization of Silicide Coating Process

### 4.1.1 Optimization of composition of salt

Various experiments were carried out to optimize the composition of the bath to obtain a uniform coating with maximum thickness.

- (a) First set of experiments were carried out with the composition of the salt as mentioned in chapter 3 (Table 3.2).
- (b) In the second set of experiments, the quantity of Si sources was varied. No significant change in the thickness of the coating was observed even when the quantity of the Si powder was doubled with respect to the first set of experiments. This set of experiment clearly

showed that to increase the thickness of coating, increasing the concentration of Si sources in form of Si powder is not effective. In the third set of experiments, only Si sources, i.e.,  $\text{Na}_2\text{SiF}_6$  and Si powder with eutectic salt mixture of NaCl-KCl were considered. In spite of varying the composition of  $\text{Na}_2\text{SiF}_6$  and Si in the molten bath, samples did not show presence of any coating. Absence of coating in spite of the presence of two sources of Si suggested the importance of role of the etchant, NaF, in the formation of coating.

Based on these observations, it was clear that to obtain the silicide coating, the presence of  $\text{Na}_2\text{SiF}_6$ , powder Si and NaF in the eutectic salt of NaCl-KCl is required. In the next step, a series of coating experiments were carried out using optimized composition of the bath. The optimum composition of the salt which could provide uniform coating is shown in Table 3.2.

#### 4.1.2 Effect of stirring

To study the effect of the continuous stirring of the salt, two sets of experiments were carried out. Samples were coated using the optimized salt composition at 800 °C; 2 h with (a) continuous stirring of the salt and (b) intermittent stirring of the salt. Fig. 4.1 shows typical SEM micrograph of the cross section of the sample coated at 800 °C in the continuous stirred molten bath. Presence of non-uniform and non-homogenous  $\text{NbSi}_2$  coating on these samples can be noticed in the Fig. 4.1. This result clearly showed adverse effect of stirring on the process of development of the coating on Nb alloy samples. Therefore, continuous stirring of the salt was not considered for further experiments to optimize time and temperature. On the other hand, intermittent stirring of the salt before lowering the sample in the molten salt showed favourable results and therefore, intermittent stirring was pursued for further experiments.

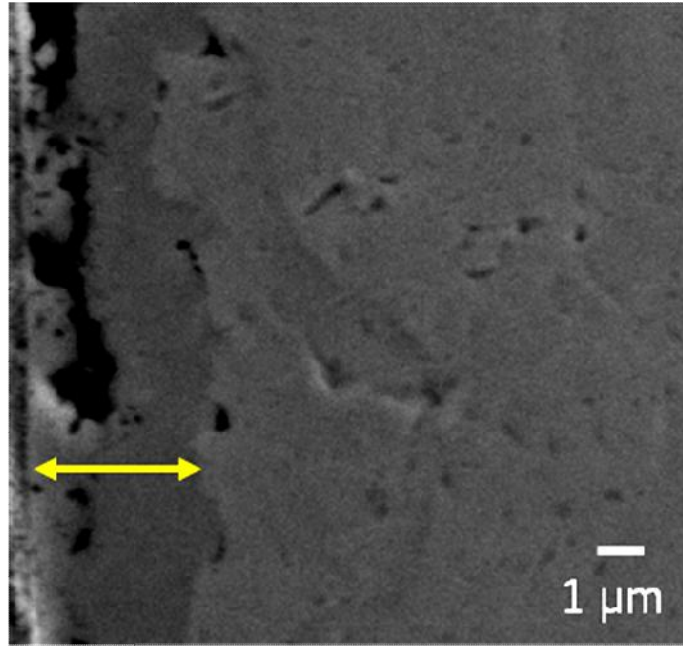


**Figure 4.1:** SEM micrographs of cross sectional view of Nb-Si coating produced by molten salt method with continuous stirred bath.

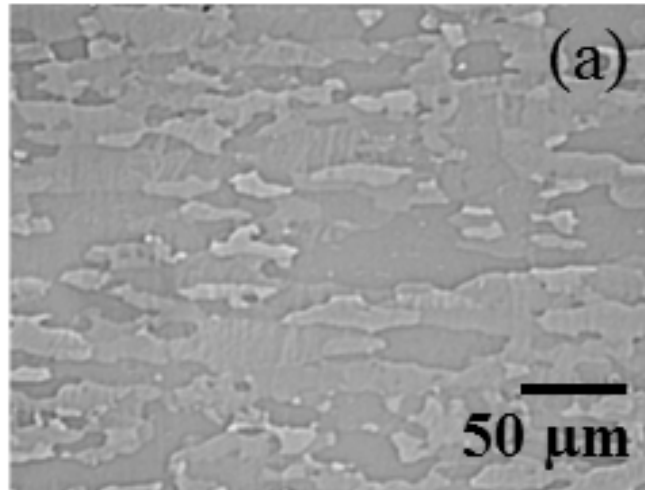
#### 4.1.3 Optimization of time and temperature

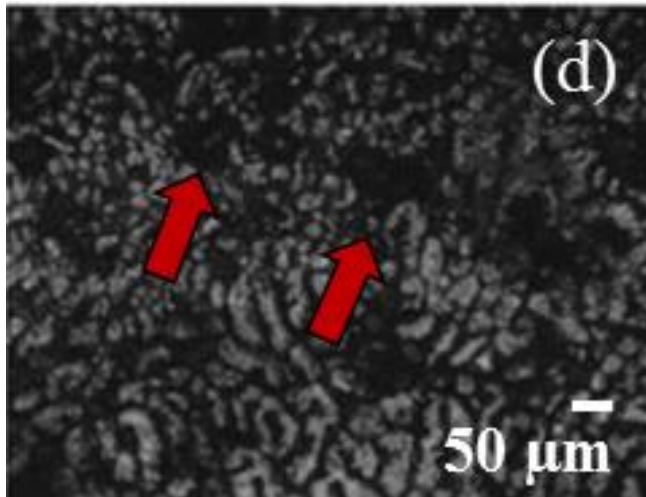
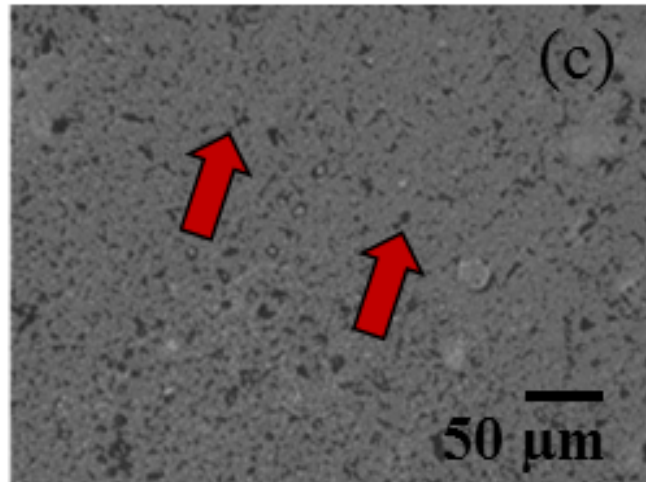
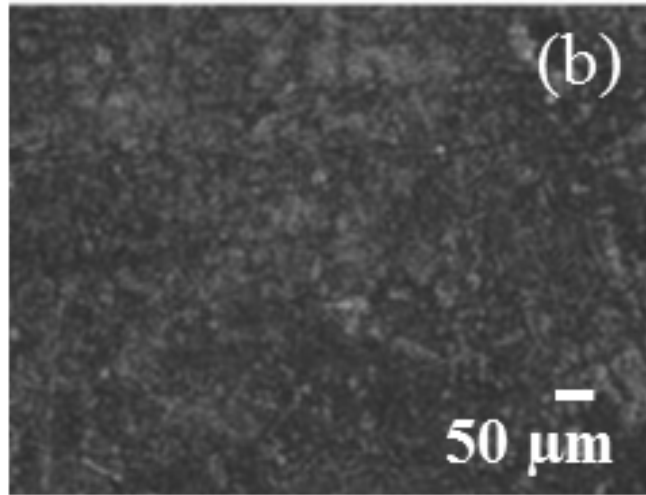
In order to obtain the optimized temperature and time window, coating experiments were carried out at different temperatures. As the eutectic temperature of the salt mixture is ( $\sim 750$  °C), all the temperatures selected for the experiments were kept above this temperature. Upon exceeding temperature of the bath above 1000 °C, extremely poor quality coatings were observed and therefore the most suitable temperatures where coating could be successfully developed were identified as 800 °C and 900 °C. By changing the duration of coating at these temperatures further optimization with respect to time was carried out.

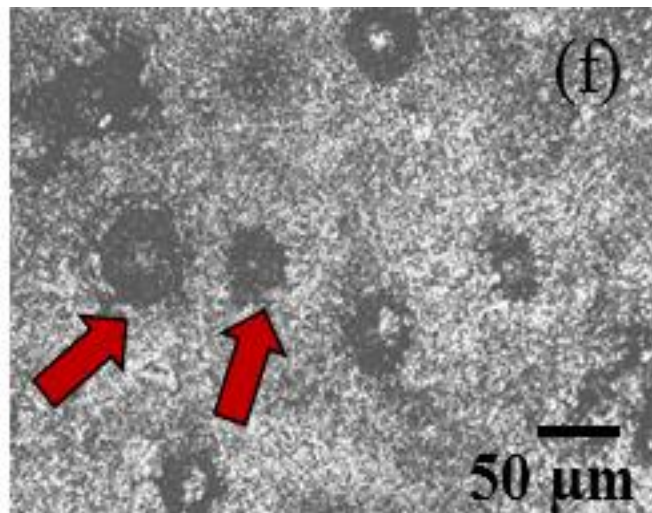
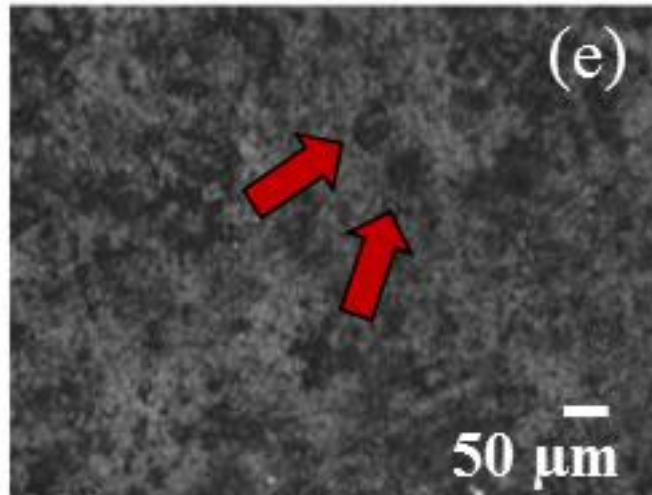
Figs. 4.2 (b-d) show optical images of the Nb alloy samples coated with Si at 800 °C. For the purpose of comparison, the surface of uncoated sample is shown in Fig. 4.2 (a). The surface morphologies of the samples dipped at 800 °C for 2 and 4 h showed presence of smooth coating (Fig. 4.2 (b-c)), whereas samples which dipped for 6 h showed granular appearance (Fig. 4.2 (d)). In many places formation of pits was observed at the surface of

samples dipped for 6 h. In contrast, samples dipped for 2 and 4 h showed nearly pit free surface. The sizes of pits increased with temperature and time. For example surface of the samples coated at 900 °C for 6h (Fig.4.2 (f)) when examined under microscope showed much larger pits (compare Fig. 4.2 (f) with Figs.4.2(d)-(e)).

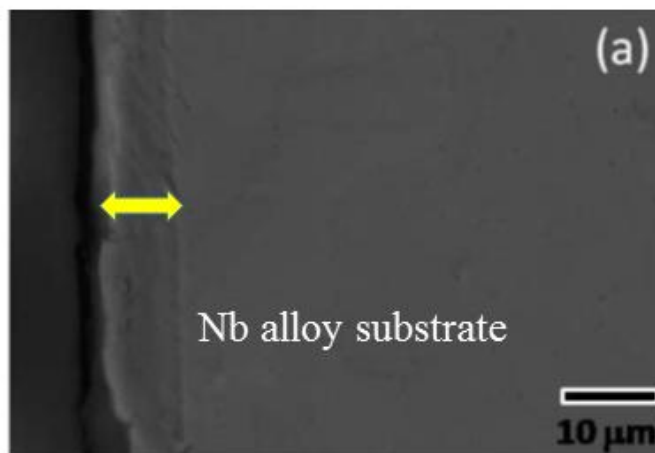
Figs. 4.3 (a-c) show SEM images of the cross sections of samples with the different dip time at 800 °C. An increase in the coating thickness from 8  $\mu\text{m}$  to 12  $\mu\text{m}$  was noticed with increase in the dip time from 2 h to 4 h. Upon further increase in the immersion time from 4 h to 6 h, a decrease in the coating thickness from 12 to 5  $\mu\text{m}$  was observed. The composition profile across the coating thickness showed that the silicide phase mainly comprised the NbSi<sub>2</sub> phase (Fig. 4.4 (a-c)).

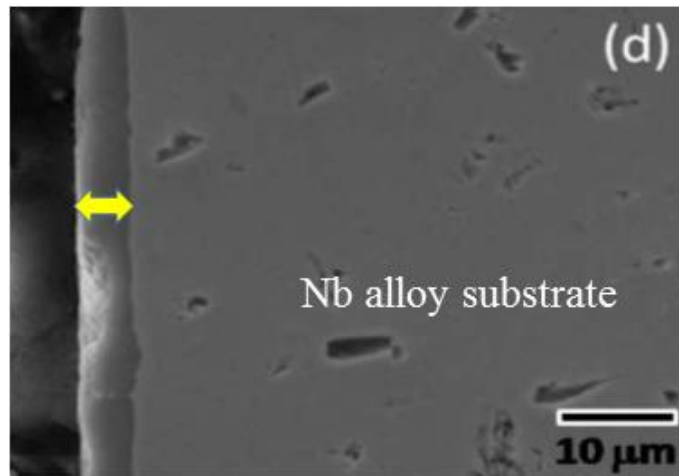
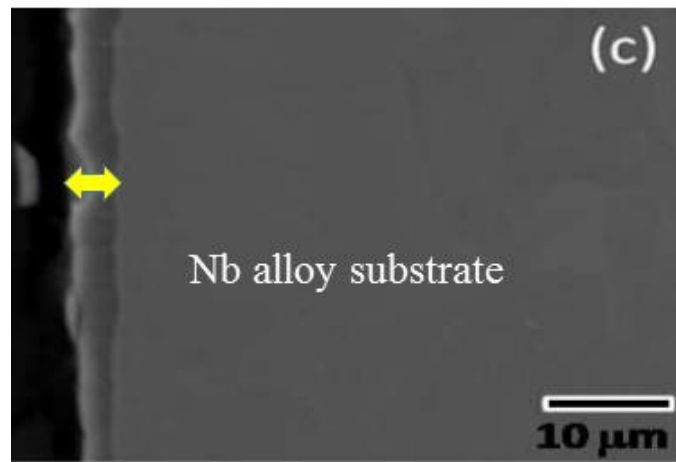
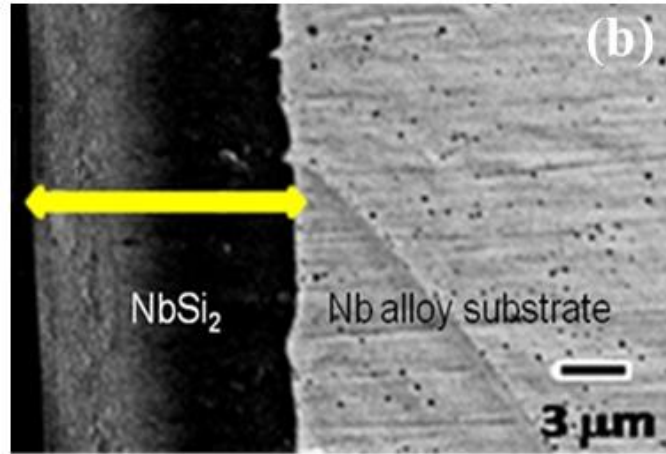


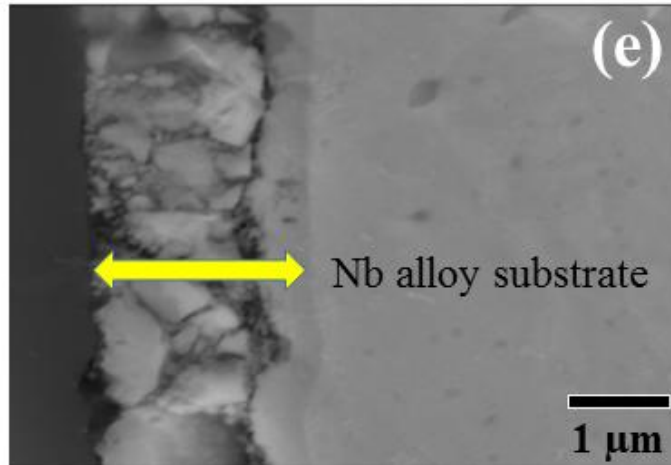




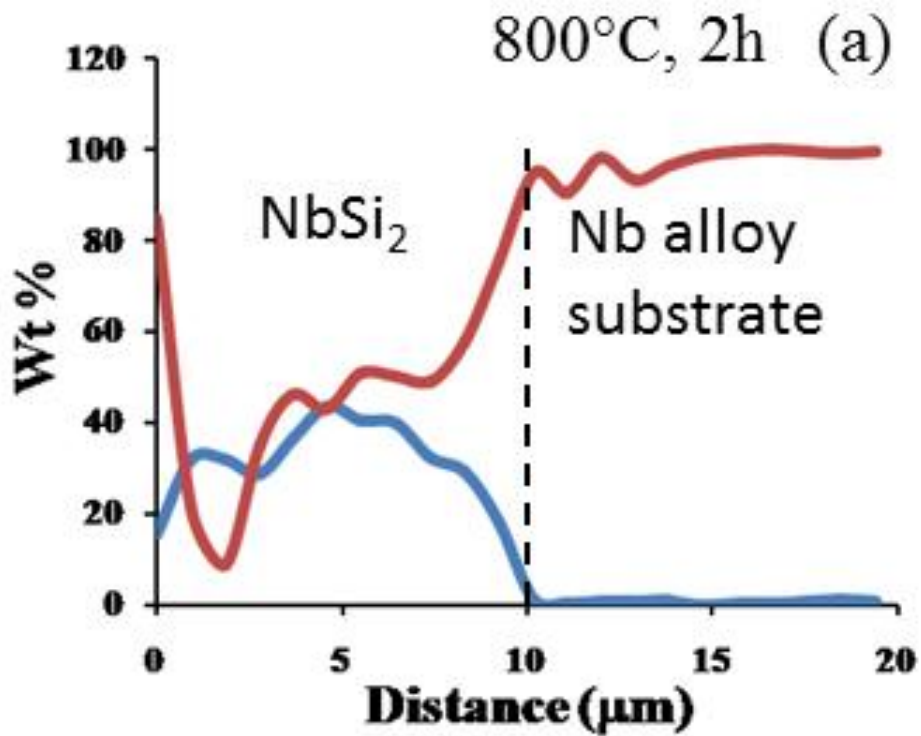
**Figure 4.2:** Optical images showing surface morphology of Si coated Nb alloy samples for dip time of (a) bare Nb alloy, (b) 2 h, (c) 4h, (d) 6 h (800 °C), (e) 2h and (f) 6 h (900 °C), location of the pits are marked in the figure.

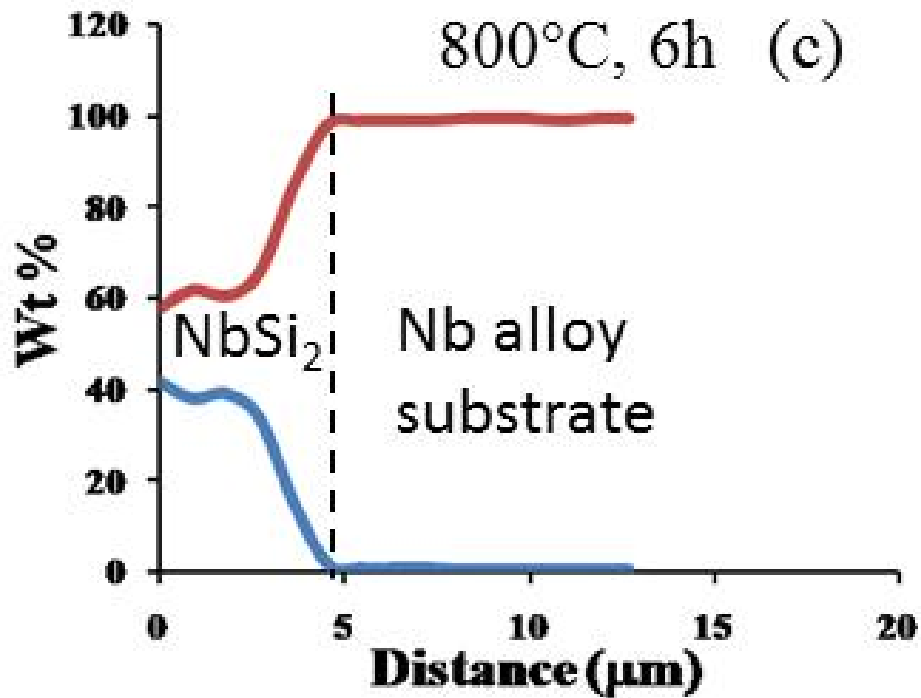
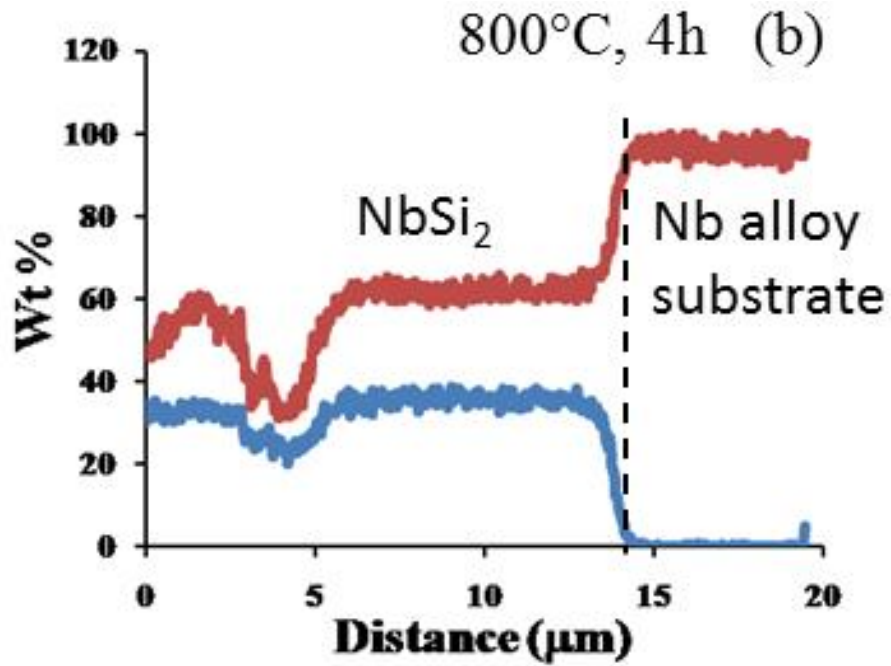






**Figure 4.3:** SEM micrographs of cross sectional view of Nb-Si coating produced by molten salt method at different time periods (a) 2 h, (b) 4 h, (c) 6 h (800 °C), (d) 2 h and (e) 6 h (900 °C).





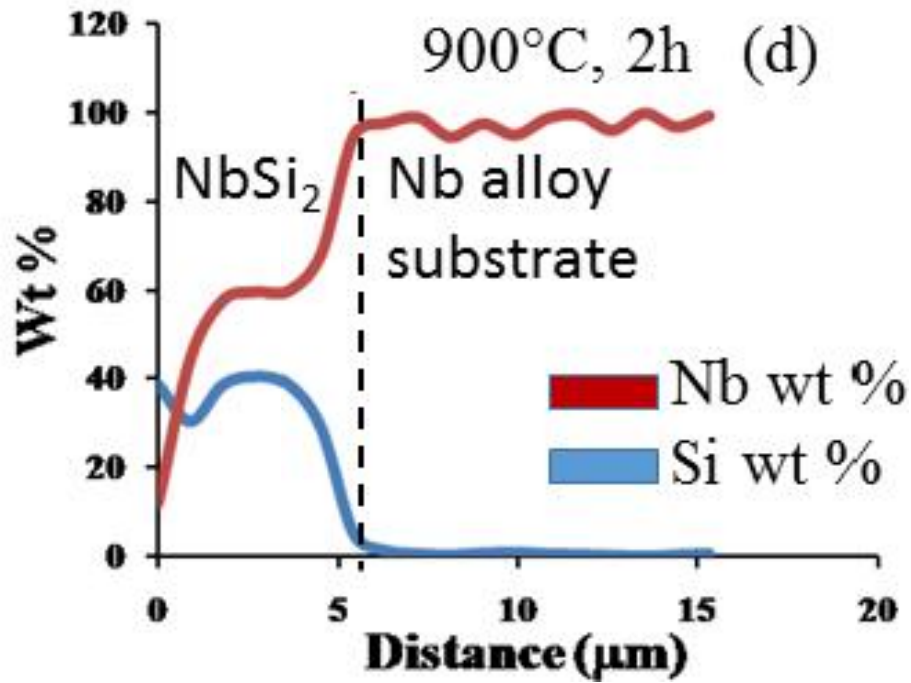


Figure 4.4: Composition profiles of Si coated samples by EDS at (a) 2 h, (b) 4 h, (c) 6 h (800 °C) and (d) 2 h (900 °C).

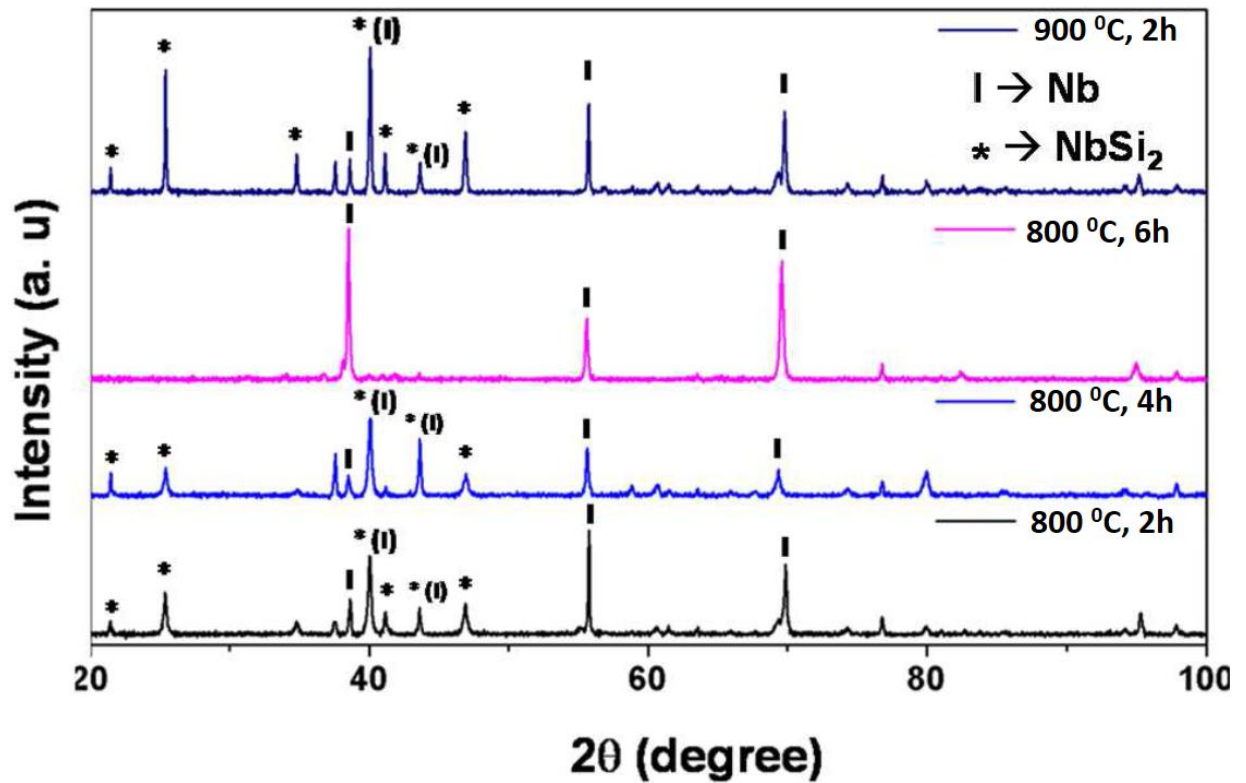


Figure 4.5: XRD patterns showing formation of different Nb-Si phases at 800 °C and 900 °C.

Fig. 4.5 shows the XRD line profiles of the coated samples at 800 °C. The sample immersed for 2, 4 and 6 h showed that the majority of the peaks pertain to the phase NbSi<sub>2</sub>. For the purpose of comparison, samples were also coated at 900 °C. Optical and SEM images of the sample dipped for 2 h are shown in Fig. 4.2(c) and 4.3(d) respectively. The surface morphology showed more number of pits on the surface in comparison to the surface of the sample coated at 800 °C for 2 h. The corresponding composition profile of the cross section of the coating is shown in Fig. 4.4 (d). The XRD pattern of this sample also showed the appearance of NbSi<sub>2</sub> reflections confirming the EDS results (Fig. 4.5).

## 4.2 Discussion

Based on the optimization study on silicide coating by the molten salt method, following inferences could be drawn:

- (i) The continuous stirring of the molten salt results in the formation of non-uniform coating.
- (ii) In order to achieve the silicide coating on the Nb alloy, presence of all the three constituents, viz., Na<sub>2</sub>SiF<sub>6</sub>, NaF and Si is required.
- (iii) The optimum temperature and time for the silicide coating is 800 °C and 4 h respectively. Increasing time or temperature of coating resulted in the formation of pits.
- (iv) Direct mixing of powder Si as single constituent or along with Na<sub>2</sub>SiF<sub>6</sub> shows deposition of silicon on the substrate is not a single step process but it is a multistep process.

It can, therefore, be understood that the continuous stirring of the salt leads to the non-uniform coating because as the salt is stirred the deposition time for each Si species i.e. time taken by this species from salt to the surface of substrate varies which results in formation of non-uniform coating.

Si produced by various chemical reactions diffuses onto the metal surface. With the consumption of Si by metal, the concentration of Si ions depletes. In addition to this, evaporation of SiF<sub>4</sub> (a volatile species) also aggravates the depletion of the concentration of Si and therefore the diffusion of silicon on the Nb surface retards with time. This suggests that if the Si is added, depletion of Si can be overcome and in such cases further deposition of Si is possible. However, present study shows that upon increasing time or temperature of coating, thickness of coating reduces as well as presence of pits is also observed. This clearly suggests dissolution of the coating, which means the process of silicide coatings is a net result of two counter processes: deposition and etching of silicon from the surface of the sample. One such possible source of etching could be the fluoride ions, as one of the constituent of the salt (Na<sub>2</sub>SiF<sub>6</sub>) which is a source of providing Si ions could also be a source of fluoride ions. This could be attributed to fluoride ion assisted etching of nascent Si layer deposited on the alloy surface. The possible source of F<sup>-</sup> ion is decomposition of Na<sub>2</sub>SiF<sub>6</sub>. In such cases, with the continuous decomposition of Na<sub>2</sub>SiF<sub>6</sub> would lead to the build-up of fluoride ions. In effect, the presence of excess fluoride ions initiates etching of the Nb surface. Therefore, the resultant silicide coating thickness on Nb is a net effect of two counter reactions of deposition of Si ions and etching of deposited Si ions by fluorides. Such effect of etching process could be noticed in the microstructures of the samples immersed for 6 h at 800 °C (Fig. 4.1 (b)). This is also corroborated by the fact that the thickness of the coating reduced in samples immersed for 6 h at 800 °C as well as in the sample which was immersed at higher temperature of 900 °C.

Recently, Vishwanadh *et al.* [82] have shown that during silicide deposition process, the Nb<sub>5</sub>Si<sub>3</sub> phase forms as thin layer sandwiched between the metal and the NbSi<sub>2</sub> phase. However, in the present study, the formation of Nb<sub>5</sub>Si<sub>3</sub> phase could not be detected from the present investigations. The absence of the Nb<sub>5</sub>Si<sub>3</sub> phase could be attributed to the low

temperature of the bath as formation of this phase occurs at and above 1200 °C during silicide coating process [61].

### **4.3 Summary**

The optimum time and temperature to produce maximum thickness (~12 µm) of silicide coating onto Nb alloy was found to be 4 h at 800 °C. XRD analysis showed the formation of single phase hexagonal NbSi<sub>2</sub> at 800 °C. An increase in the immersing time and temperature resulted in buildup of F<sup>-</sup> ions which etched out the silicide phases resulting in the reduction of the coating thickness. Also, continuous stirring of the molten bath leads to the formation of non-uniform NbSi<sub>2</sub> coating.



## Mechanisms of molten salt coating process

In the present chapter, systematic attempts made to study the mechanism of silicide coating on the Nb alloy are discussed. For this purpose, experiments containing different Si species as starting reagents and their combinations to deposit Si on the Nb alloy substrate have been carried out. Three sets of experiments with different salt compositions, S1, S2, S3, (given in Table 5.1) were carried out at the optimized conditions of coating (shown in Chapter 4) of 800 °C for a time period of 4 h.

**Table 5.1** Composition of molten salts used in the study.

Salt	Composition (mol %)				
	NaCl	KCl	NaF	Na <sub>2</sub> SiF <sub>6</sub>	Si
<b>S1</b>	36.58	36.58	21.95	4.89	-
<b>S2</b>	36.58	36.58	21.95	-	21.85
<b>S3</b>	36.58	36.58	21.95	4.89	21.85

By varying concentrations of Na<sub>2</sub>SiF<sub>6</sub> and Si, three salts were produced to develop coatings on samples at 800°C. The surface morphologies of the coated samples were examined under optical microscope. X-ray diffraction (XRD) patterns taken from the surface of the samples were analyzed to identify different Nb-Si phases formed. Also, cross sections specimens were prepared from the coated samples. Cross sectional microstructures were examined under field emission scanning electron microscope (FESEM) equipped with energy dispersive X-ray (EDS) analyzer.

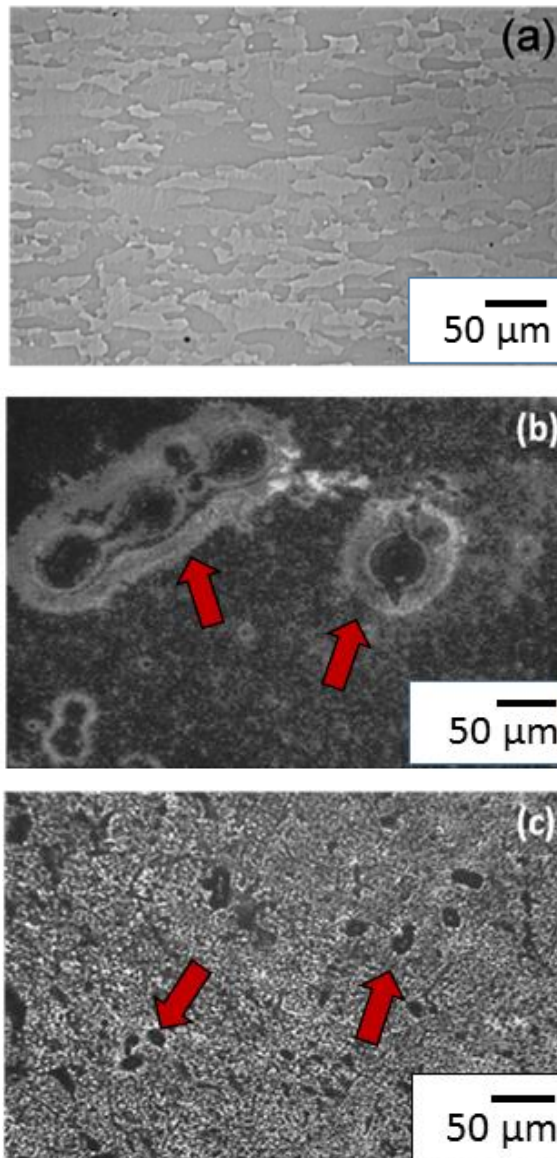
Post experiments, all the salts were examined by X-ray Photoelectron spectroscopy (XPS) to determine various states of ions present in the salts and by ion chromatography to determine the concentration of ions and the etched Nb in the salts. Based on these findings a mechanism of formation of silicide coating on Nb alloys by molten salt technique has been proposed. Thermochemical calculation software, FactSage 7.0, was used to examine the feasibility and applicability of the all-possible reactions involved during coating.

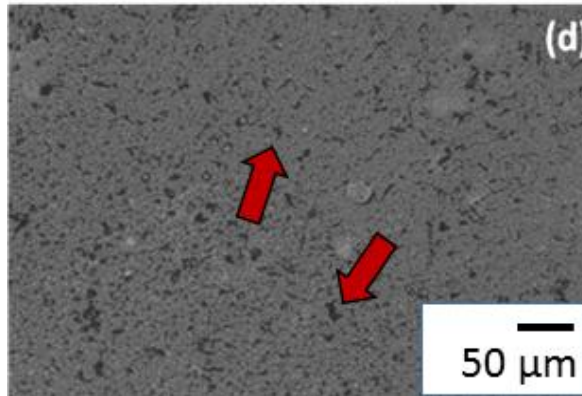
### 5.1 Microstructural Characterization

Fig. 5.1 shows surfaces of samples subjected to silicide coating using various salt compositions. For the purpose of comparison, image of bare Nb alloy sample is also included (Fig. 5.1 (a)). Surface morphologies of the samples which were dipped in S1 salt showed formation of large number of pits (indicated by arrows) on the surface (Fig. 5.1 (b)), whereas the samples dipped in S2 and S3 showed presence of relatively smooth coating surface (Fig. 5.1 (c-d)). Typical diameters of pits were close to 50  $\mu\text{m}$ . It may be noted that S1 salt does not contain any Si powder. Therefore, etching effect of  $\text{F}^-$  ions is more pronounced in this case. Appearance of peripheral rings around each pit suggests that growth of pits has occurred on the surface as well as along the depth. Detailed investigations on the surface failed to show the presence of Si coating on the samples dipped in salt S1. This suggests that the kinetics of deposition of Si is very sluggish in this case. Such large pits have not been observed in the samples dipped in salts S2 and S3. Rather, entire surfaces were covered with Si coating in these samples. It may be noted that in both the molten salts (S2 and S3) Si was present in the powdered form. It, therefore, clearly suggests that the kinetics of Si deposition can be increased with the addition of Si powder.

The surface morphology of the coating obtained from molten salt S3 is smoother in comparison to the coating surfaces of the samples obtained from salt S2 (compare Fig. 5.1 (c-d)). In the case of samples dipped in salts S2, isolated pits ( $\sim 15 \mu\text{m}$ ) were observed (Fig. 5.1

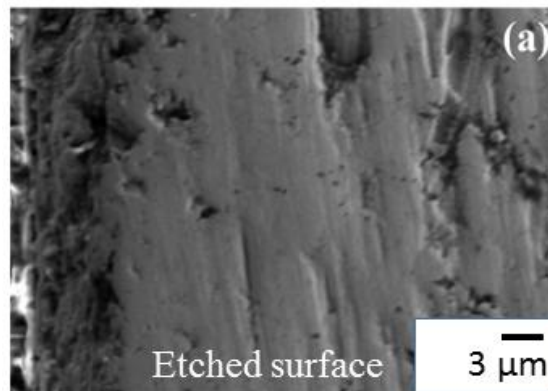
(c) whereas for the samples dipped in salt S3, the size of the pits as well as their number density was considerably low (Fig. 5.1 (d)). This difference in the size of pits and density is suggestive of the fact that the kinetics of depositions were faster in the case of the samples dipped in salts S3.





**Figure 5.1:** Optical images showing surface morphology of Si coated Nb alloy produced when samples were dipped into (a) bare Nb alloy, (b) S1, (c) S2 and (d) S3; location of the pits are marked in the figure.

In order to examine the thickness of the coating, cross-section samples were examined under SEM (Figs. 5.2 (a-c)). No coating was observed in the case of samples dipped in salt S1 (Fig. 5.2 (a)). This observation is consistent with the results reported in the literature [60]. The coating thickness of  $\sim 7 \mu\text{m}$  was observed when the samples were dipped into salt (S2) comprising pure Si powder as a Si source. In comparison, coating thickness was found to increase to  $\sim 12 \mu\text{m}$  when the samples were dipped into salt (S3) comprising pure Si powder and  $\text{Na}_2\text{SiF}_6$  in the supporting salt.



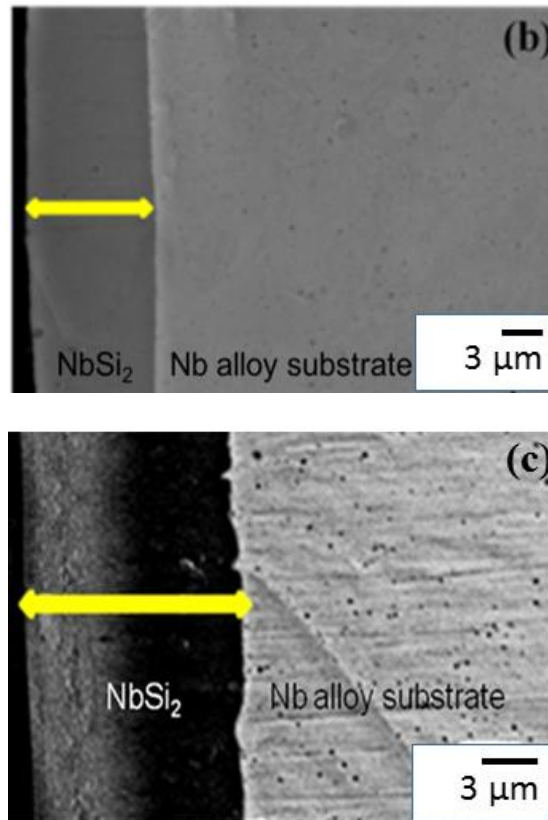
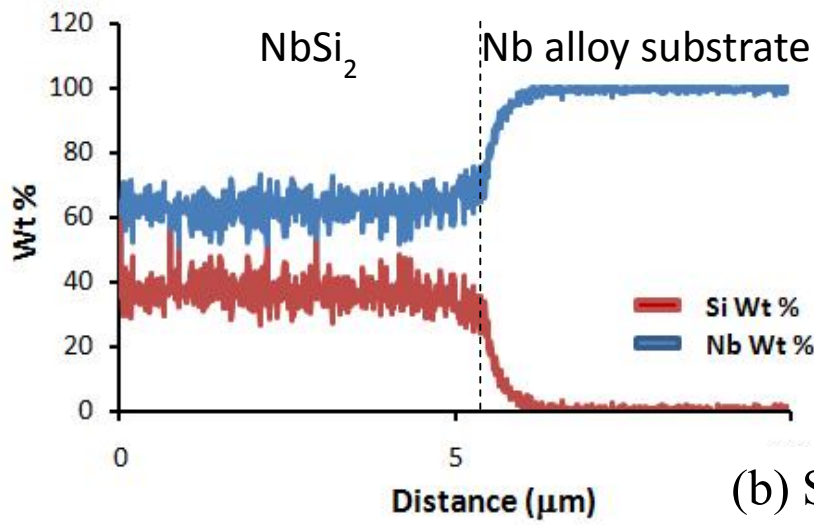


**Figure 5.2:** SEM micrographs of cross sectional view of Nb-Si coating produced when samples were dipped into salt (a) S1, (b) S2 and (c) S3

In the latter two cases, the composition profile obtained from EDS across the coating thickness showed that Nb:Si atomic ratio is 67:33 ( $\pm 0.5$ ), which is close to the ideal ratio of NbSi<sub>2</sub> (Figs. 5.3 (a-b)). Therefore, the phase could be assigned as NbSi<sub>2</sub>. In order to confirm the presence of this phase, XRD patterns from the coated surfaces of the samples were obtained (Figs. 5.4 (a-c)). The XRD patterns obtained from the coated surface of the samples dipped into the salt S1 showed presence of metallic- Nb, as all high intensity peaks could be indexed in terms of bcc structure (JCPDS no. 35-0789). This observation along with the observation of the cross-section microstructure confirmed that no coating has been developed on samples dipped into salt S1. The XRD profiles of the samples dipped in molten salts S2 and S3, on the other hand, showed the presence of peaks pertaining to NbSi<sub>2</sub> reflections (Fig. 5.4 (b-c)) (JCPDS no. 72-1032) and thereby confirming the EDS results.

(a) S2



(b) S3

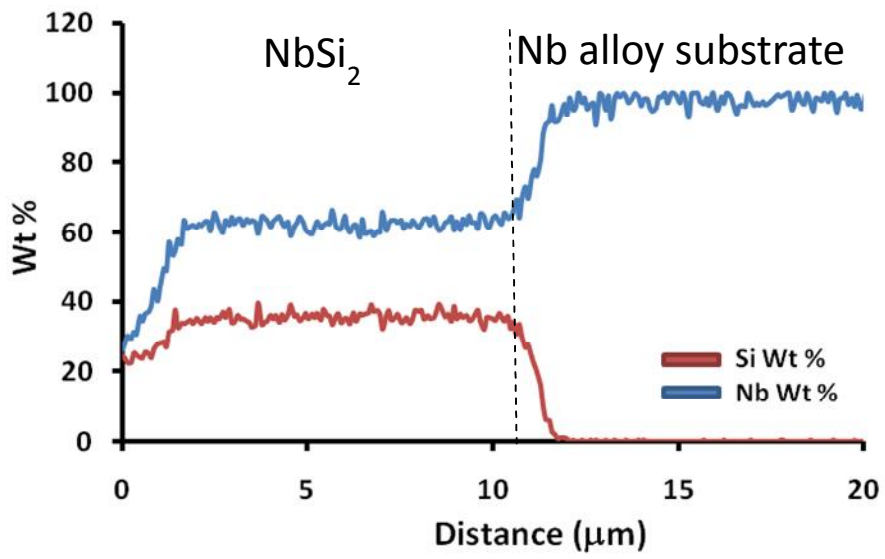


**Figure 5.3:** Composition profiles of Si coated samples by EDS dipped in salt (a) S2 and (b) S3.

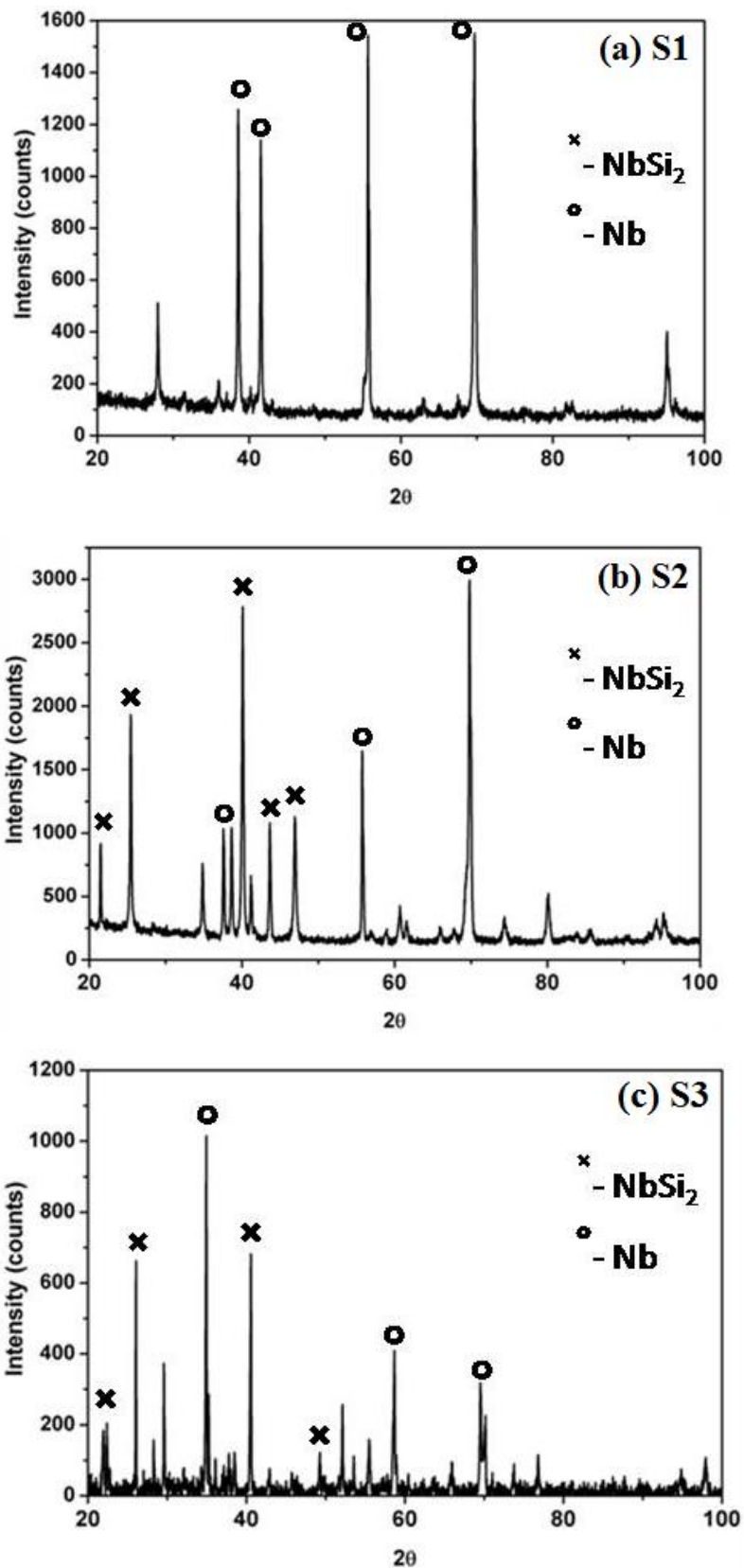


**Figure 5.4:** XRD patterns showing formation of  $\text{NbSi}_2$  phase formed when samples were dipped into salt (a) S1, (b) S2 and (c) S3.

Rietveld analysis of the XRD data was carried out to determine the volume fraction of the phases present in the samples dipped in various salts. The results obtained are presented in Table 5.2. Based on this analysis, it is established that NbSi<sub>2</sub> has a hexagonal structure with lattice parameters a = 4.80 Å, c = 6.59 Å and Nb has a bcc structure with a = 3.30 Å. These lattice parameters match closely with the values reported in the literature. (JCPDS no. 72-1032, JCPDS no. 35-0789)

**Table 5.2** *Volume percentage of phases present in samples dipped in various salts estimated by Rietveld analysis.*

<b>Salt</b>	<b>% Nb present</b>	<b>% NbSi<sub>2</sub> present</b>
<b>S1</b>	100	-
<b>S2</b>	12.3	87.7
<b>S3</b>	4.3	95.7

Ion chromatographic analysis (Table 5.3) showed highest fluoride concentration in salt S1 and lowest in salt S2. This concentration variation in the salts could be attributed to the formation of larger number of pits on the samples dipped in salt S1.

**Table 5.3** *Nb and F<sup>-</sup> ion concentration in various molten salts estimated by ion chromatography.*

<b>Salt</b>	<b>F<sup>-</sup> ion (mg/g)</b>	<b>Nb(µg/g)</b>	<b>SiO<sub>2</sub> (mg/g)</b>	<b>Ratio of F<sup>-</sup> /SiO<sub>2</sub></b>
<b>S1</b>	287	2367	100	2.87
<b>S2</b>	51.1	49.4	40	1.27
<b>S3</b>	86	17.9	160	0.54

In order to determine the electronic state of the Si in salts, XPS spectrum was obtained from each salt. Figs. 5.5 (a-c) show the Si-2p core level for the molten salt bath with

three different salt compositions where XPS peaks are observed at 101.9 eV, 101.25 eV, 100.9 eV for the salts –S1, S2 and S3, respectively.

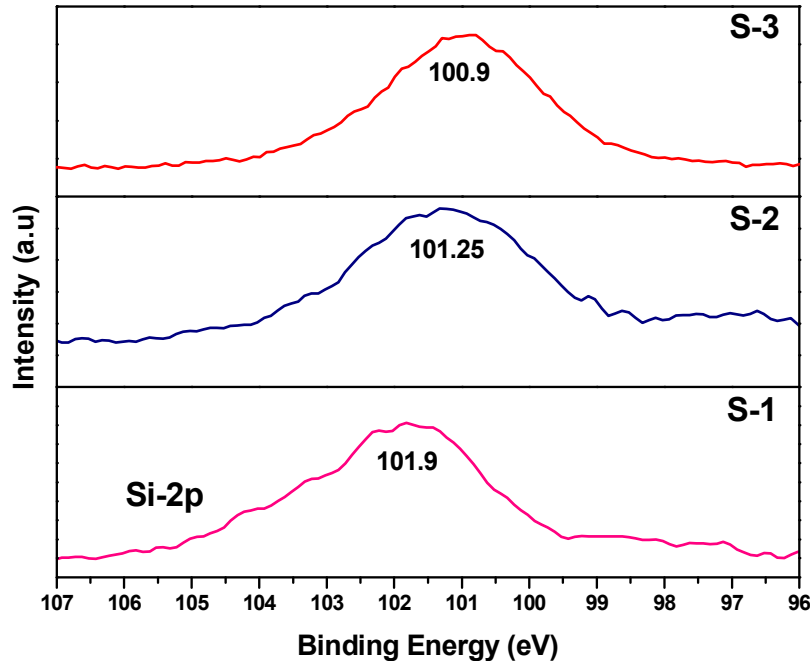


**Figure 5.5:** Si-2p XPS spectra of the molten salt bath (a) S1, (b) S2 and (c) S3.

The binding energy of Si-2p for SiO<sub>2</sub> is 103.6 eV [83]. The  $\Delta E$  between the Si-2p<sub>1/2</sub> and Si-2p<sub>3/2</sub> is reported to be 0.6 eV with a FWHM of 0.65 eV [84,85]. Thereby it is quite clear that there is a very narrow margin of difference between the Si-2p<sub>1/2</sub> and Si-2p<sub>3/2</sub> binding energies. The Marstein group provided the XPS spectra of the surface and bulk photoetched silicon which were fabricated for the antireflection properties. They have fitted the Si-2p<sub>3/2</sub> peak with a binding energy of 99.4, 100.4 eV, 101.4 eV, 102.5 eV, 103.6 eV, and 99.7 eV. The above initial five peaks represents Si (Si<sup>0</sup>), Si<sub>2</sub>O (Si<sup>+1</sup>), SiO (Si<sup>+2</sup>), Si<sub>2</sub>O<sub>3</sub> (Si<sup>+3</sup>), and SiO<sub>2</sub> (Si<sup>+4</sup>) respectively. The peak with binding energy of 99.7 eV was not exactly identified by them [86]. They have used a monochromated (X-ray) source of Al K $\alpha$  (1486.6 eV) at zero angle of emission operated at 1 mA and 15 kV. Rochet group similarly has identified for the (n+) Si (001)-2 and the hydrated surface the resultant effect of the spin –

orbit splitting for Si-2p, however, the  $\Delta E$  between the Si2p<sub>3/2</sub> and Si2p<sub>1/2</sub> was found to be 0.65 eV [87]. They have attributed the different Si<sup>1+</sup> and Si<sup>2+</sup> of the Si2p<sub>3/2</sub> to 99.65 and 100.31 eV, respectively, primarily motivated by the earlier works of Uhrberg group and Yeom group [88,89]. They have utilized a Synchrotron beamline source of 130 eV with a very high resolution of 30meV. However, in the present study the exact spin orbit splitting in the Si-2p core level XPS peak was not observed. A non-monochromatised source of Al K $\alpha$  (1486.6 eV) with the best resolution of 0.89 eV was used. Upon deconvolution it was obtained that the 2p<sub>1/2</sub> and that of 2p<sub>3/2</sub> were consistent with the earlier literature [90]. Primarily, the Si-2p XPS peaks were observed at 101.9 eV, 101.1 eV, 100.9 eV for the salts – S1, S2 and S3 respectively (Fig. 5.6). The Fig. 5.6 represents de-convoluted spectrum of Si-2p<sub>3/2</sub> for the three different samples, where Shirley function for the base line correction and the Gaussian function for the deconvolution of the peaks were used. Progressive shift in the position of peak observed in different salts was an indicator of the fact that Si in these salts was present in the different electronic environment. Upon deconvoluting these peaks (Fig. 5.6), it was observed that XPS data from salt S1 could be best fitted with single peak at 102.7 eV. The data from salt S2 sample could also be fitted into three peaks with value of 101.31, 104.5, 96.9 eV. The data from salt S3 has three deconvoluted peaks at (103.1, 100.9 and 97.6) eV respectively.

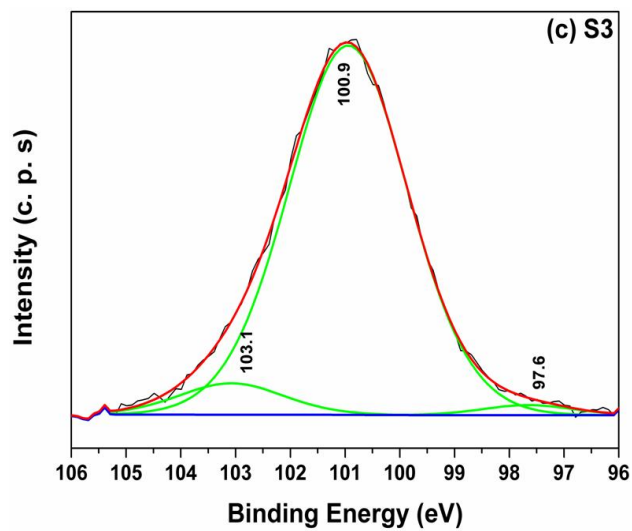
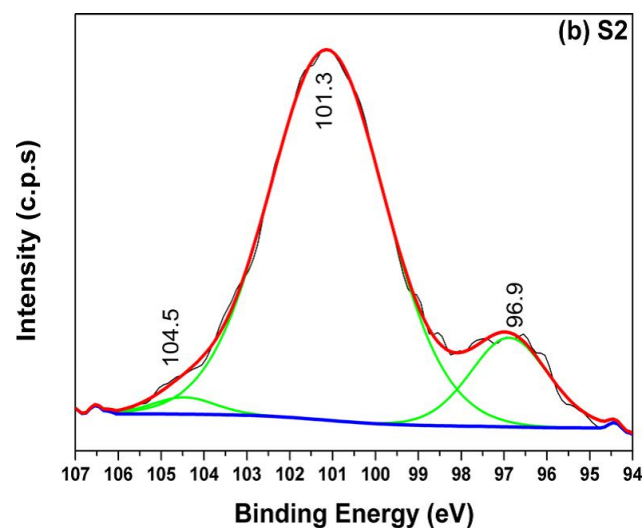
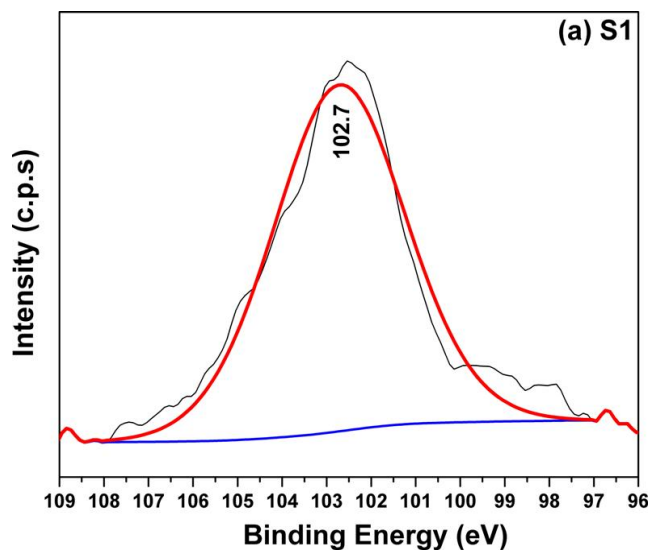
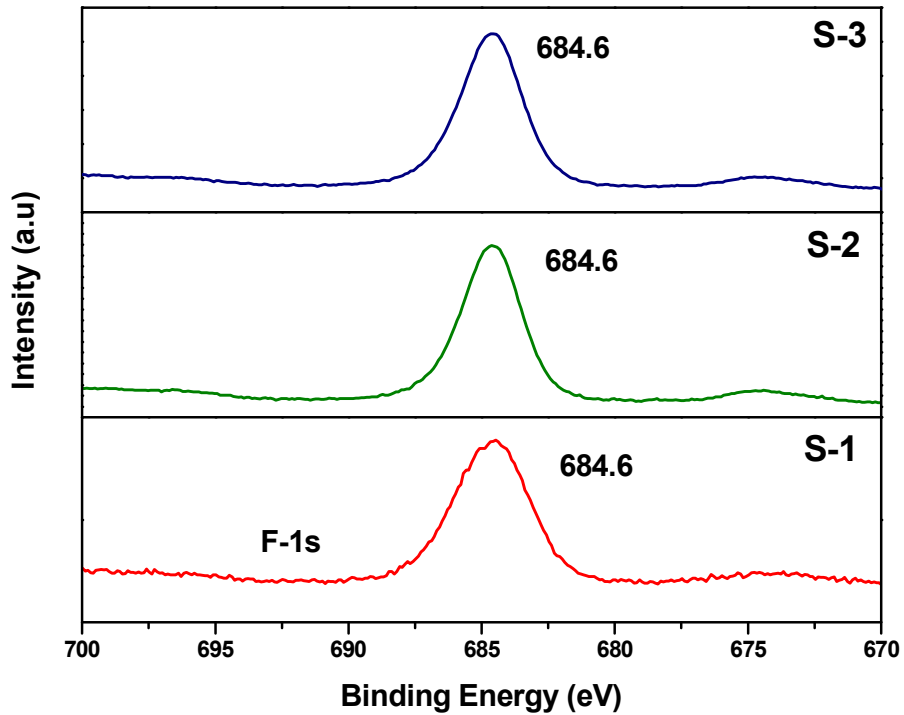


Figure 5.6: De-convoluted Figures for the Si-2p XPS spectra of the different samples.

Fig. 5.7 shows the core level peaks XPS spectra of F-1s. The binding energy of F-1s obtained from all the three salts was estimated at 684.6 eV which is in agreement with the literature value of F-1s.



**Figure 5.7:** F-1s XPS spectra of the molten salt bath (a) S1,(b) S2 and (c) S3.

## 5.2 Discussion

In the current study of producing silicide coating on Nb-1Zr-0.1C alloys, composition of the salt played an important role. The major findings of the results could be summarized as follows:

1. The molten salt comprising NaCl-KCl-NaF with only  $\text{Na}_2\text{SiF}_6$  as Si source (salt-S1) could not produce any silicide coating on the samples, whereas pits were observed on the surface of the samples. Loss of weight was also observed in these samples. Peaks in the XRD pattern were indexed in terms of single bcc Nb phase (Fig. 5.4 (a)).
2. The salt comprising NaCl-KCl-NaF with only Si powder as Si source (salt S2), produced a coating of  $\sim 7 \mu\text{m}$  with weight gain in the sample,  $\sim 20.23 \text{ g/m}^2$ . The XRD patterns obtained from the coated surface of the samples showed presence of the  $\text{NbSi}_2$  phase (Fig.

5.4 (b)). The surface morphology of the coated sample showed the presence of smaller pits.

3. A thick NbSi<sub>2</sub> layer (~12μm) with the weight gain of 28.9 g/m<sup>2</sup> was obtained on the samples dipped into the salt (S3) comprising NaCl- KCl- NaF – Na<sub>2</sub>SiF<sub>6</sub>- Si powders. Addition of two Si sources (Na<sub>2</sub>SiF<sub>6</sub>- Si powder) maintained Si concentration in the bath for the same time period. The XRD patterns obtained from the surface of the coated samples showed the presence of the NbSi<sub>2</sub> and Nb phase (Fig.5.4(c)). The surface morphology showed the presence of smaller and fewer pits than the samples dipped in salt S1 and S2.

These results are summarized in Table 5.4

Post experiment XPS analysis of the salts provided an insight about the different electronic environments in which Si was present in the molten salt bath which could be correlated with the formation of the silicide (NbSi<sub>2</sub>) coating. XPS results showed that Si in the salt S1 was present in the Si<sup>4+</sup> state (Table 5.5).

**Table 5.4** Summary of the thickness of the coating phases present and weight gain in various salts.

Characterization technique	Optical	XRD	EDS	Weight gain per unit area(ΔM) g/m <sup>2</sup> of the dipped samples
S1	Larger pits	Nb	No coating	-89.59
S2	Smaller and lesser pits	NbSi <sub>2</sub>	~7 μm	20.23
S3	Smaller and lesser pits	NbSi <sub>2</sub>	~12 μm	28.9

A single peak fitting for the salt S1 sample at 102.7 eV was obtained. It corresponds mainly to Si<sup>4+</sup> state. This value is lower than the value of binding energy of Si<sup>4+</sup> in the

standard state, which is 103.4 eV [86,87]. Lowering of the binding energy value could be attributed to the presence of several SiF<sub>x</sub> (x = 4, 3, 2) forming due to thermal dissociation of the Na<sub>2</sub>SiF<sub>6</sub> compound [91]. The concentration of each of the SiF<sub>x</sub> species is very low, peaks of these species was not observed in XPS spectra but being lower in electronic state, presence of these species shifts Si<sup>4+</sup> peak towards lower binding energy value of 102.7 eV [86,87]. This argument is supported by the fact that the FWHM for the F-1s for the salt S1 possess a value of 3.31 which is higher than the values of FWHM of F-1s in others two salts. These values of FWHM are 2.78 and 2.66 for salts S2 and S3 respectively. Difference in the FWHM in the case of salt S1 indicates that though all fluorine is present in F<sup>-1</sup> state, yet they are in the vicinity of Si with differential electronic density. This would lead to the formation of a wider FWHM for the salt S1 as compared to that of S2 and S3.

The presence of Si<sup>4+</sup>, Si<sup>2+</sup>, Si<sup>0</sup> ions in the salt S2 was confirmed by XPS analysis. The XPS signal obtained from the analysis of salt S2 could be fitted in to three peaks with value of 104.5, 101.3, 96.9 eV, respectively, which primarily are for Si<sup>4+</sup>, Si<sup>2+</sup>, Si<sup>0</sup>. This is in parity with the earlier reports of Si<sup>2+</sup> found from the Si 2p peak [86,87].

The salt S3 has three deconvoluted peaks at (103.1, 100.9 and 97.6) eV respectively. Therefore, there is a definite presence of the Si<sup>4+</sup> (103.1eV), Si<sup>2+</sup> (100.9) and Si<sup>0</sup> (97.6) in this salt. The FWHM, peak area and probable percent of these peaks are described in the Table 5.5. The maximum value was observed for 100.9 eV peak representing Si<sup>2+</sup> state. A negative shift in the binding energy of Si in salt S1 and that of S2 by 0.8 eV and that between S1 and that of S3 of 1.0 eV was observed. However, the negative shift in the XPS signal definitely hints towards the fact that both the salts, S2 and the S3 possess Si in lower oxidation states as compared to that of S1.

**Table 5.5** Post experiment salt analysis of salt S1,S2 and S3.

<b>Sample</b>	<b>Peak Position</b>	<b>FWHM</b>	<b>Area</b>	<b>% Present</b>	<b>Si state Identified</b>
<b>Salt-S1</b>	102.7	3.39	2460	100	Si <sup>4+</sup>
<b>Salt-S2</b>	96.9	2.13	5901	13.57	Si <sup>0</sup>
	101.3	3.2	36665.3	84.38	Si <sup>2+</sup>
	104.5	1.7	889.9	2.05	Si <sup>4+</sup>
<b>Salt-S3</b>	97.6	1.93	1945	1.87	Si <sup>0</sup>
	100.9	2.58	94866	91.36	Si <sup>2+</sup>
	103.1	2.25	7021	6.77	Si <sup>4+</sup>

*Mechanism for the formation of silicide coating*

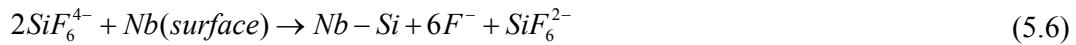
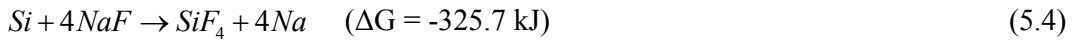
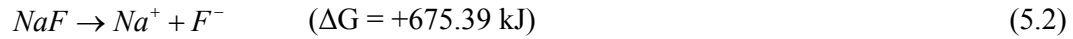
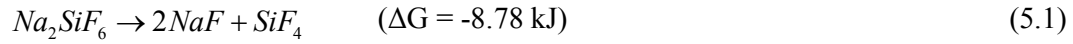
In the present study, it has been observed that whenever the concentration of F<sup>-</sup> ions increases with respect to the Si ions, etching effect of F<sup>-</sup> ions on the surface of the substrate as well as on newly formed silicide coatings was realised. For example, samples dipped in S1 salt, where concentration of F<sup>-</sup> is maximum (Table 5.3), showed the presence of large pits (~ 50 µm) (Fig. 5.1 (b)). Extending this argument for the case of samples dipped in S3. This salt had two sources of Si, namely powdered Si and Na<sub>2</sub>SiF<sub>6</sub>, and higher concentration of F<sup>-</sup> as compared to S1. Samples dipped in this salt showed least numbers of pits. Sizes of these pits were also smallest among all the three cases. Samples dipped in S2, where concentration of F<sup>-</sup> and Si ions is minimum, on the other hand, showed more numbers of pits as compare to samples dipped in S3. Other observations, like formation of a maximum thickness of silicides which upon extending time period of coating start reducing the thickness, corroborate this

finding [92]. The reason for reduction in thickness with extending time could be explained on the basis of etching effect of  $F^-$  concentration due consumption of Si ions [92].

To understand the role of Si present in  $Na_2SiF_6$  and in powder form, three extreme cases were considered; (i)  $Na_2SiF_6$  only (S1), (ii) Si powder only (S2) and (iii) both Si powder and  $Na_2SiF_6$  (S3). It has been observed in present study that  $Na_2SiF_6$  alone could not produce coating (Fig 5.3 (a)), whereas Si powder alone could produce silicide coating on the samples (Fig. 5.3 (b)). This observation indicates that Si powder plays an important role. In the first case, post experiment analysis of the molten salt showed that most of the Si was present in  $Si^{4+}$  state whereas in the second case, it was mostly present in  $Si^{2+}$  state. Therefore, it can be inferred that for the silicide coating, formation of  $Si^{2+}$  ionic species in the molten bath is a prerequisite. This observation is in agreement with those reported by Suzuki *et al.* [61]. In the case where both the sources of Si ( $Na_2SiF_6$ -Si powder) were present (salt S3) a coating of 12  $\mu m$  was observed. In addition, XPS analysis of this salt showed the presence of all electronic states of silicon, namely Si,  $Si^{+2}$  and  $Si^{+4}$ .

Based on these results, it can be proposed that  $Na_2SiF_6$  and NaF dissociate into several species (equations 5.1 and 5.2). Dissociation of NaF (equation 5.2) is not spontaneous as the free energy of the reaction is positive ( $\sim 675.4$  kJ). Therefore, this reaction involves consumption of energy. However, the reaction can be moved forward by the consumption of  $F^-$  by  $SiF_4$  to produce  $SiF_6^{2-}$  (equations 5.3). Elemental Si (powder) reacts with NaF to produce  $SiF_4$  (equation 5.4) and reaction further proceeds as presented in equation 5.3. Elemental Si and  $F^-$  ions in the molten bath react with  $SiF_6^{2-}$  species to form  $SiF_6^{4-}$  ions (equation 5.5). Later,  $SiF_6^{4-}$  species oxidise on the Nb substrate giving free Si which subsequently diffuses into the substrate to form  $NbSi_2$  layer (equation 5.6). Therefore, the silicide coating formation could be attributed to the inward diffusion of the silicon ions deposited by  $SiF_x$  species on the surface of the substrate and the counter effect of the  $F^-$  ions.

The coating mechanism based on the observations could be expressed in terms of the following equations



In case of the salt S1, the reactions 5.1-5.3 are possible. Reactions 5.4-5.5 will be observed only in the salts S2 and S3, where Si powder was added as a source of Si. Owing to the high stability of the  $\text{SiF}_6^{2-}$  species, coating could not be observed in the case of salt S1. Presence of elemental Si (powder) in the salts S2 and S3 lead to a disproportional reaction in the molten salt producing metastable species,  $\text{SiF}_6^{4-}$ . This species eventually produces free Si on the Nb substrate which reacts with Nb to produce  $\text{NbSi}_2$  coating (equation 5.6).

### 5.3 Summary

In the present study, the formation of silicide coating on the Nb-1Zr-0.1C alloy using different sources of Si ( $\text{Na}_2\text{SiF}_6$  and Si powder) has been studied. For this purpose NaCl–KCl–NaF–salt was used as supporting medium. Main observations from the study could be summarised in the following points:

- (i)  $\text{Na}_2\text{SiF}_6$  as the source of Si could not produce coating on Nb alloys. Si powder and the combination of Si powder and  $\text{Na}_2\text{SiF}_6$  could produce coating on the Nb-alloy.
- (ii) A coating of 12  $\mu\text{m}$  could be produced in the sample dipped in salt containing both  $\text{Na}_2\text{SiF}_6$  and Si powder as silicon sources at 800°C for 4 h.

- (iii) XRD analysis of the samples dipped in salts S2 and S3 showed the formation of single phase hexagonal NbSi<sub>2</sub> at 800°C. EDS analysis of the cross sections of these samples also confirmed that the chemistry of the coating was close to the NbSi<sub>2</sub> phase.
- (iv) Post experiments XPS analysis of the salts revealed the presence of Si in various electronic states. Salt, containing only Na<sub>2</sub>SiF<sub>6</sub> showed the presence of Si in Si<sup>4+</sup> state only. Whereas other salts, containing Si powder and combination of Na<sub>2</sub>SiF<sub>6</sub> and Si powder, showed presence of Si<sup>0</sup>, Si<sup>2+</sup> and Si<sup>4+</sup> states of silicon. Post experiment ion chromatographic analysis showed the presence of etched Nb in all the three salts thereby confirming the etching effect of F<sup>-</sup> ions.
- (v) Based on the, microstructural, chemical and thermodynamic analyses it was possible to show that the formation of SiF<sub>6</sub><sup>4-</sup> state is a prerequisite for the producing the layer of silicide coating. Based on this observation a mechanism of silicide coating has been proposed.



## High Temperature Behaviour of Silicide Coatings

---

Development of the silicide coatings on the Nb alloys using molten salt has been presented in previous chapters. These coatings were produced to withstand high temperatures and also provide protection against high temperature oxidation. In order to evaluate the performance of the silicide coatings, effects of temperature has been studied in detail and described in the present chapter. It may be noted that the silicide phase formed by the molten salt technique is a single NbSi<sub>2</sub> phase. At high temperatures, the following possibilities may occur:

- (i) In the presence of metallic Nb, the NbSi<sub>2</sub> phase may react and form other silicon lean silicide phases, like Nb<sub>3</sub>Si Nb<sub>5</sub>Si<sub>3</sub>*etc.*
- (ii) The excess release of Si due to the formation of silicon lean silicide phases may form other metastable silicide phases or this Si may dissolve in the Nb phase.
- (iii) In addition, in the presence of oxygen apart of the occurrence of various phase reactions, formation of oxide phase at the surface may occur which may or may not provide sufficient barrier to the Nb alloy.
- (iv) The temperature variation may induce stresses at the interface between silicide phase and the matrix phase because of which the coating may prematurely peel off at high temperatures revealing a fresh surface of Nb for oxidation.

The high temperature study was, therefore, divided into two parts. In part one, silicide coated samples were subjected to various heat treatments to study possible phase reactions at high temperatures. To avoid interference by the formation of any oxide phase or ingress of oxygen into the sample, these heat treatments were carried out in a vacuum furnace operating

at  $\sim 10^{-6}$  bar. To study the possible high temperature reactions, several heat treatments by varying temperature and time have been carried out, as listed in Table 6.1. In part two, oxidation study to compare the oxidation behaviour of heat treated, as-coated and re-coated sample post heat treatment was carried out. In this experiment, samples were exposed to air in open atmosphere at 1000 °C for a period of 1 h. This allowed the free flow of oxygen to oxidize the silicide layers. To study the microstructures and the chemical compositions of the constituent phases formed during heat treatment, re-coating of the samples after heat treatment and oxidation of the coated Nb samples, cross-section specimens of the samples were prepared and analyzed using a field emission scanning electron microscopy (FESEM) equipped with an energy dispersive spectroscopy (EDS).

**Table 6.1** *Time and temperature considered for heat treatment*

<b>Temperature (°C)</b>	<b>Time( h)</b>
1200	2,4
1350	6,10
1400	10

### **6.1 High temperature studies on the silicide coated samples**

In order to study the high temperature behaviour of as-coated Nb alloy samples, set of samples were subjected to various temperatures in the range of 1200 -1400°C for time period of 2-10 h. As it is reported in the literature [61,82] that the formation of Nb<sub>5</sub>Si<sub>3</sub> initiates above 1200 °C, the first temperature and time for the heat treatment was chosen as 1200 °C for 2 h. Post heat treatment experiments , cross section samples were prepared and their detailed microstructural characterization was carried out. The results are discussed in the following section.

### 6.1.1 Microstructural characterization

Fig. 6.1 (a) shows cross section of the samples heat treated at 1200 °C and 2 h. Formation of two distinct layers, i.e., a ~4µm porous layer (layer 1) and a ~6.2 µm non-porous layer (layer 2) were observed. EDS analysis of these layers revealed that the major phase is Nb<sub>5</sub>Si<sub>3</sub> in both the layers (table 6.2). Extending the time of heat treatment upto 4 h showed that the distinction between the two layers became more evident. Fig. 6.1(b) shows the cross section of silicide coated samples after heat treatment at 1200 °C for 4 hr. In this sample, the formation of at least 2 distinct layers could again be observed where the outer layer was found to have high porosity. The EDS analysis of these layers confirmed that Nb<sub>5</sub>Si<sub>3</sub> is the major phase present in both the layers. Since porosity was observed in the outermost layer, it was decided to increase time and temperature of heat treatment to facilitate the reaction to form a homogenous layer of Nb<sub>5</sub>Si<sub>3</sub>. Consequently, temperature and heat treatment time were increased to 1350 °C; 6 and 10 h. Selection of this temperature for the next treatment was based on the fact that at and above 1400 °C any free Si would have the tendency to melt down.

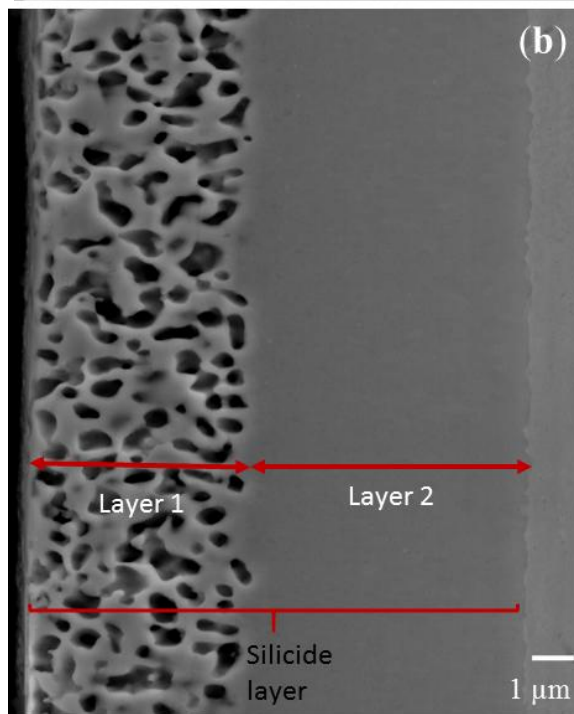
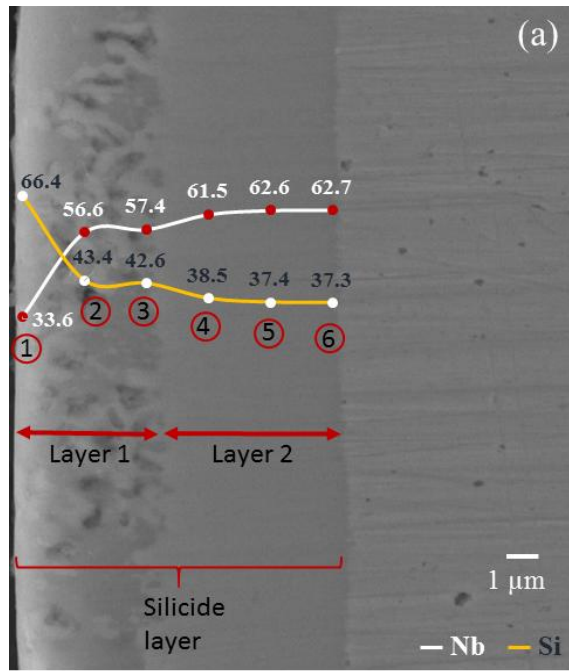
In order to examine changes in the coating after heat treatment, cross section samples (Fig 6.1 (d)) were analysed using FESEM. Porosity was again observed in the coating. The composition profile obtained from EDS across the coating thickness showed that Nb:Si atomic ratio in localized region is 63:37(±0.5), which is close to the ideal ratio of Nb<sub>5</sub>Si<sub>3</sub>. Therefore, the phase could be assigned as Nb<sub>5</sub>Si<sub>3</sub>. As homogenous and non-porous layer was not observed, another attempt was made to increase the temperature of heat treatment to 1400 °C.

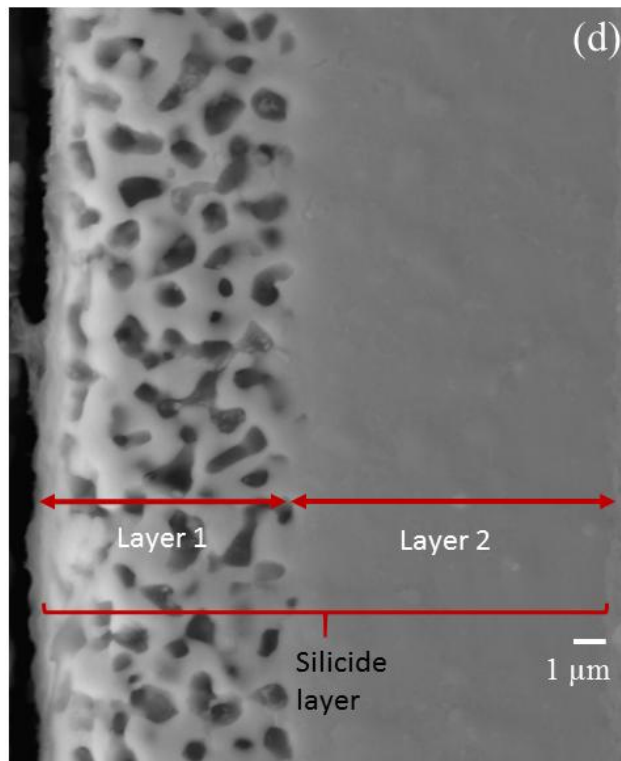
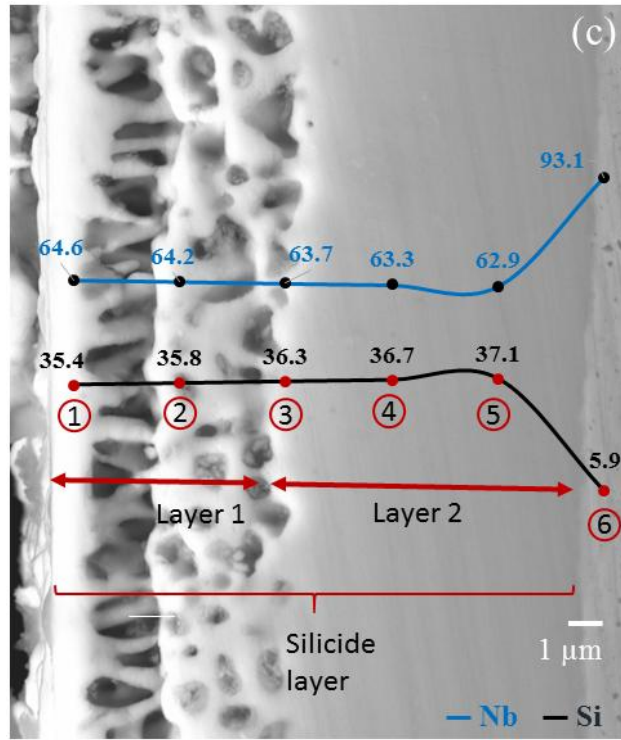
Fig. 6.1(e) shows the cross section of samples heat treated at 1400 °C for 10 h. It was observed that even further increasing time of heat treatment, formation of homogenous layer

of  $\text{Nb}_5\text{Si}_3$  was not observed. Cross section of this post heat treated sample examined under FESEM showed that the layer was consisted of the  $\text{Nb}_5\text{Si}_3$  phase.

The approach of varying time and temperatures of heat treatment of the coated samples to overcome the problem of porosity discussed above clearly indicates that the increase in time and temperature did not produce any favourable results. Therefore, to overcome the problem of porosity in the post heat treated coatings another approach was considered, *i.e.*, by re-coating the sample. For this purpose, pre-coated samples containing single  $\text{NbSi}_2$  phase were heat treated to form the pores. Subsequent to the formation of pores, these samples were again subjected to coating again at  $800^\circ\text{C}$  for 4 h.

When effect of the second coating was examined by investigating the cross sections of the re-coated samples under FESEM, it revealed the formation of three distinct layers (Fig. 6.2) - one porous layer and two non-porous layers. The composition profile obtained from EDS across the outermost layers (porous and non-porous layer; marked by points 7 to 4 in Fig. 6.2)) showed that Nb:Si atomic ratio is  $67:33(\pm 0.5)$  (Table 6.3), which is close to the ideal ratio of  $\text{NbSi}_2$ . The innermost non porous layer showed the Nb:Si atomic ratio as  $63:37(\pm 0.5)$ , which is close to the ideal ratio of  $\text{Nb}_5\text{Si}_3$  (marked as points 1 to 3 in Fig. 6.2) (Table 6.3). Therefore, the phase could be assigned as  $\text{Nb}_5\text{Si}_3$ .





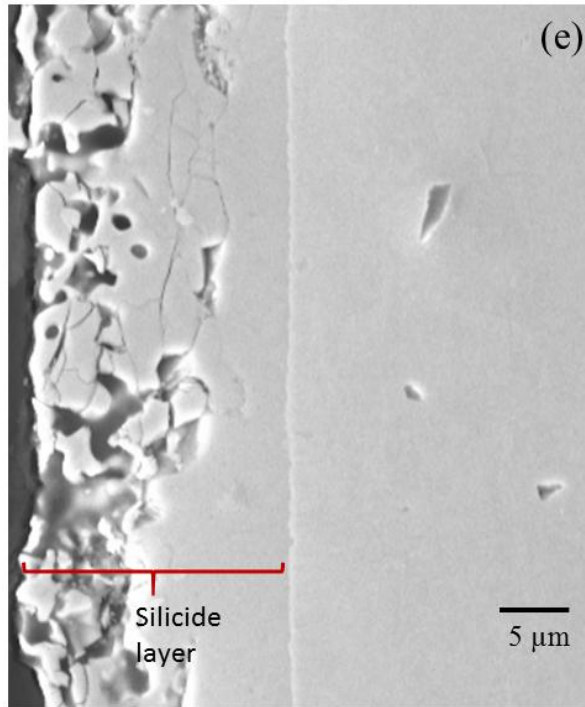


**Figure 6.1** SEM Micrographs of cross section samples after heat treatment at (a) 1200°C- 2h, (b)1200°C- 4h, (c)1350°C- 6h, (d)1350°C- 10h and (e)1400°C- 10h, \*Layer 1- porous ; Layer 2 – non-porous layer. The points marked show the region from where composition of the silicide layer was identified which is listed in Table 6.2.

**Table 6.2** Chemical Composition Determined by EDS at the Positions Marked on the SEM Micrographs Fig. 3(a) and 3(c)

Position Fig. 3(a)	Element(at. %)		Positions Fig. 3(c)	Element(at.%)	
	Nb	Si		Nb	Si
1	33.6	66.4	1	64.6	35.4
2	56.6	43.4	2	64.2	35.8
3	57.4	42.6	3	63.7	36.3
4	61.5	38.5	4	63.3	36.7
5	62.6	37.4	5	62.9	37.1
6	62.7	37.3	6	93.1	5.9

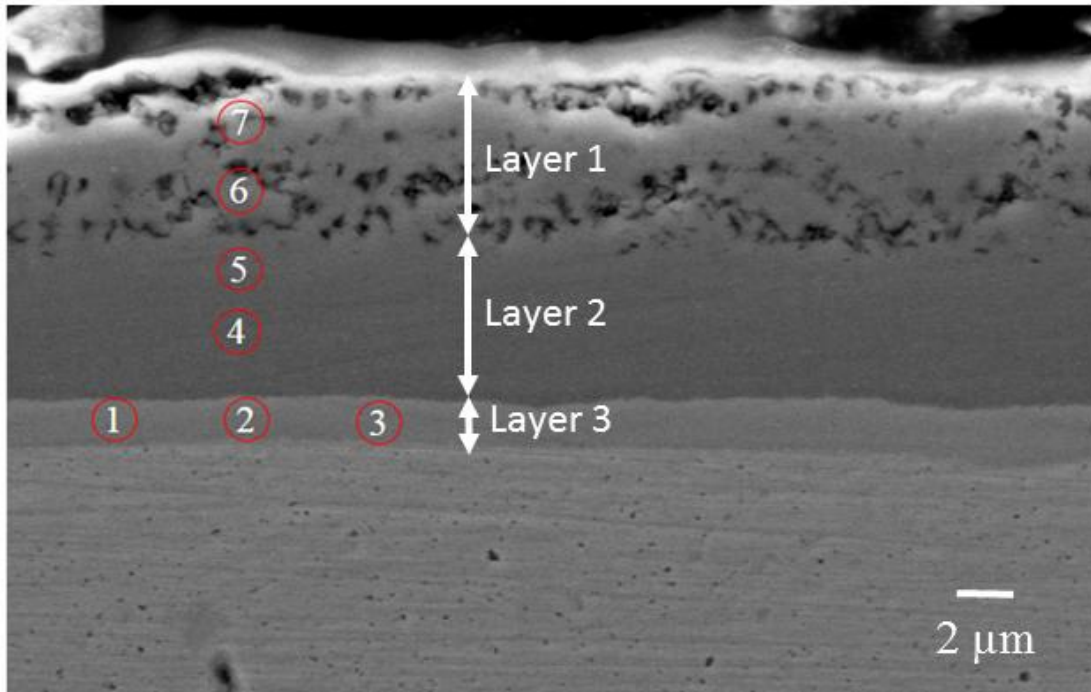


**Figure 6.2:** SEM Micrograph of cross section sample after re-coating post heat treatment. Three distinct layers of silicides could be observed in the image. The points marked show the region from where composition of the silicide layer was identified which is listed in Table 6.3.

**Table 6.3** Chemical Composition Determined by EDS at the Positions Marked on the SEM Micrographs Fig. 6.3

Position	Element(at. %)		Phase
	Nb	Si	
1	62.4	37.6	Nb <sub>5</sub> Si <sub>3</sub>
2	63	37	Nb <sub>5</sub> Si <sub>3</sub>
3	62.2	37.8	Nb <sub>5</sub> Si <sub>3</sub>
4	34.1	65.9	NbSi <sub>2</sub>
5	35.3	64.9	NbSi <sub>2</sub>
6	34	66	NbSi <sub>2</sub>
7	33.6	66.4	NbSi <sub>2</sub>

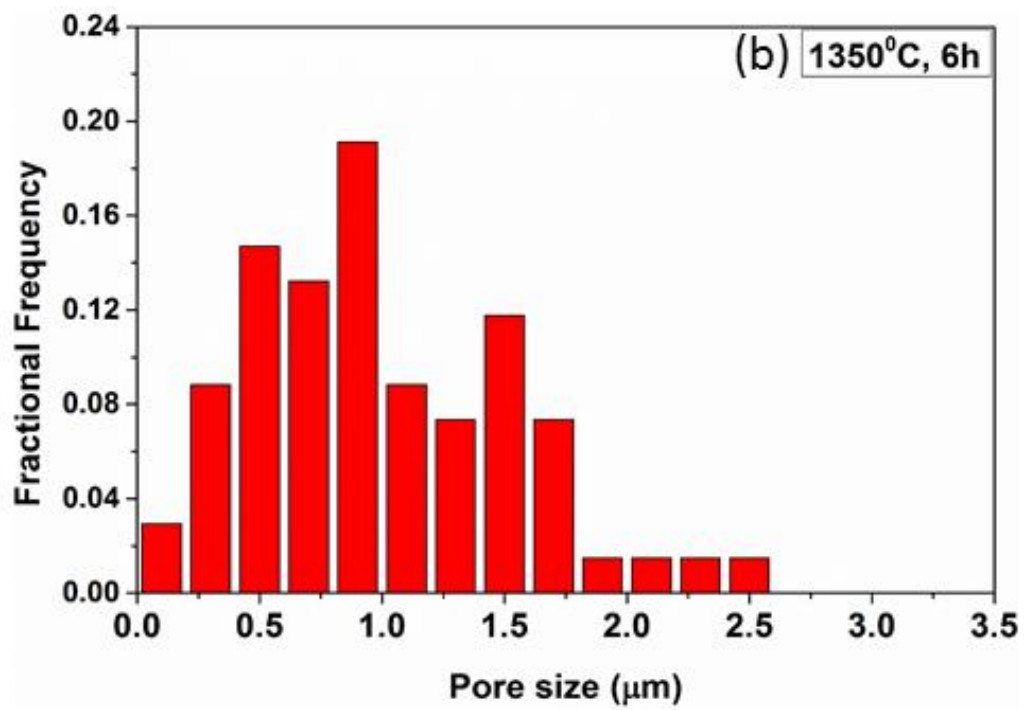
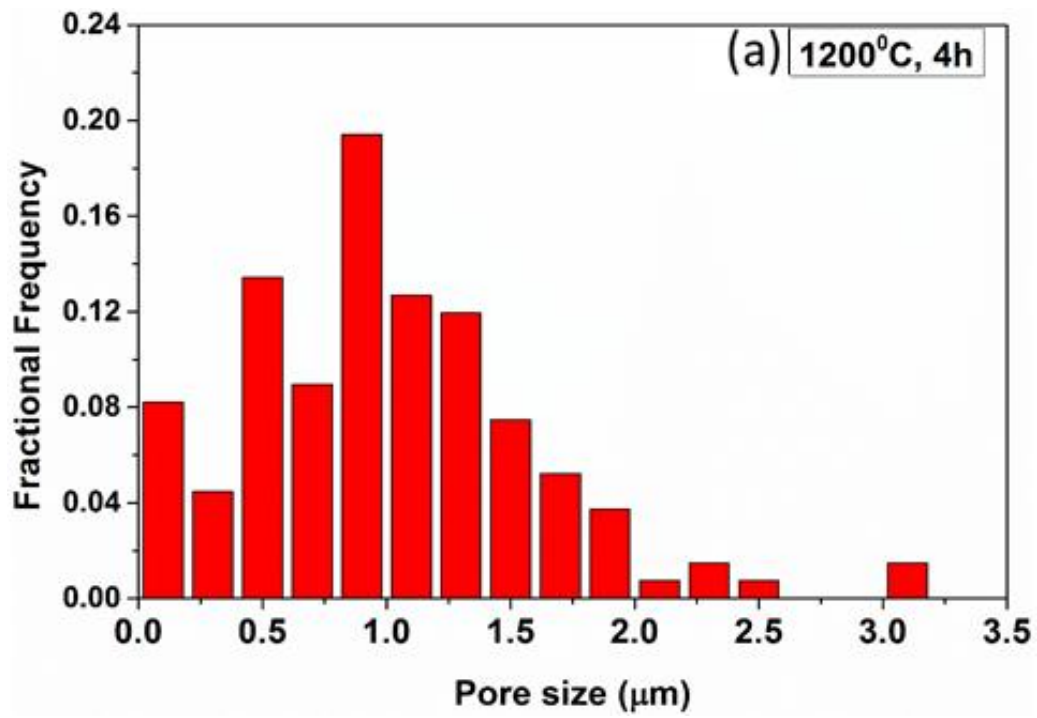
To understand the root cause of porosity in the silicide coating, the porosities observed in the outermost layer after heat treatment and recoating followed by heat treatment were analysed in depth to study the effect of time, temperature and re-coating.

Figure 6.3 shows pore size distribution in the form of histogram. Average pore size distribution was found to be between 0.5  $\mu\text{m}$  to 1.5  $\mu\text{m}$  for the temperature range 1200- 1350  $^{\circ}\text{C}$ . The histogram also shows that maximum pores were having size  $\sim 1 \mu\text{m}$ .

**Table 6.4** Pore size data analysis.

Pore Size	1200 $^{\circ}\text{C}$ , 4h	1350 $^{\circ}\text{C}$ ,6h	1350 $^{\circ}\text{C}$ ,10 h
<b>X<sub>0</sub>(&lt;1<math>\mu\text{m}</math>)</b>	0.542	0.652	0.668
<b>X<sub>1</sub>(&gt;1<math>\mu\text{m}</math>)</b>	0.45	0.410	0.326

Pore size analysis revealed that the number of pores increased when temperature was increased from 1200 $^{\circ}\text{C}$  to 1350 $^{\circ}\text{C}$ . Size distribution analysis of pores (Table 6.4) showed that the population of the pores which were smaller than 1 $\mu\text{m}$  increased whereas the population of pores which were larger than 1  $\mu\text{m}$  decreased with the increasing time and temperature of the heat treatment. This suggests that bigger pores (>1 $\mu\text{m}$ ) breaks down into smaller size pores with increasing time and temperature. It is also evident in SEM micrographs (Fig.6.2) that with increasing temperature from 1200 $^{\circ}\text{C}$  (4 h) to 1350 $^{\circ}\text{C}$  (6, 10 h) the shape of pores changed from elliptical to dumbbell shaped pores. In the case of re-coated sample, the average pore diameter was found to decrease. This clearly suggests that during heat treatment at higher temperatures and re-coating experiments, formation of silicide has filled some of the pores.



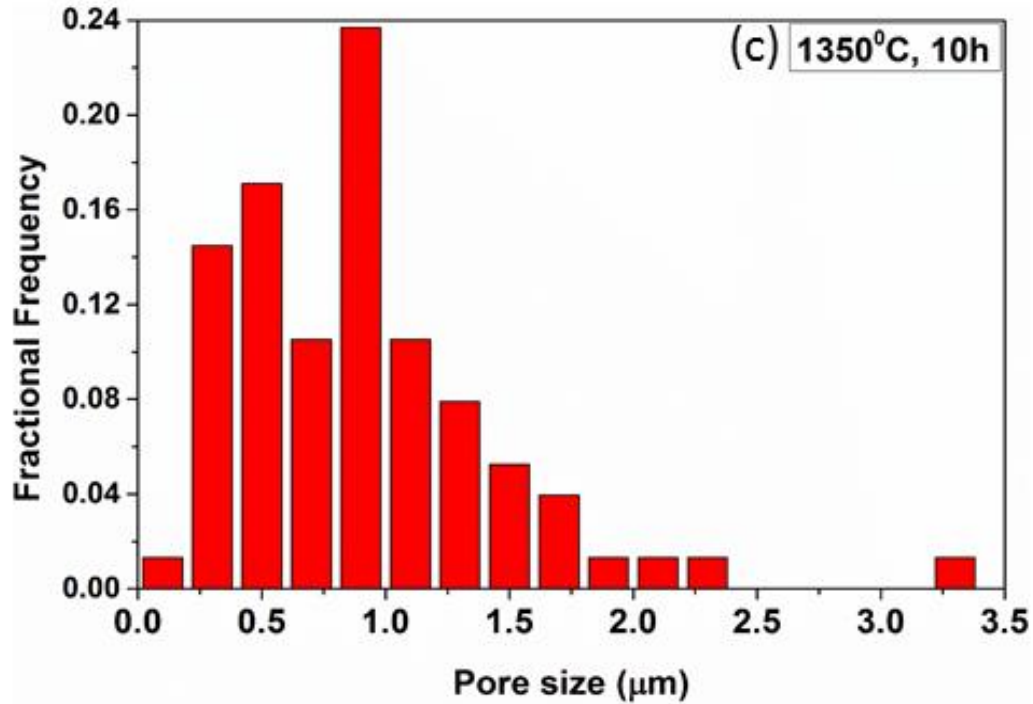


**Figure 6.3:** Plot of fractional frequency Vs pore size for the samples heat treated at (a)1200°C- 4 h, (b)1350°C- 6 h and (c) 1350°C- 10 h

## 6.2 Isothermal oxidation study

Isothermal oxidation behaviour of silicide coating Nb alloy samples prepared under different condition was studied. Three sets of samples, Set-1, Set-2 and Set-3 comprising as-coated, heat treated and re-coated post heat treatment samples respectively were prepared. Samples from each set were subjected to oxidation 1000 °C for the period of 1 h.

Fig. 6.4 shows that subsequent to oxidation experiment, nearly all the samples from Set-1 (as-coated) converted into the powder form indicating poor oxidation resistance of the silicide coating. On the other hand, samples from the Set-2 (heat treated) showed better oxidation behaviour as compared to the Set-1 samples as these samples did not turn into powder completely and when kept under same oxidizing conditions for same time period

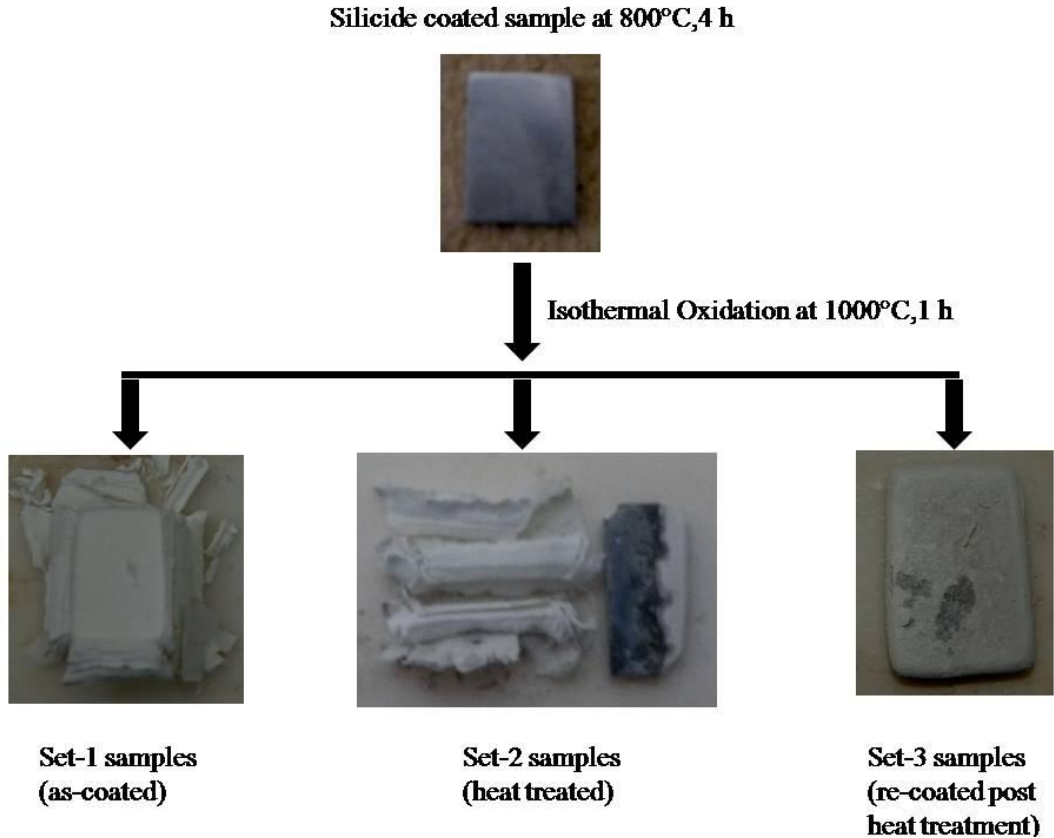


**Figure 6.4:** Isothermal oxidation behaviour of (a) Set-1 (as-coated), (b) Set-2 (heat treated); (c) Set-3 (re-coated post treatment) samples.

This suggested that layer of  $\text{Nb}_5\text{Si}_3$  played an important role in improving the oxidation resistance behaviour of Nb alloy systems. Upon oxidation at 1000 °C for 1 h, further improvement in the oxidation behaviour was observed for Set-3 (re-coated post heat treatment) samples. They showed better oxidation resistance behaviour in comparison to single heat treated samples indicating that re-coating of the samples post heat treatment step assisted in filling up the pores formed during heat treatment and thereby made the surface of the samples impervious to oxygen to some extent.

Upon analysing these powdered samples by XRD, the identity of the powder was established as  $\text{Nb}_2\text{O}_5$  (Fig. 6.5) (JCPDS 72-1484). Presence of  $\text{Nb}_2\text{O}_5$  clearly suggested that the silicide formed on the surface was not impervious to oxygen and the entire matrix got oxidised. In fact, the oxidation was so rapid that it did not allow formation of sufficient

thickness of protective SiO<sub>2</sub> layer, as reflected by absence of SiO<sub>2</sub> peak in the XRD pattern. Therefore, it can be inferred that the presence of the single NbSi<sub>2</sub> phase in the silicide coating failed to provide surface protection against oxidation. These results corroborate with those reported in the literature [93,94], where it has been shown that NbSi<sub>2</sub> alone cannot prevent oxidation.

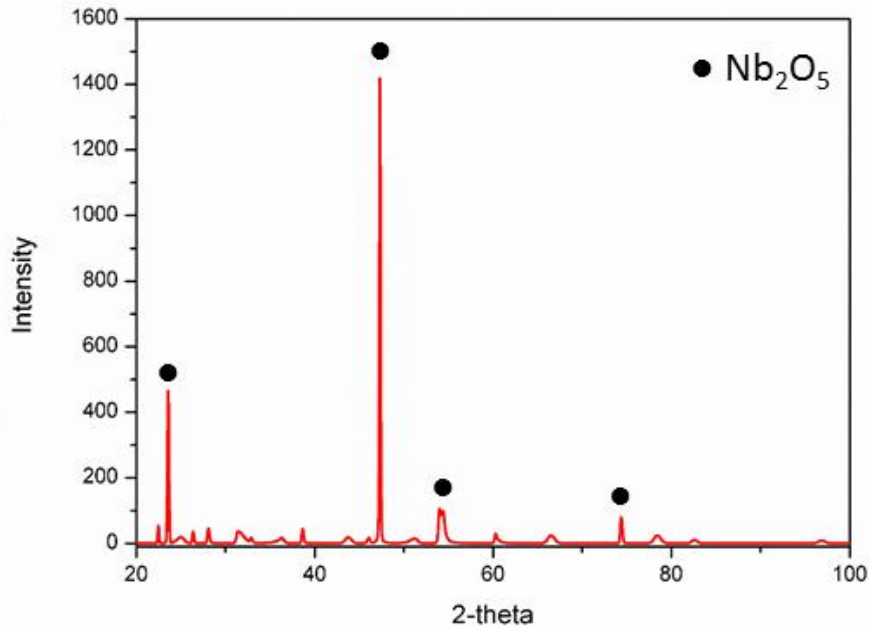


**Figure 6.5:** XRD patterns of powder of the samples oxidized at 1000°C for 1 h showing formation of Nb<sub>2</sub>O<sub>5</sub>.

### 6.3 Discussion

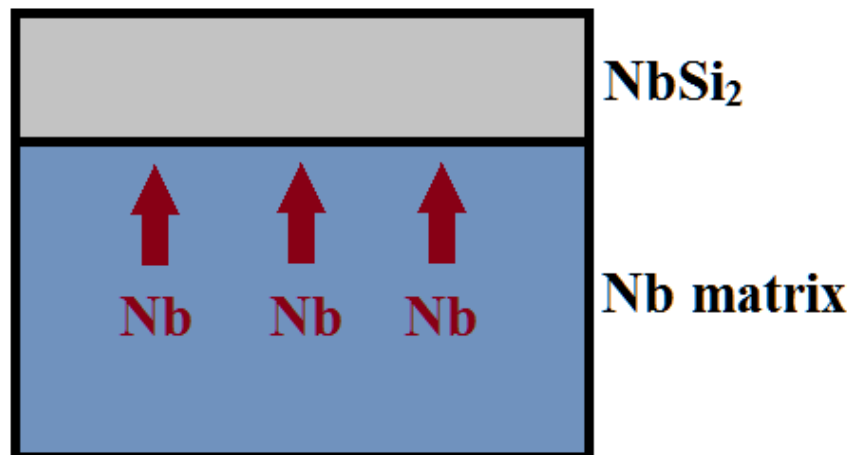
In the present study, attempts were made to study the high temperature behaviour of silicide coating and form the additional layer of the Nb<sub>5</sub>Si<sub>3</sub> between the Nb matrix and NbSi<sub>2</sub> silicide layer by suitable heat treatment of the coated samples. It has been reported that for the formation of Nb<sub>5</sub>Si<sub>3</sub> phase, temperature in the vicinity of 1200°C is required [82].

In the present study, therefore, the temperature range of heat treatment of the silicide coated samples was selected between 1200 to 1400°C. These heat treatments, however, led to

the development of a porous layer at the outer side of the coating (Fig. 6.1) followed by formation of the  $\text{Nb}_5\text{Si}_3$  phase as confirmed by EDS analysis. Formation of porous structure clearly indicates changes in volumes are involved during the formation of the  $\text{Nb}_5\text{Si}_3$  phase. In addition, to address the problem of porosity when time and temperature of heat treatments were increased, it was observed that porosity in the outer layer was still existing (Fig.6.1). However, it is interesting to note that the porosity is confined to the outer layer and it also display sharp interface running almost parallel to the metal-silicide interface.

To understand the mechanism of formation of  $\text{Nb}_5\text{Si}_3$  as well as pores in the  $\text{NbSi}_2$  layer, three reaction mechanisms, as shown in Fig 6.6, could be proposed:

- (i) Only Nb from the matrix diffusing outwards reacting with  $\text{NbSi}_2$  to form  $\text{Nb}_5\text{Si}_3$  and free Si. (Fig. 6.6 (a))
- (ii) Due to high temperatures,  $\text{NbSi}_2$  disintegrating to form  $\text{Nb}_5\text{Si}_3$  and free Si. This free Si must be reacting with Nb to form  $\text{Nb}_5\text{Si}_3$ . (Fig. 6.6 (b))
- (iii) Nb diffusing outwards and simultaneously Si diffusing inwards. Nb in the silicide reacting with  $\text{NbSi}_2$  and Si in the matrix reacting with Nb to form  $\text{Nb}_5\text{Si}_3$ . (Fig. 6.6 (c))



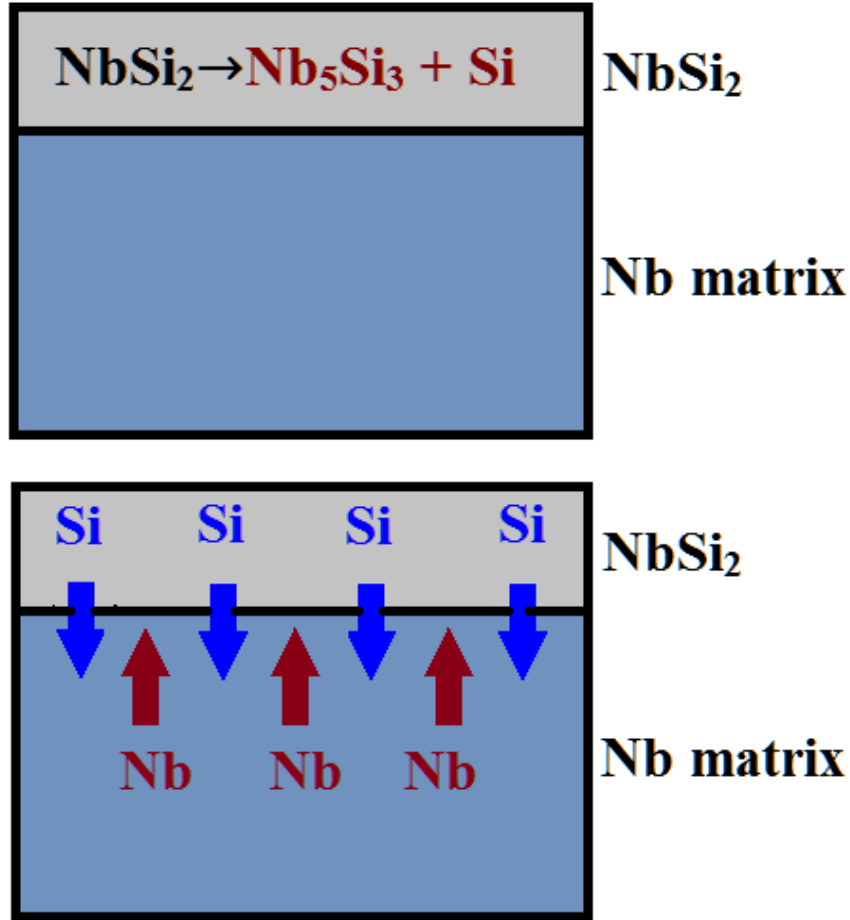
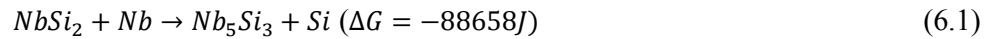


**Figure 6.6:** Schematic representation of proposed reaction mechanisms.

The above mentioned scenarios could be expressed in terms of reactions as follows



The changes in the Gibbs free energy for equations 6.1-6.3 have been calculated using thermochemical software, Factsage 7.0. It was observed that the dissociation of  $\text{NbSi}_2$  (equation 6.2) is not spontaneous as the free energy of the reaction is positive ( $\Delta G = +35421\text{J}$ ). Therefore, equations 6.1 and 6.3 must be the governing reactions for the formation of  $\text{Nb}_5\text{Si}_3$  phase. According to this proposed scheme, for the formation of  $\text{Nb}_5\text{Si}_3$ , outward diffusion of Nb is required and as a consequence of the reaction, free Si produced should diffuse inward.

These propositions could easily be validated by EDS analysis. Following major observations in this regard could be mentioned as:

- (i) EDS examination of samples heat treated at 1200°C showed that from the bulk-Nb to the outermost layer (porous layer), the concentration of Nb decreased and the concentration of Si increased. This clearly suggests inward diffusion of Si and outward diffusion of Nb has taken place (Fig. 6.1)
- (ii) It was also observed that concentrations Nb and Si were close to that of Nb<sub>5</sub>Si<sub>3</sub> i.e. (Nb-62.5 and Si-37.5 at.%) towards the matrix, whereas point scans at the outermost layer showed the presence of NbSi<sub>2</sub>. Therefore, it could be inferred that Nb could not diffuse across the entire length at lower time and temperature of heat treatment (1200°C, 2h).
- (iii) As temperature and time of the heat treatment were increased, higher Nb concentration in porous layer was observed, revealing that Nb could diffuse across the length. In these samples the NbSi<sub>2</sub> phase was absent suggesting nearly complete consumption of NbSi<sub>2</sub>.
- (iv) With the consumption of the NbSi<sub>2</sub> phase, arrest of the growth of porous layer was observed, as the thickness of the porous layer remained stagnant even when the time of heat treatment was increased (1350°C from 10 h); the average thickness of porous layer and non-porous layer is listed in Table 6.5.

**Table 6.5** *Effect of temperature and time on silicide coated samples.*

<b>Temp.(°C)</b>	<b>Time(h)</b>	<b>Porous layer(μm)</b>	<b>Non-porous layer(μm)</b>
<b>1200</b>	2	~ 4	~ 6
<b>1200</b>	4	~ 5	~ 6.2
<b>1350</b>	6	~ 6.7	~ 8.3
<b>1350</b>	10	~ 6.7	~ 9.9

Based on these observations, the sequence of the steps involved in the silicide coating when subjected to high temperatures could be presented as-

- (i) In the initial stage, Nb started diffusing outwards under the driving force represented by equation 6.1. The first reaction, therefore, should take place at metal-silicide interface. As a consequence of this reaction (equation 6.1)  $Nb_5Si_3$  and free Si would be produced.
- (ii) As Si has solubility in Nb, the matrix start acting as a sink for the excess Si formed at the interface according to step (i). As a consequence of diffusion of Si from the newly formed  $Nb_5Si_3$  layer towards the matrix, pores will be generated in the  $Nb_5Si_3$  layer.
- (iii) The diffusion of Si in the matrix would initiate the formation of  $Nb_5Si_3$  according to equation 6.3. As a consequence, the thickness of  $Nb_5Si_3$  would increase towards the bulk-Nb matrix.
- (iii) The pores formed in the  $Nb_5Si_3$  layer provide the sites for the reaction and thereby led to the formation of monolithic  $Nb_5Si_3$  layer near the metal-silicide interface (Fig.6.1) as continuous and simultaneous diffusion of Si and Nb in the  $Nb_5Si_3$  layer would undergo the same reaction at these reaction sites(equation 6.3). This argument is supported by the fact that with increasing time and temperature larger pores have tendency to reduce to smaller pores (Fig.6.3 and Table 6.4).
- (iv) The formation of the layer retards the inter-diffusion of Nb and Si, because of which the kinetics of the reaction become sluggish which manifests itself by the retarded growth of both the layers (Table 6.5).
- (v) Simultaneous to the inward diffusion of Si, Nb also diffuses outwards through the layer formed at interface and reacts with  $NbSi_2$  as per equation 6.1. This contributes to the increase in the thickness of  $Nb_5Si_3$  towards the interface between  $NbSi_2$  and  $Nb_5Si_3$  layer, and generation of more free Si.

(vi) With continuous generation of free Si, according to equation 6.1, difference in concentration is generated which causes Si to continuously diffuse inwards which leaves out porosity in the outermost region (Fig. 6.1).

Between porous and non-porous layers, stagnancy observed in the thickness of porous layer (Table 6.5) could be attributed to the complete consumption of NbSi<sub>2</sub>. With the consumption of NbSi<sub>2</sub> phase, further formation of Nb<sub>5</sub>Si<sub>3</sub>, according to equation 6.1, cannot proceed. In this scenario equation 6.3 becomes the dominant mechanism for the formation of Nb<sub>5</sub>Si<sub>3</sub> and thus increase in the thickness is observed only in the non-porous layer.

In the present study, however, it was observed that silicide coating failed to provide any protection. It is well documented in literature that at elevated temperatures silicide coatings on Nb alloys provide necessary oxidation protection [4]. In fact, the specimens crumbled into powder. In fact, the specimens crumbled into powder. The crumbling of the entire sample into powdered form could be attributed to the formation of Nb<sub>2</sub>O<sub>5</sub>. The high Pilling Bedworth ratio of Nb<sub>2</sub>O<sub>5</sub>/Nb (i.e. 2.68), suggests that volume of the oxide is larger than the metal oxidised and thus compressive stresses will be developed. As the thickness of the oxide increases, cracking and buckling phenomenon is observed in the coating.

This difference between the two (protective and non-protective) silicide coatings could be attributed to the formation of the single NbSi<sub>2</sub> phase in the present case which could not prevent oxidation of the base material [93,94]. One of the possible reason for its inability to provide protective layer, which at room temperature appears very smooth could be due to large differences in their coefficients of thermal expansions (Nb- $7.3 \times 10^{-6} \text{ K}^{-1}$ , NbSi<sub>2</sub>- $9.8 \times 10^{-6} \text{ K}^{-1}$ ) [63,64]. Therefore, during thermal cycles, these differences in the coefficients of thermal expansions induce stresses at the Nb-alloy/NbSi<sub>2</sub> interface and thereby initiating cracks in the NbSi<sub>2</sub> layer leading to direct exposure of bare Nb-metal surface to oxygen. Subsequent rapid oxidation of Nb-alloy consumes the entire sample within a short duration of 1 h.

This study has clearly shown that simultaneous formation of  $\text{Nb}_5\text{Si}_3$  and  $\text{NbSi}_2$  layers provide better high temperature oxidation resistance properties in comparison to single  $\text{NbSi}_2$  coating. It appears two-layer silicide structure  $\text{NbSi}_2/\text{Nb}_5\text{Si}_3$  acts as a stress reducing layer during thermal cycling and thus providing better protection [82]. In addition, this phase also provides an impervious layer to retard ingress of oxygen into the matrix phase [79,82]. Post formation of  $\text{Nb}_5\text{Si}_3$  by heat treatments of the  $\text{NbSi}_2$  layer leads to the formation of pores in the outer layer which are not easy to remove from the system; even after providing another coating of silicides.

#### **6.4 Summary**

In the present study high temperature behaviour of silicide coated Nb-1Zr-0.1C has been studied. Main observations from this study could be summarized as follows

- (i) Heat treatment provided to convert the single layer  $\text{NbSi}_2$  into a two-layer system comprising  $\text{Nb}_5\text{Si}_3$  and  $\text{NbSi}_2$  led to the formation of a porous and a non-porous layer.
- (ii) The porous layer is mainly confined to the outmost layer. Pore size analysis showed that the fractional frequency of porosities increases with increase in temperature of heat treatment.
- (iii) Based on microstructural and thermodynamic analyses, a mechanism explaining the formation of various phases and porosities in the outermost layer has been proposed.
- (iv) Single layer of  $\text{NbSi}_2$  on the Nb alloy could not prevent oxidation of the material.



## Conclusions

---

In the present study, silicide coatings on the Nb-1Zr-0.1C alloy have been developed using molten salt technique. By systematically varying parameters, like, composition of the salts, concentration of various species, time and temperature of coating experiments, optimized conditions to produce smooth coating of uniform thickness on the surface of the samples have been worked out. Detailed characterization of coating, examination of cross-sections of samples and by determination of composition of various phases, a mechanism of silicide coatings on the Nb alloy has been proposed. High temperature behaviour of the coating has been systematically studied. This study has shown that at elevated temperatures, formation of the Nb<sub>5</sub>Si<sub>3</sub> phase led to the formation of voids which once formed were difficult to remove. A detailed mechanism explaining formation of various phases and voids during high temperature heating has also been proposed.

Some of the important conclusions that have been drawn from the present investigation are listed below-

### 7.1 Optimization of coating parameters

1. Silicide coating experiments using molten salt experiments showed formation of single NbSi<sub>2</sub> phase coating on the surface. These experiments have shown that
  - (i) Increasing concentration of Si does not have significant effect on the thickness of the coating. Even adding additional Si during experiment does not give desired results.
  - (ii) Continuous stirring of the molten salt showed an adverse effect on the coating leading to the formation of non-uniform and non-homogeneous coating. Intermittent stirring is also not a suitable option to produce a uniform coating.

- (iii) In order to produce smooth coating on the surface, presence of all three constituents in the salt are necessary. These are  $\text{Na}_2\text{SiF}_6$ ,  $\text{NaF}$  and  $\text{Si}$ .
2. Optimized time and temperature determined in the present study are 4 h and  $800\text{ }^\circ\text{C}$  which produced  $12\text{ }\mu\text{m}$  thick uniform silicide coating of the  $\text{NbSi}_2$ . Increasing time or temperature of the bath led to the formation of pits and reduced thickness of the silicide phase.
  3. Microstructural characterization of the samples dipped in the salt at higher temperatures ( $> 800^\circ\text{C}$ ) and for longer time periods ( $> 4\text{ h}$ ) showed more pronounced effect of etching. The phenomenon of etching could be attributed to the increase in  $\text{F}^-$  ions concentration with increase in time and temperature.

## 7.2 Reaction Kinetics

In order to understand the kinetics of the silicide coatings, three salts with different composition, each carrying different species, were used in the present study. Detailed post experiments characterization of coatings and salts were carried out to identify the species present in the silicide phase as well as in the salts. Major highlights of the work are summarized as:

1. XPS analysis of the salts with different compositions revealed the presence of Si in various electronic states. Salt, containing only  $\text{Na}_2\text{SiF}_6$  showed the presence single ionic state of Si as  $\text{Si}^{4+}$ . Whereas other salts, containing Si powder and combination of  $\text{Na}_2\text{SiF}_6$  and Si powder showed presence of  $\text{Si}^0$ ,  $\text{Si}^{2+}$  and  $\text{Si}^{4+}$  states of silicon.
2. Microstructural characterization of the samples dipped in the salt containing only  $\text{Na}_2\text{SiF}_6$  showed no coating on the samples. On the other hand, samples dipped in the salt containing only Si powder could produce a layer of coating. However, maximum thickness of coating could be achieved only when both Si sources,  $\text{Na}_2\text{SiF}_6$  and Si powder are

present in the salt. Therefore, presence of Si in all three states;  $\text{Si}^0$ ,  $\text{Si}^{2+}$  and  $\text{Si}^{4+}$  is necessary to obtain silicide coating.

3. Cross-sectional microstructure of the silicide coating obtained in the presence of  $\text{Na}_2\text{SiF}_6$  and Si powder showed that  $\text{NbSi}_2$  had hexagonal crystal structure with lattice parameters of  $a = 0.48 \text{ nm}$  and  $c = 0.66 \text{ nm}$ .
4. Ion chromatographic analysis carried out to study the effect of increase in the  $\text{F}^-$  ions concentration, revealed the presence of etched Nb in the molten salt and thereby confirmed the etching effect of  $\text{F}^-$  ions.
5. Based on the detailed chemical and thermodynamic analyses, it was revealed that the formation of  $\text{SiF}_6^{4-}$  state is a prerequisite for the producing the layer of silicide coating on Nb-1Zr-0.1C alloy.

### **7.3 High temperature behaviour of silicide coating**

Based on the high temperature studies on silicide coated Nb-1Zr-0.1C alloy, it could be concluded that

1. Cross-sectional microstructure of the as-coated samples subjected to high temperatures showed that single layer of  $\text{NbSi}_2$  transforms into a two-layer system comprising  $\text{Nb}_5\text{Si}_3$  and  $\text{NbSi}_2$ .
2. Detailed microstructure characterization of the heat treated sample showed that the transformation of  $\text{NbSi}_2$  into two layer system led to the formation of a porous and a non-porous layer. The confinement of the porous layer at the outmost edge could be attributed to outward diffusion of Nb and inward diffusion of Si towards the Nb matrix. Also, pore size data analysis showed that the fractional frequency of porosities increased with increase in temperature of heat treatment.
3. In order to understand the oxidation behaviour of the silicide coatings, three sets of silicide coated samples with different conditions were used in the present study. Oxidation studies

showed that single layer of  $\text{NbSi}_2$  in as-coated Nb alloy samples cannot prevent oxidation due to the formation of  $\text{Nb}_2\text{O}_5$ . Presence of additional layer,  $\text{Nb}_5\text{Si}_3$  and re-coating of samples post heat treatment considerably improved the oxidation resistance behaviour of the Nb-1Zr-0.1C.

4. Silicide coating with co-formation of  $\text{NbSi}_2$  and  $\text{Nb}_5\text{Si}_3$  has better high temperature performance than the coating where the formation of  $\text{Nb}_5\text{Si}_3$  is assisted by additional heat treatments.

---

## **Scope of Further Research**

---

Based on the work carried out in this dissertation, the following are a few suggestions for further work:

1. Development of Mo-based surface coatings to improve the high temperature properties of the Nb-Zr-C alloys can be carried out.
2. Development of low oxidation Nb alloys by the addition of other refractory based alloying elements can be explored.

## References

- [1] X. Zheng, R. Bai, D. Wang, X. Cai, F. Wang, M. Xia, J. Yu, Research development of refractory metal materials used in the field of aerospace, *Rare Met. Mater. Eng.* 40 (2011) 1871–1875.
- [2] B.P. Bewlay, M.R. Jackson, P.R. Subramanian, J.-C. Zhao, A review of very-high-temperature Nb-silicide-based composites, *Metall. Mater. Trans. A.* 34 (2003) 2043–2052.
- [3] J.R. Stephens, D.W. Petrasek, R.H. Titran, *Refractory metal alloys and composites for space power systems*, National Aeronautics And Space Administration Cleveland Oh Lewis Research Center, 1988.
- [4] B.P. Bewlay, M.R. Jackson, P.R. Subramanian, Processing high-temperature refractory-metal silicide in-situ composites, *JOM.* 51 (1999) 32–36.
- [5] P. Subramanian, M. Mendiratta, D. Dimiduk, M. Stucke, Advanced intermetallic alloys—beyond gamma titanium aluminides, *Mater. Sci. Eng. A.* 239 (1997) 1–13.
- [6] B.P. Bewlay, J.J. Lewandowski, M.R. Jackson, Refractory metal-intermetallic in-situ composites for aircraft engines, *JOM.* 49 (1997) 44–45.
- [7] R.L. Fleischer, Ion Tracks, in: *Intermet. Compd. - Princ. Pract.*, Wiley-Blackwell, 2002: pp. 263–273.
- [8] M.S. El-Genk, J.-M. Tournier, A review of refractory metal alloys and mechanically alloyed-oxide dispersion strengthened steels for space nuclear power systems, *J. Nucl. Mater.* 340 (2005) 93–112.
- [9] K.S. Chan, Cyclic-Oxidation Resistance of Niobium-Base in situ Composites: Modeling and Experimentation, *Oxid. Met.* 61 (2004) 165–194.
- [10] J.R. Davis, A.S.M.I.H. Committee, *ASM Specialty Handbook: Heat-Resistant Materials*, in: *ASM Spec. Handb. Heat-Resist. Mater.*, 1997.

- [11] E.N. Sheftel, O.A. Bannykh, Niobium-Base Alloys, *Hit J Refracto Met. Hard Mater.* 12 (1994) 303–314.
- [12] M. Uz, R.H. Titran, Thermal stability of the microstructure of an aged Nb-ZrC alloy, in: *AIP Conf Proc*, 1991.
- [13] T.B. Massalski, H. Okamoto, P.R. Subramanian, L. Kacprzak, *Binary Alloy Phase Diagrams*, 1990.
- [14] F. Ostermann, Controlling carbide dispersions in niobium-base alloys, *J. Common Met.* 25 (1971) 243–256.
- [15] D.L. Olson, B. Mishra, D.W. Wenman, *Welding, Brazing and Joining of Refractory Metals and Alloys*, *Miner. Process. Extr. Metall. Rev.* 22 (2001) 1–23.
- [16] E.J. Delgrosso, C.E. Carlson, J.J. Kaminsky, Development of niobium-zirconium-carbon alloys, *J. Common Met.* 12 (1967) 173–201.
- [17] J.F. Smith, O.N. Carlson, R.R. De Avillez, The niobium-carbon system, *J. Nucl. Mater.* 148 (1987) 1–16.
- [18] H. Tanaka, Y. Tan, C.L. Ma, A. Kasama, R. Tanaka, Report of the 123rd Committee on Heat-resisting Materials and Alloys, *Jpn. Soc. Promot. Sci.* 41 (2000) 223–227.
- [19] S. Nomura N; Yoshimi, K; Hanada, Mechanical properties of Mo-Nb-TiC in-situ composites synthesized by hot-pressing, *Mater. Trans. JIM.* 41 (2000) 1599 – 1604.
- [20] T. Suzuki, S. Hanada, N. Nomura, K. Yoshimi, Microstructure and creep of Mo-ZrC in-situ composite, *Mater T JIM.* 41 (2000) 1164–1167.
- [21] Y. Tan, C. Ma, A. Kasama, R. Tanaka, Y. Mishima, S. Hanada, J.-M. Yang, Effect of Alloy Composition on Microstructure and High Temperature Properties of Nb–Zr–C Ternary Alloys, *Mater. Sci. Eng. -Struct. Mater. Prop. Microstruct. Process. - Mater Sci Eng -Struct Mater.* 341 (2003) 282–288.

- [22] D. Goldberg C., G. Dicker, S.A. Worchester, Niobium and Niobium alloys in nuclear power, *Nucl. Eng. Des.* 22 (1972) 95–123.
- [23] M. Uz, R.H. Titran, Characterization of the microstructure of Nb-1wt%Zr- 0.1wt%C tubes as affected by thermomechanical processing, *AIP Conf Proc.* 301 (1994) 393–402.
- [24] E. M. Lyutyi, O. S. Tsvikilevich, G. G. Maksimovich, Quantitative analysis on the distribution of hardening-phase particles in an Nb-Zr-C alloy, *Sov Mater Sci.* 14 (1978) 284 – 288.
- [25] A. E. Kissil, P. A. Khandarov, A. D. Rapp, L. P. Onisenko, L. Z. Polyak, A. G. Arakelov, and I. I. Maksimov, Study of the structure and morphology of the strengthening phase in an Nb-Zr-C alloy during the prolonged action of high temperature and pressure in vacuo, *Sov Mater Sci.* 12 (1977) 640–643.
- [26] G. G. Maksimovich, O.S. Tsvikilevich, E. M. Lyutyi, A. E. Kissil, L. P. Onisenko, P. A. Khandarov, Structure and morphology of the hardening phase in an Nb-Zr-C alloy after strain aging at 900°C, *Sov Mater Sci.* 13 (1977) 576–578.
- [27] P.A. Khandarov, A.N. Luk'yanov, A.G. Arakelov, O.S. Tsvikilevich, E.M. Lyutyi, G.G. Maksimovich, Kinetics of structural changes in an Nb-Zr-C alloy with prolonged holding under load at high temperatures, *Sov. Mater. Sci.* 14 (1978) 431–435.
- [28] M. Levy, J.J. Falco, R.B. Herring, Oxidation of columbium (niobium) and coated columbium alloys, *J. Common Met.* 34 (1974) 321–343.
- [29] T. Hurlen, Oxidation of niobium, *J Inst Met.* 89 (1960) 273–280.
- [30] I. McKee, G.R. Wallwork, The oxidation of tantalum and niobium in the temperature range 400 - 600 °C, *J. -Common Met.* 30 (1973) 249–258.
- [31] O. Kubaschewski, B.E. Hopkins, Oxidation mechanisms of niobium, tantalum, molybdenum and tungsten, *J. -Common Met.* 2 (1960) 172–180.

- [32] P. Kofstad, High Temperature Oxidation of Metals. John Wiley & Son, New York, 1966.
- [33] C. Nico, T. Monteiro, M.P.F. Graça, Niobium oxides and niobates physical properties: Review and prospects, Prog. Mater. Sci. 80 (2016) 1–37.
- [34] J.F. Stringer, High Temperature Corrosion of Aerospace Alloys, AGARDograph. (1975).
- [35] R. Svedberg, Properties of High Temperature Alloy, in: Electrochemical Society, Pennington, NJ, 1976: p. 331.
- [36] M. Steinhorst, H.J. Grabke, Oxidation of niobium aluminide NbAl<sub>3</sub>, Mater. Sci. Eng. A. 120–121 (1989) 55–59.
- [37] C.S. Wukusick, Oxidation Behavior of Intermetallic Compounds in the Nb-Ti-Al System, US Atomic. Energy Commission, 1963.
- [38] H. Lavendel, Investigation of modified silicide coatings for refractory metal alloys with improved low pressure oxidation behaviour, Lockheed, 1965.
- [39] High-Temperature Oxidation-Resistant Coatings: Coatings for Protection From Oxidation of Superalloys, Refractory Metals, and Graphite, The National Academies Press, Washington, DC, 1970.
- [40] H. Chen, Y. Gang, C. Wenbin, L. Kaijun, L. Feng, Simulation of the organic thin film thickness distribution for multi-source thermal evaporation process, Vacuum. 85 (2010) 448–451.
- [41] C.W. Draper, C.A. Ewing, Laser surface alloying: a bibliography, J. Mater. Sci. 19 (1984) 3815–3825.
- [42] M. Halvarsson, H. Nordén, S. Vuorinen, The microstructure of bonding layers for CVD alumina coatings, Surf. Coat. Technol. 68–69 (1994) 266–273.

- [43] M. Halvarsson, S. Vuorinen, Microstructure and performance of CVD  $\kappa$ -Al<sub>2</sub>O<sub>3</sub> multilayers, *Mater. Sci. Eng. A.* 209 (1996) 337–344.
- [44] A.S. Khanna, A. Gasser, K. Wissenbach, M. Li, V.H. Desai, W.J. Quadackers, Oxidation and corrosion behaviour of mild steel laser alloyed with nickel and chromium, *J. Mater. Sci.* 30 (1995) 4684–4691.
- [45] B. Lux, C. Colombier, H. Altena, K. Stjernberg, Preparation of alumina coatings by chemical vapour deposition, *Thin Solid Films.* 138 (1986) 49–64.
- [46] K. Matsuura, T. Koyanagi, T. Ohmi, M. Kudoh, Aluminide Coating on Niobium by Arc Surface Alloying, *Mater. Trans.* 44 (2003) 861–865.
- [47] B. Navinšek, Improvement Of Cutting Tools By TiN PVD Hard Coatings, *Mater. Manuf. Process.* 7 (1992) 363–382.
- [48] I. Milošev, B. Navinšek, A corrosion study of TiN (physical vapour deposition) hard coatings deposited on various substrates, *Surf. Coat. Technol.* 63 (1994) 173–180.
- [49] B. Bhushan, B.K. Gupta, *Handbook of Tribology: Materials, coatings, and surface treatments*, (1991).
- [50] K.K. Biswas, S. Datta, S.K. Das, M.C. Ghose, A. Mazumdar, N. Roy, Glass-ceramic Coatings for Steel and Nimonic Alloy, *Trans. Indian Ceram. Soc.* 45 (1986) 43–45.
- [51] D. Chatterji, R.C. DeVries, G. Romeo, Protection of Superalloys for Turbine Application, in: M.G. Fontana, R.W. Staehle (Eds.), *Adv. Corros. Sci. Technol. Vol. 6*, Springer US, Boston, MA, 1976: pp. 1–87.
- [52] V.S. Smentkowski, Trends in sputtering, *Prog. Surf. Sci.* 64 (2000) 1–58.
- [53] R. Sakidja, F. Rioult, J. Werner, J.H. Perepezko, Aluminum pack cementation of Mo-Si-B alloys, *Scr. Mater.* 55 (2006) 903–906.

- [54] Z.D. Xiang, S.R. Rose, P.K. Datta, Codeposition of Al and Si to form oxidation-resistant coatings on  $\gamma$ -TiAl by the pack cementation process, *Mater. Chem. Phys.* 80 (2003) 482–489.
- [55] R.W. Chan, *Physical Metallurgy*, Elsevier, 1996.
- [56] R.O. Suzuki, T. Nishibata, K.-I. Nakanishi, M. Ishikawa, K. Ono, Electroless coating of Fe<sub>3</sub>Si on steel in the molten salt, *Steel Res.* 71 (2000) 130–137.
- [57] R.O. Suzuki, M. Ishikawa, K. Ono, MoSi<sub>2</sub> coating on molybdenum using molten salt, *J. Alloys Compd.* 306 (2000) 285–291.
- [58] T. Ueda, T. Goto, Y. Ito, *Surf. Finish. Soc. Jpn.* 46 (n.d.) 1173–1179.
- [59] A.J. Gay, J. Quakernaat, A study of electroless siliconizing of nickel, *J. Common Met.* 40 (1975) 21–28.
- [60] R.O. Suzuki, Y. Nagaso, K.-I. Nakanishi, K. Ono, Growth of Fe<sub>3</sub>Si layer deposited from the molten salt, *Steel Res.* 71 (2000) 138–143.
- [61] R.O. Suzuki, M. Ishikawa, K. Ono, NbSi<sub>2</sub> coating on niobium using molten salt, *J. Alloys Compd.* 336 (2002) 280–285.
- [62] K. Tatemoto, Y. Ono, R.O. Suzuki, Silicide coating on refractory metals in molten salt, *J. Phys. Chem. Solids.* 66 (2005) 526–529.
- [63] F. Meng, H. Lu, *Electrochemical Fabrication of Niobium Silicon Alloys from Oxide Powder Mixtures*, 2013.
- [64] B. Song, P. Feng, J. Wang, Y. Ge, G. Wu, X. Wang, F. Akhtar, Oxidation properties of self-propagating high temperature synthesized niobium disilicide, *Corros. Sci.* 85 (2014) 311–317.
- [65] G. Slama, A. Vignes, Coating of niobium and niobium alloys with aluminum. Part I. Pack-cementation coatings, *J. Common Met.* 23 (1971) 375–393.

- [66] S. Majumdar, A. Arya, I.G. Sharma, A.K. Suri, S. Banerjee, Deposition of aluminide and silicide based protective coatings on niobium, *Appl. Surf. Sci.* 257 (2010) 635–640.
- [67] L. Yin, L. Yang, D. Yi, High temperature oxidation resistance coating on niobium, *Mater. Sci. Technol.* 21 (2005) 579–582.
- [68] K. Hosokawa, *J Jpn Inst Met.* 39 (1975) 345–351.
- [69] G.I. Belyaeva, A.I. Anfinogenov, N.G. Ilyushchenko, *Met. Sci. Heat Treat.* 13 (1971) 63–65.
- [70] T. Oki, J. Tanikawa, *J Met. Finish. Soc.* 31 (1980) 561–566.
- [71] W.M.M. Huijbregts, M.J. Brabers, Oxidation of niobium and of niobium coated with aluminium in steam-air mixtures, in: *Proc. SERAI Journee Int. Détude Sur Lóxydation Metaux*, 1965: p. 12.
- [72] T. Murakami, S. Sasaki, K. Ito, H. Inui, M. Yamaguchi, Microstructure of Nb substrates coated with Mo(Si,Al)<sub>2</sub>-Al<sub>2</sub>O<sub>3</sub> composite and B-doped Mo<sub>5</sub>Si<sub>3</sub> layers by spark plasma sintering, *Intermetallics.* 12 (2004) 749–754.
- [73] T. F. K., Ryosuke O S., Katsutoshi O., Oxidation Resistant Coating for Niobium by Combining Hot Dipping in Molten Aluminum Coating and Anodic Oxidation, *J. Jpn. Inst. Met. Mater.* 59 (1995) 967–972.
- [74] T. Yamada, H. Sato, H. Yamane, Preparation of Niobium Disilicide Coating by Heating Niobium in a Sodium&ndash;Silicon Melt, *Mater. Trans.* 53 (2012) 2141–2144.
- [75] S. Priceman, L. Sama, No Title, *Electrochem Tech.* 6 (1968) 315.
- [76] M. Li, L. Song, J. Le, X. Zhang, B. Pei, X. Hu, Effect of Copper Addition on the Niobium Disilicide Coatings by Pack Cementation, *Mater. Trans.* 45 (2004) 2785–2787.
- [77] J.-K. Yoon, G.-H. Kim, J.-H. Han, I.-J. Shon, J.-M. Doh, K.-T. Hong, Microstructure and oxidation property of NbSi<sub>2</sub>/Si<sub>3</sub>N<sub>4</sub> nanocomposite coating formed on Nb substrate

- by nitridation process followed by pack siliconizing process, *Intermetallics*. 13 (2005) 1146–1156.
- [78] C. Milanese, V. Buscaglia, F. Maglia, U. Anselmi-Tamburini, Reactive growth of niobium silicides in bulk diffusion couples, *Acta Mater.* 51 (2003) 4837–4846.
- [79] S. Majumdar, P. Sengupta, G. Kale, I. G. Sharma, Development of Multilayer Oxidation Resistant Coatings on Niobium and Tantalum, *Surf. Coat. Technol.* 200 (2006) 3713–3718.
- [80] M. Ukegawa, A. Yamauchi, A. Kobayashi, K. Kurokawa, Interfacial reactions in Nb/NbSi<sub>2</sub> and Nb/NbSi<sub>2</sub>–B systems, *Vacuum*. 83 (2008) 157–160.
- [81] B. Vishwanadh, K. Vaibhav, S.K. Jha, K.V. Mirji, I. Samajdar, D. Srivastava, R. Tewari, N. Saibaba, G.K. Dey, Development of Nb-1%Zr-0.1%C alloy as structural components for high temperature reactors, *J. Nucl. Mater.* 427 (2012) 350–358.
- [82] B. Vishwanadh, R.H. Naina, S. Majumdar, R. Tewari, G.K. Dey, A study on the oxidation behavior of Nb alloy (Nb-1 pct Zr-0.1 pct C) and silicide-coated Nb alloys, *Metall. Mater. Trans. Phys. Metall. Mater. Sci.* 44 (2013) 2258–2269.
- [83] C. Wagner, D. Passoja, H. Hillery, T. Kinisky, H. Six, W. Jansen, J. Taylor, Auger and photoelectron line energy relationships in aluminum–oxygen and silicon–oxygen compounds, *J. Vac. Sci. Technol.* 21 (1982) 933–944.
- [84] C.H.F. Peden, J.W. Rogers, N.D. Shinn, K.B. Kidd, K.L. Tsang, Thermally grown Si<sub>3</sub>N<sub>4</sub> thin films on Si(100): Surface and interfacial composition, *Phys Rev B*. 47 (1993) 15622–15629.
- [85] F.J. Himpsel, F.R. McFeely, A. Taleb-Ibrahimi, J.A. Yarmoff, G. Hollinger, Microscopic structure of the SiO<sub>2</sub>-Si interface, *Phys Rev B*. 38 (1988) 6084–6096.
- [86] A. Thøgersen, J.H. Selj, E.S. Marstein, Oxidation effects on graded porous silicon anti-reflection coatings, *J. Electrochem. Soc.* 159 (2012) D276–D281.

- [87] J.-J. Gallet, F. Bournel, F. Rochet, U. Köhler, S. Kubsky, M.G. Silly, F. Sirotti, D. Pierucci, Isolated Silicon Dangling Bonds on a Water-Saturated n+-Doped Si(001)-2 × 1 Surface: An XPS and STM Study, *J. Phys. Chem. C*. 115 (2011) 7686–7693.
- [88] C.J. Karlsson, E. Landemark, Y.-C. Chao, R.I.G. Uhrberg, Photoemission study of the Si(111)- $\sqrt{3} \times \sqrt{3}$  -Pb mosaic phase: Observation of a large charge transfer, *Phys Rev B*. 45 (1992) 6321–6324.
- [89] H. Koh, J.W. Kim, W.H. Choi, H.W. Yeom, Reinvestigation of the Si 2p photoemission line shape from a clean Si(001)c(4x2) surface, *Phys Rev B*. 67 (2003) 073306-4.
- [90] N. Tomita, Y. Kawabata, S. Adachi, Characterization of Si (111) surfaces treated in aqueous H<sub>2</sub> SiF<sub>6</sub> solution, *Mater. Sci. Eng. B*. (2000).
- [91] P. Chiotti, Dissociation pressure and thermodynamic properties of Na<sub>2</sub>SiF<sub>6</sub>, *J. Common Met.* 80 (1981) 97 – 104.
- [92] M. Tyagi, B. Vishwanadh, S.K. Ghosh, R. Tewari, Synthesis and characterization of silicide coating on niobium alloy produced using molten salt method, *Mater. Sci. Forum*. 830–831 (2015) 683–686.
- [93] Y.-J. Choi, J.-K. Yoon, G.-H. Kim, W.-Y. Yoon, J.-M. Doh, K.-T. Hong, High temperature isothermal oxidation behavior of NbSi<sub>2</sub> coating at 1000–1450°C, *Corros. Sci.* 129 (2017) 102–114.
- [94] K. Kurokawa, A. Yamauchi, Classification of oxidation behavior of disilicides, *Solid State Phenom.* 127 (2007) 227–232.

